

Incipient stages of collagen mineralization monitored by atomic force microscopy

by

©Ionela Alina Stetco

A Dissertation submitted to the School of Graduate Studies in partial fulfillment of
the requirements for the degree of

Ph.D.

Department of Chemistry

Memorial University of Newfoundland

November 2015

St. John's

Newfoundland

Abstract

The process of collagen mineralization represents a current challenge in tissue engineering and is extensively studied, since collagen and calcium phosphate are the main constituents of natural human bone. *In vitro* biomineralization of collagen can lead to biomaterials which could resemble the bone structure and may be appropriate for use as bone substitutes and implants in medical fields.

Due to the fact that *in vitro* mineralization of collagen contributes to the understanding of mechanisms of mineralization *in vivo*, our research focused on the *in situ* monitoring of the incipient stages of collagen/calcium phosphate composite formation as it happened, with the help of atomic force microscopy (AFM). Since AFM is an appropriate tool for characterizing the morphologic features of a surface and is able to show the modification of the surface by depositions, the effect of calcium and phosphate ion concentrations upon the mineralization process of a collagen matrix in aqueous medium has been studied and the stimulation of mineral deposition by collagen has been established. Raman spectroscopy enabled us to identify the mineralization products as well as obtain a qualitative measure of mineralization efficiency.

According to literature, glycosaminoglycans may enhance the efficiency of the collagen mineralization. Glucuronic acid, a major component of glycosaminoglycans (e.g. hyaluronic acid) in the extracellular matrix, has been previously shown to stimulate collagen mineralization *in vitro* and to lead to the formation of the desired calcium

phosphate phase, i.e. hydroxyapatite. We performed a comparison of glucuronic acid with galacturonic acid (an epimer) which reveals differences in their effects on collagen fibrillogenesis. Our approach shows that while the presence of uronic acids in the collagen matrix may build an efficient scaffold for collagen calcification, it also brings modifications to the collagen matrix assembly. Using a surface-induced process for collagen alignment and fibril formation, we can observe changes in fibril and film structure with AFM.

In order to gain insight on how the glucuronic acid may potentially affect the collagen matrix during fibrillogenesis, we studied the behaviour of glucuronic acid in alkaline and acidic media using AFM. In addition to AFM visualization of the various pH-dependent aggregates formed by glucuronic acid in solution, our experiments led to the synthesis of α -polyglucuronic acid starting from glucuronic acid monomers in an acidic solution. The α -polyglucuronic acid fibers were observed by AFM and its structure was confirmed by ^{13}C solution NMR.

Acknowledgements

First and foremost, I would like to thank my supervisor, Prof. Erika F. Merschrod S., for providing me with the opportunity to study and complete my Ph.D. program in her research group, at Memorial University, on such an interesting topic. The expertise, support and excellent guidance of Prof. Erika F. Merschrod S. made my thesis work possible. There are not enough words to express my gratitude to my supervisor for always being available to advise me and answer all of my questions, and for her understanding, kindness and endless patience.

I would like to thank Prof. Raymond Poirier and Prof. David Thompson, the members of my supervisory committee, for their advice throughout the program and for reading the first draft of this thesis.

Many thanks to Ming Sun and Shaheen Fatima, former members of the group, for teaching me the collagen fibrillogenesis technique by incubation on mica and by “cold-start” approach.

I would also like to thank Dr. Kristin Poduska for discussions and comments, during joint group meetings, concerning my research topic and interpretation of Raman data.

Furthermore, I thank Dr. Céline Schneider (CREAIT) for technical assistance with NMR experiments, and Dr. K. Nag (Biochemistry, Memorial University) and C-CART for the use of Raman spectrometer.

I have really appreciated the administrative assistance of Ms. Mary Flinn and the late Ms. Viola Martin.

I am very grateful to the School of Graduate Studies, Memorial University, for providing me with a graduate scholarship, which enabled me to pursue the Ph.D. program. This work was supported, with funding for stipend, equipment and materials, by the Natural Sciences and Engineering Research Council of Canada (NSERC), the Canada Foundation for Innovation (CFI), and the Industrial Research and Innovation Fund, and they are thankfully acknowledged.

Finally, I would like to thank my whole family, my daughter, my husband, my mother and my sisters, for all their continuous support and encouragement.

Table of Contents

Abstract	ii
Acknowledgments	iv
List of Figures	xv
List of Tables	xvi
1 Introduction	1
1.1 Biom mineralization and mineralized tissues	1
1.2 Extracellular matrix and tissue engineering applications	2
1.2.1 Collagens	4
1.2.2 Collagen self-assembly <i>in vitro</i>	6
1.2.3 Glycosaminoglycans (GAGs) and proteoglycans	7
1.3 Collagen mineralization	8
1.3.1 Mineral phase: calcium phosphates	11
1.4 AFM as a morphological characterization tool	11
1.4.1 AFM imaging in fluid	13
1.4.2 AFM imaging of biom mineralization	14
1.5 Raman spectroscopy and biom mineralization	16
1.6 NMR and polysaccharides	18

1.7	Summary	19
	Bibliography	20
	Co-authorship Statement	37
2	Incipient stages of collagen mineralization monitored by atomic force microscopy	39
2.1	Introduction	39
2.2	Materials and methods	41
2.2.1	Materials	41
2.2.2	Methods for growing collagen fibrils	42
2.2.3	AFM	43
2.2.4	Raman spectroscopy	43
2.3	Results and discussion	44
2.3.1	Collagen mineralization revealed by AFM	44
2.3.2	Calcium phosphate mineral phases characterized by Raman spectroscopy	48
2.4	Conclusions	53
	Bibliography	54
3	Structural effects of uronic acids on collagen-based mineralization matrices	60
3.1	Introduction	60
3.2	Experimental	62
3.2.1	Reagents and apparatus	62
3.2.2	Methods for growing collagen fibrils	62
3.3	Results and discussion	63
3.3.1	Collagen on mica	63

3.3.2	Collagen with sugar acids on mica	64
3.3.3	Collagen on mica pre-treated with sugar acids	66
3.3.4	Collagen fibrils with sugar acids by the cold start method	68
3.3.5	Raman spectroscopy	69
3.4	Conclusions	71
	Bibliography	72
4	Supramolecular structure and anomer-selective formation of polyglucuronic acid	77
4.1	Introduction	78
4.2	Materials and methods	79
4.2.1	Materials	79
4.2.2	Methods for growing polyglucuronic fibrils on mica for AFM	80
4.2.3	AFM	80
4.2.4	Solid-state NMR	80
4.2.5	¹³ C - solution NMR	81
4.3	Results and discussion	81
4.3.1	Polyglucuronic acid fibres on mica revealed by AFM	81
4.3.2	Polyglucuronic acid fibres characterized by NMR	87
4.4	Conclusions	95
4.5	Acknowledgments	97
	Bibliography	97
5	Conclusions and future perspectives	103
5.1	Conclusions	103
5.2	Future perspectives:	105
5.2.1	Understanding the role of acidic groups in collagen mineralization	105

5.2.2	Mechanical properties of <i>in vitro</i> mineralized collagen fibrils	106
5.2.3	Characterization of α -polyglucuronic acid	106
	Bibliography	107
A	Raman evidence for mineralization	110
B	^1H NMR spectra of glucuronic acid in monomeric and polymeric forms	114

List of Figures

1.1	Structure of a generic collagen fibril. A D-periodic collagen fibril from tendon is presented at the <i>top of the panel</i> . The negative stained fibril has a characteristic alternating light/dark pattern representing the gap (<i>dark</i>) and overlap (<i>light</i>) regions of the fibril. The diagram represents the staggered pattern of collagen molecules giving rise to this D-periodic repeat. The collagen molecules (<i>arrows</i>) are staggered N to C. The fibrillar collagen molecule is approximately 300 nm (4.4 D) in length and 1.5 nm in diameter. Reproduced from [30] with permission from Springer.	5
-----	--	---

- 2.1 Phosphate ion addition to cold start collagen protofibrils enriched with calcium leads to partial disappearance of collagen fibrils. A) Collagen protofibrils enriched with calcium, imaged in water (control image) B) 20 minutes after the addition of 50 μL KPb - dramatic change in fibrils thickness is observed due to mineral precipitation on top of the fibrils C) after 40 minutes since the addition of KPb (the next scan) - deposition of calcium phosphate occurs more even on the imaged surface, not only on collagen fibrils where the calcium concentration was the highest, leading to thinner fibrils D) after 80 minutes since the addition of KPb - the fibrils are becoming less prominent and fewer in number Note: the duration of an AFM image is approximately 20 minutes; all images 5 μm \times 5 μm 45
- 2.2 The effect of calcium ion concentration upon the *in situ* mineralization process with imaging in phosphate buffer pH 7.5. 20 μL 1 mM CaCl_2 solution are added every 60 minutes at the imaging spot. A) No calcium is added. B) After 5 hours the amount of added CaCl_2 is 100 μL ; image shows the mineralized fibrils. C) The next scanned image after addition of CaCl_2 shows the growth in size of the crystallite objects at the expense of decrease in height of the collagen fibrils. D) After 6 hours there is more mineral coverage. Image sizes are (A) 5 μm \times 5 μm and (B)-(D) 3 μm \times 3 μm 47
- 2.3 Mineralization of the collagen scaffold created by incubation on mica by slight exposure to calcium ion solution. AC mode capture of the incipient stages of mineralization stimulated by collagen fibrils (on top of fibrils) exposed A) once (3 μm \times 3 μm) or B) twice (5 μm \times 5 μm) to CaCl_2 48

2.4	Raman spectra: A) mica (intensity multiplied by 2) B) collagen monomers on mica (original intensity; x axis offset of 12.5 cm ⁻¹) C) collagen fibrils on mica (intensity multiplied by 2) D) mica and calcium phosphate phases (mixed KPB and CaCl ₂) (original intensity; x axis offset of 12.5 cm ⁻¹) E) collagen fibrils incubated on mica in KPB exposed once to CaCl ₂ (intensity multiplied by 2); F) collagen fibrils incubated on mica in KPB saturated with CaCl ₂ and KPB (intensity multiplied by 2). Note: The offset along the x axis was adjusted for some spectra so that the major mica Raman band at 701 cm ⁻¹ is aligned in all spectra in this plot. The intensity of selected spectra in this plot was doubled with the purpose of enhancing the visualisation of the spectral features of interest and to facilitate their interpretation.	49
3.1	AFM images of glucuronic acid's effects on a collagen matrix. a) Collagen fibrils grown by incubation on mica. b) Collagen fibrils grown with the sugar acid (early stages of hole formation). c) Mature collagen/sugar film showing the "laddered stockings" motif.	65
3.2	AFM images showing how sugar interactions with mica initiate the pore formation. GlcA on mica looks like a), while collagen films grown on a pre-treated surface of mica saturated with GlcA look like b), which is similar to the films from pre-mixed GlcA/collagen c). Similar images for GalA are shown in d)–f), with the GalA film on mica in d), the collagen film grown on a GalA-treated mica surface in e), and a film of pre-mixed coll/GalA in f).	66
3.3	AFM images of a) collagen and b) collagen and glucuronic acid, after cold-start treatment.	68

3.4	Raman spectra of: a) glucuronic acid, b) a sample of collagen monomers with glucuronic acid, c) collagen with GlcA after cold start, d) collagen after cold start.	70
4.1	Atomic force micrograph of (a) glucuronic acid monomers, unadjusted pH, and (b) polyglucuronate fibrils prepared in an acidified solution and dried on a mica substrate.	83
4.2	AFM images of a sample dried from a glucuronic acid solution (a) at pH 2, (b) at pH 13, (c) at pH 2 switched to basic pH and (d) at pH 13 switched to acidic pH.	84
4.3	Atomic force micrograph of polyglucuronate fibrils prepared in an acidified solution, dried on a mica substrate, and imaged in ultrapure water to check stability.	85
4.4	Structure of glucuronic acid monomer and polymer: (a) α anomer and (b) β anomer. The carbon atoms are numbered, as referred to in the text. (c) Possible structure of synthesized polyglucuronic acid featuring the α -(1,4) linkage.	88
4.5	^{13}C NMR spectra of glucuronic acid in monomeric and polymeric forms: (a) solid state CPMAS; (b) unadjusted pH 6, monomer; (c) basic pH 13, monomer; (d) acidic pH 2, monomer; (e) acidic to basic after 10 min, mixture monomer-polymer; (f) acidic to basic after 30 min, polymer. The intensity in the solid state spectrum (a) is scaled to match those of the solution spectra (b)–(f).	89

A.1	Raman spectra: A) collagen fibrils incubated on mica in KPB in the presence of glucuronic acid and saturated with CaCl_2 and KPB B) collagen fibrils incubated on mica in KPB C) collagen fibrils incubated on mica in KPB, without addition of glucuronic acid, and saturated with CaCl_2 and KPB.	111
A.2	Raman spectra: A) collagen fibrils incubated on mica in KPB in the presence of glucuronic acid and saturated with $\text{Ca}(\text{NO}_3)_2$ and KPB B) collagen fibrils incubated on mica in KPB in the presence of galacturonic acid and saturated with $\text{Ca}(\text{NO}_3)_2$ and KPB C) collagen fibrils incubated on mica in KPB, without addition of uronic acids, and saturated with $\text{Ca}(\text{NO}_3)_2$ and KPB.	112
A.3	Raman spectrum of collagen monomers after exposure to calcium and phosphate ions.	113
B.1	^1H NMR spectra of glucuronic acid in monomeric and polymeric forms.	115
B.2	^1H NMR spectrum of glucuronic acid in monomeric form at basic pH = 12.	116

List of Tables

2.1	Raman band assignment of calcium phosphate phases	50
-----	---	----

Chapter 1

Introduction

1.1 Biomineralization and mineralized tissues

The process of biological mineralization, also known as biomineralization, refers to the formation of inorganic minerals *in vivo* (so-called, biominerals) by living organisms, within or outside cells, under well-controlled conditions [1–3]. These biomineral phases are composite materials comprised of both inorganic and bioorganic components [4]. Given the great variety of minerals and macromolecules involved in this process, the central point of the biomineralization field is a thorough comprehension of their structure and in particular of the interaction between them [5].

Mineralized tissues in vertebrates are represented by bones, enamel, dentin, and cementum, and their mineral phase is mainly formed from calcium phosphates [6]. These inorganic calcium phosphate salts present in the calcified tissues of vertebrates, especially bones and teeth, are known as biological apatites and are characterized by the presence of low-rate stoichiometric and non-stoichiometric substitution [7] which may play a significant role in the pathophysiological processes in these biological materials [8].

The degree of mineralization as well as the size, shape and organization of the mineral crystals is tissue-specific [6]. For instance, the average mineral content of bone tissue is species dependent and lies within the range of 30 to 55 volume % or 50 to 74 dry weight % [9]. Since bone tissue is formed from a composite, besides the mineral part it contains about 30 % organics by dry weight [10]. Dentin is the calcified tissue that represents the largest part of the tooth and has a similar composition to the bone, consisting of type I collagen and carbonated apatite, which is similar to the mineral in bone and calcified tendon [11].

The basic building block of bones is the mineralized collagen fibril [12]. The mineral phase is essentially carbonated hydroxyapatite [9]. Other constituents of bone tissue consist of water, organic molecules such as glycosaminoglycans, glycoproteins, lipids and peptides, and ions like sodium, magnesium, fluoride, and citrate [13].

1.2 Extracellular matrix and tissue engineering applications

The extracellular matrix (ECM) is a complex three-dimensional structural support network [14] representing the cell's direct environment in the body [15]. The extracellular matrix is built from two main classes of macromolecules: (1) polysaccharide chains of the class called *glycosaminoglycans (GAGs)*, which are usually found covalently linked to protein in the form of *proteoglycans*, and (2) fibrous proteins, including *collagen*, *elastin*, *fibronectin*, and *laminin*, which have both structural and adhesive functions [16].

The composition and ultrastructure of the ECM is tissue-specific and the combination of cells and ECM defines the tissues in our body based on the physiologic requirements of the particular tissue [17]. For example, tissues like cartilage and

bone are primarily constituted by ECM, which in the case of bone is highly mineralized [16], thus conferring the rigidity typical of that tissue as well as resistance to load and strain [14]. The macromolecules that constitute the ECM of most connective tissues are mainly produced by cells called fibroblasts, which may have even more specific names for certain types of connective tissues, for example osteoblasts for bone, chondroblasts for cartilage, etc. [16].

The ECM is ubiquitously distributed throughout the body, surrounding the cells, and it is a fundamental element during regeneration and physical maintenance of all cells responsible for structural support for tissues and organs [18]. Therefore, it represents a significant factor in successful tissue engineering, as well [14].

Tissue engineering is an interdisciplinary field that combines engineering and biology concepts with the aim of developing biological substitutes that can be used to restore, maintain, or enhance tissue function [19, 20]. The field of tissue engineering uses the natural repair processes to inspire and motivate the creation *in vitro* of synthetic materials for various human tissues, which eventually would allow prevention, diagnosis, and treatment of diseases that are of current interest for tissue engineering [19].

The ECM is the nature's ideal biological scaffold material, and intact ECM has been employed in various therapeutic applications [21] for the reconstruction of many different tissue types following injury [17]. Advances in areas such as biology, engineering, physics and chemistry enable the exploration of new and improved scaffolds capable of mimicking the cell's environment and which may lead to the successful fabrication of engineered tissues. Several scaffold materials such as hydroxyapatite and natural polymers including collagen and chitin, aiming to sustain biological processes and support the repair of defective tissues, have been evaluated for suitability to be used in the tissue engineering for bone and cartilage [22]. Additionally, syn-

thetic polymer scaffolds consisting of glycosaminoglycan and collagen were used to regenerate cartilaginous tissue and may be useful for a variety of tissue engineering applications [23].

1.2.1 Collagens

Collagen is the primary and most abundant structural protein within the ECM [17,24]. In addition, type I collagen is the major organic component of the bone ECM [25]. The appeal of collagen as a biomaterial is based on the fact that it is a natural material of low immunogenicity, thus being recognized by the body as a normal constituent rather than foreign matter [26,27].

More generally, collagens are a family of proteins exhibiting extensive structural variety. There are currently 28 distinct types of collagen identified in humans and more than 20 in animal tissues, which can be classified in several subfamilies based on their diverse shape and size [28,29]. The collagens assemble into various supramolecular organizations, e.g. fibrils, filaments, or networks [30]. However, the subfamily of fibrillar collagens (collagen type I, II, III, V, XI, XXIV and XXVII) is the most abundant in vertebrates and is also the most important from a biomechanical standpoint owing to the ability to assemble into cross-striated collagen fibrils [31] that display a repeating banding pattern with a so-called D axial periodicity characteristic to collagen [28]. The length of the D-period, which is proposed to be a stagger between adjacent fibrillar collagen molecules due to the formation of a gap-overlap structure [30], is tissue-specific (e.g. 67 nm in rat tail tendon and 64 nm in human dermis). These collagens co-assemble into banded fibrils usually in the extracellular matrix of connective tissues [32] including bone, dentin, tendons, cartilage, dermis, sclera, cornea, and the interstitial connective tissues in and around many organs [30]. The D-periodic banding of collagen is schematically represented in Figure 1.1 [30].

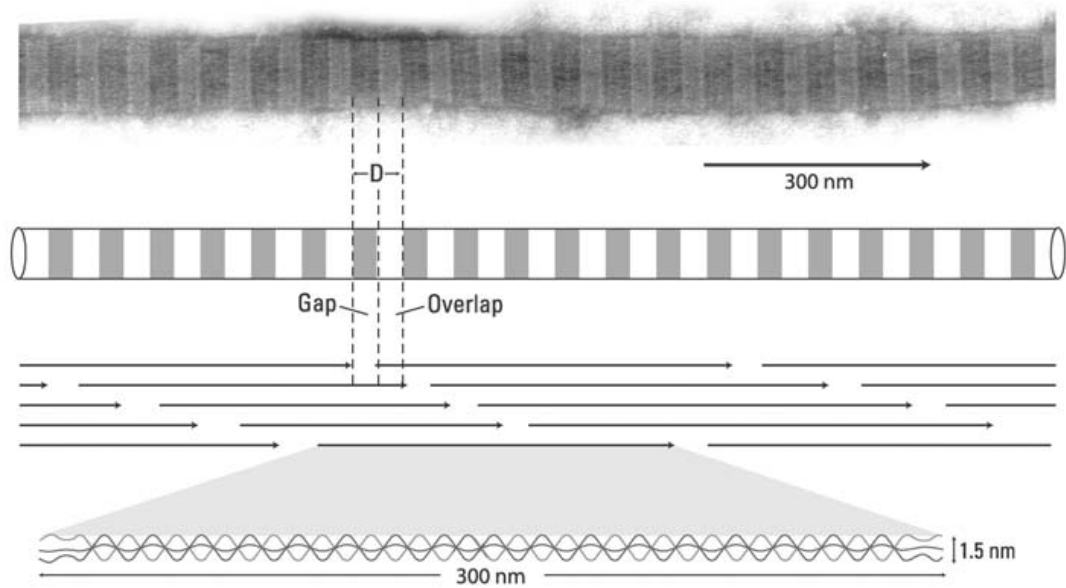


Figure 1.1: Structure of a generic collagen fibril. A D-periodic collagen fibril from tendon is presented at the *top of the panel*. The negative stained fibril has a characteristic alternating light/dark pattern representing the gap (*dark*) and overlap (*light*) regions of the fibril. The diagram represents the staggered pattern of collagen molecules giving rise to this D-periodic repeat. The collagen molecules (*arrows*) are staggered N to C. The fibrillar collagen molecule is approximately 300 nm (4.4 D) in length and 1.5 nm in diameter. Reproduced from [30] with permission from Springer.

Type I collagen is the major protein of banded fibrils displaying various supras-structures based on the type of tissue and is also the major structural protein present in bones [30]. The triple helical domain of collagen I is composed of 338 amino acid triplets Gly-X-Y per chain, where Gly represents glycine [30]. While X and Y can be any amino acid, typically they are represented by proline and hydroxyproline [29,31]. Type-I collagen molecules share a common feature in that they consist of three polypeptide α -chains that constitute a unique and uninterrupted right handed triple helix called tropocollagen, approximately 300 nm in length and 1.5 nm in diameter [29,32]. The triple helical structure is stabilized by the formation of hydrogen bonding between two NH groups of a chain and two oxygens from the other two chains [33,34]. This characteristic feature makes collagen distinctive from other proteins [29].

Staggered arrays of collagen molecules (triple helical tropocollagen) assemble into fibrils, which further organize to form collagen fibers [29,33]. Collagen is characterized by high elasticity and lower levels of strength and toughness [35]. Therefore, the knowledge of the function of collagen fibrils is of general interest for material researchers. The investigations of the structure and the mechanical properties of collagen have been done mostly on type I collagen, due to the fact that it has the most well-organized structure of all collagen types [36].

1.2.2 Collagen self-assembly *in vitro*

Purified collagen molecules in solution *in vitro*, at neutral pH and room temperature conditions, will spontaneously assemble into fibrils similar to those seen *in vivo* showing the characteristic 67 nm periodicity, as observed in electron microscopy studies [37]. Despite the fact that the assembly of collagen molecules into fibrils has been attracting intense research interest since the 1950s, the mechanism by which the

assembly occurs is not completely elucidated [24, 37].

According to the research studies found in literature the assembly of type I collagen entails that subfibrillar components congregate into fibrils and bundles of fibrils which may be responsible for controlling the mechanical properties of collagen fibers [24]. An AFM study of type I collagen fibrillogenesis indicates that this is a four stage assembly process and represents a progression from oligomers to small microfibrils, then larger microfibrils followed by mature collagen fibrils, formed through lateral interactions [38].

1.2.3 Glycosaminoglycans (GAGs) and proteoglycans

Connective tissue glycosaminoglycans (GAGs) are linear, unbranched polysaccharide chains composed of repeating disaccharide units [39], where one of the two sugars in the repeating disaccharide is always an amino sugar (N-acetylglucosamine or N-acetylgalactosamine), which in most cases is sulfated. The second sugar is usually a uronic acid (glucuronic or iduronic) [16]. Polysaccharide chains are strongly hydrophilic, forming gels even at very low concentrations and incorporating large amounts of water into their matrix. This swelling enables the matrix to resist compressive forces, thus conferring mechanical support to the tissue, in contrast to collagen fibrils, which resist stretching forces [16, 40]. These supramolecular structures formed by anionic GAGs assist the collagen fibrils in maintaining the shape of the extracellular matrices in connective tissues [41].

Due to the presence of sulfate or carboxyl groups on most of their sugar units, GAGs are highly negatively charged, being the most anionic molecules produced by animal cells [16]. Four main groups of GAGs are distinguished according to their constituting sugars, the type of linkage between the sugars, and the number and location of sulfate groups: (1) *hyaluronan* (non-sulfated), (2) *chondroitin sulfate* and

dermatan sulfate, (3) *heparan sulfate*, and (4) *keratan sulfate* [16,39].

Except for hyaluronan (also known as hyaluronic acid), all GAGs are found covalently attached to a core protein in the form of proteoglycans, which are made by most animal cells [16]. Proteoglycans are believed to have a major role in chemical signaling between cells [16]. By definition, at least one of the sugar side chains of a proteoglycan must be a GAG, thus they are usually easily distinguished from other glycoproteins [16].

The ECM macromolecules, proteins and glycoconjugates, are bound by mutual interactions, which are mainly non-covalent. The driving force of these hydrophilic/hydrophobic and electrostatic interactions is thermodynamic [42]. Based on the knowledge achieved so far with respect to intermolecular interactions in the ECM it is believed that the small proteoglycans bind collagen fibrils at specific sites through their protein core, while their carbohydrate chains interact with each other in the interfibrillar space [42]. The specific interactions between collagen fibrils and anionic GAGs help in the organization of collagen fibrils by forming interfibrillar bridges [41].

The GAG–collagen matrices have made a significant contribution in the development of artificial skin and other biomaterials, thus it is essential to understand the chemical binding of GAGs and collagen. The collagen-proteoglycan interaction has been studied by high-resolution SEM on reconstituted collagen fibrils in the presence of proteoglycans or GAGs (*dermatan / chondroitin sulphate*) under controlled conditions *in vitro* [42].

1.3 Collagen mineralization

It is believed that the collagen mineralization occurs in a manner similar to most biomineralization processes and that it comprises two steps. The first step corresponds

to the nucleation of the inorganic material which subsequently will lead to crystal growth and complete mineralization of the collagen matrix. The initiation of the collagen mineralization process is believed to be controlled either by non-collagenous proteins [43–45] or by the collagen matrix [46]. Although the extracellular matrix is saturated with the precursor ions of the crystal phase to be formed, no uncontrolled or spontaneous precipitation occurs *in vivo*, and the crystal growth in terms of rate, size, and shape is controlled by the macromolecules involved in the mineralization process [6].

While a recent research study posits that the collagen matrix is essential for the nucleation and growth of bone apatite *in vivo* [25], it is still not completely understood how the collagen interacts with the apatite crystals [43] nor the function that the collagen matrix plays in the biomineralization process [47], starting from the incipient phases of biomineralization (i.e., the infiltration of collagen fibrils with amorphous calcium phosphate (ACP)), followed by the growth of apatite crystals [46].

In an attempt to understand the role of the collagen matrix in the apatite formation, individual mineralized collagen fibrils in calcified turkey tendons were examined by transmission electron microscopy (TEM). The study concluded that the hydroxyapatite crystals are mainly intrafibrillar, primarily at the level of the gap regions observed in collagen [48]. In 1996, Landis and al. [49] observed for the first time the presence of crystals on the surface of the collagen fibrils in calcified turkey tendon, reinforcing the hypothesis that collagen may have a significant role in biomineralization. A schematic diagram by Landis et al. [50] illustrating the mineralization of turkey tendon is presented in Figure 1.2 reproduced from [51] with permission from Elsevier.

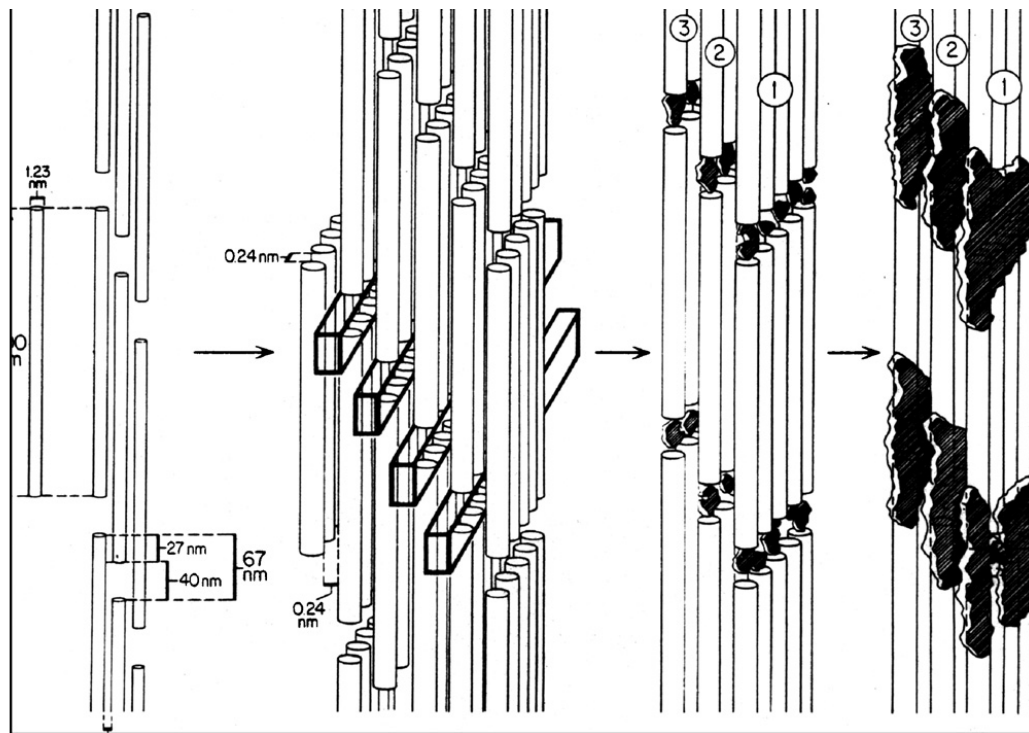


Figure 1.2: Schematic by Landis et al. [50] illustrating the mineralization of turkey tendon, based on *ex situ* observations using high-voltage TEM and tomographic reconstruction imaging. The cylindrical rods represent tropocollagen units composed of triple helical collagen molecules that assemble into fibrils in a quarter-staggered fashion, which leaves periodic gaps and grooves within the fibrils. The 67 nm repeat (64 nm when dehydrated) results from the combination of a 40 nm hole zone and 27 nm overlap zone. The space between assembled tropocollagen units is 0.24 nm. Upon mineralization, the more electron dense mineral can be seen as striations within the collagen fibrils, and the crystals are “oriented such that the crystallographic *c*-axes lie parallel to the long axes of the molecules and their (1 0 0) planes are all approximately parallel to each other. Irregularly shaped, large and small mineral deposits may occupy several hole zones, and preferential growth in the *c*-axial length follows the long axis of the collagen”. Reprinted from Reference 51 (Materials Science and Engineering: R: Reports) with permission from Journal of Structural Biology and Elsevier.

1.3.1 Mineral phase: calcium phosphates

The bone tissue, as introduced in the previous chapters, consists primarily of two components: the inorganic mineral phase, which is a poorly crystalline hydroxyapatite containing variable amounts of carbonate [9], and an organic phase constituted essentially of type I collagen fibers. However, it has been suggested that other calcium phosphate phases such as octacalcium phosphate and amorphous calcium phosphate may also be components of the mineral phase in bone [13].

Compared to other calcium phosphate phases, hydroxyapatite is the most stable phase under physiological conditions, being the least soluble form of calcium phosphate [6]. The hydroxyapatite in bone is highly substituted, thus the calcium ions may be substituted by sodium and magnesium ions, the phosphate groups may be replaced by carbonate ions or hydrogen phosphate ions, while the hydroxyl groups may be exchanged by carbonate, chlorine or fluorine ions [9].

1.4 AFM as a morphological characterization tool

The invention of the Atomic Force Microscope (AFM) by Binnig et al. [52] led to progress in the domain of imaging molecular structures [32]. AFM is a technique capable of investigating surface topography on an atomic scale of both conductors and non-conductors, in air or in aqueous solutions [53]. The generated AFM images are obtained by measurement of the force on a sharp tip attached to a cantilever that is scanned over the surface of the sample [38, 52]. The most common imaging modes of AFM are contact and tapping. In tapping mode the cantilever vibrates at its resonance frequency. Tapping mode operation avoids damaging the sample surface and is particularly useful for imaging soft samples (i.e. biological samples) [54], thus being a non-invasive tool suitable for protein morphological characterization.

AFM is appropriate for biological applications since, unlike electron microscopy, it entails minimal sample preparation and perturbation [38, 55]. AFM is a widely used technique for characterizing surface properties of biological macromolecules [56] and the AFM images can be used to obtain quantitative or qualitative information about the properties of biomaterials [57]. For example, glycosaminoglycans, which are constituents of cartilage aggrecan macromolecules, were visualized by AFM [58]. The unfolding and folding of single protein molecules can also be studied with AFM [59].

AFM confirmed the axial periodicity of mature collagen fibrils and the results from AFM studies agree well with axial periodicity measurements obtained by TEM and SEM [38, 60]. AFM was also used to study the structure of native collagen [61] type I fibrils [32] from rat tail and from reconstituted bovine dermal collagen and the 60-70 nm distinct periodicity of type I collagen was observed in almost all images [60]. AFM was also used to determine modifications of the banding pattern and diameter in collagen fibrils unmodified and modified with glucuronic acid at different concentrations (50 and 250 $\mu\text{g}/\text{mL}$) [62].

AFM was successfully used to characterize the stable transient structural intermediates formed during the *in vitro* assembly of collagen and helped in the visualization of the different stages of assembly in the fibrillogenesis of type I collagen [38]. The AFM technique was used to elucidate the ultrastructure of a fibrillar variant of type I collagen, named fibrous long spacing collagen (FLS), characterized by a periodicity in the banding pattern much larger than that in normal collagen, typically 200–300 nm. The AFM imaging was carried out on FLS collagen fibrils formed *in vitro* in presence of α 1-acid glycoprotein and the measurement data regarding the fibril diameters and periodicities was in good agreement with electron microscopy (SEM and TEM) results, confirming that the AFM technique is suitable for the study of collagen fibrils produced by *in vitro* assembly [55, 56, 63].

In an attempt to understand the thermomechanical properties of the collagen fibril and to characterize the effect of heat denaturation on the topology of the collagen fibril samples, a study was carried out on native tendon collagen using a thermally controlled AFM probe. The AFM technique successfully identified the related structural differences between the collagen long fibrils with the characteristic D-banding along the length of the fibril, associated with the native state of the fibrils, and gelatin (denatured collagen), characterized by random coil instead of triple helix [64].

Another feature that makes AFM a useful research tool is the technique of phase mode imaging, which in tapping AFM can reveal surface characteristics that are not detectable with other imaging modes, height imaging or amplitude imaging, based on differentiation between the hydrophilic and hydrophobic regions present in the sample [57].

1.4.1 AFM imaging in fluid

One powerful capability of AFM is that it allows investigating the structure and dynamics of biological molecules under aqueous environments, from the visualization of complex biochemical processes, such as transcription, in real time, to the mechanical manipulation of individual proteins [65]. By achieving high resolution imaging under liquid [65–67], AFM makes accessible the study of complex biological structures in conditions close to those that exist in living organisms [68, 69]. The operation of the AFM in tapping mode under liquid is very useful since the disruption and deformation of soft samples are significantly reduced owing to the removal of the high adhesion forces due to the water film [54].

The atomic force microscope was used to image biological structures in fluids, including physiological buffer solutions [70], after immobilization on a flat substrate, and therefore has the potential to monitor structural changes of a biological system

in its native environment [71]. Atomic-scale resolution was achieved on a variety of solid-liquid interfaces [72] for samples fixed to a flat solid support which prevents their displacement by the scanning tip [73]. Hence, AFM enables direct visualization of function-related structural changes of proteins and supramolecular assemblies and produces reliable high-resolution images of protein surfaces in an aqueous [71] and non-aqueous environments [60].

1.4.2 AFM imaging of biomineralization

The atomic force microscope proved to be a suitable tool to monitor biomineralization in general, by providing insights into molecular level interactions that occur at the biomaterial interface [74,75]. Mineralization studies report the use of AFM to analyze the nucleation and growth of calcite on native [76] versus pyrolyzed oyster shell folia [77] and the specific alignment of oyster shell protein molecules on calcite surfaces [78]. AFM was successfully used in the characterization of the early stages of calcium carbonate mineralization templated *in vitro* by proteins such as elastin and fibronectin [79], as well as in providing evidence of different calcite biomineralization in various species of coccoliths by being able to observe fine structure on rough samples [80]. However, whilst AFM is suitable to image crystalline surfaces, one of its limitations is represented by the difficulty to characterize samples that feature large variations in height since the Z piezo scanning element in the majority of AFM instruments is restricted to a full vertical range of about 10 μm [81]. In addition, the AFM images should be interpreted with care given that the radius of curvature of the AFM cantilever tip causes broadening of the structure in the lateral dimensions [81,82].

Since calcified turkey tendon displays less dense calcification than bone, it is suitable to study the early stages of bone mineralization with respect to the intra-fibrillar organization of the mineral crystals [50,83]. Literature reports AFM imaging of dem-

ineralized [84] and fully mineralized turkey leg tendon [85, 86], as well as isolated apatite crystals from calcified turkey tendon [87].

The AFM imaging of partially demineralized human dentin tissues [11, 88], as well as AFM imaging of sutural mineralization of rat calvaria [89], zebrafish skeletal bone [90], native trabecular bone [91–93], native cortical bone and ivory dentin has been reported, which demonstrated the effectiveness of AFM imaging in the structural analysis of bone and dentin and of its collagenous components [94]. AFM permitted three-dimensional visual evidence of the size and shape of native protein-free mineralites isolated from mature bovine bone [95, 96] and isolated crystals from rat femoral cortical bone, bound to negatively and positively charged self-assembled monolayers [97]. Furthermore, AFM enabled the visualization of brushite and hydroxyapatite crystals [98] and the *in situ* investigation at atomic scale of hydroxyapatite crystal growth under physiological conditions [99, 100] and also in the presence of an osteocalcin-containing buffer solution [101].

AFM images from a study aimed to compare the *in vitro* mineralization of native-like collagen peptides and collagen-like peptides designed to mimic normal to severe states of the *Osteogenesis imperfecta* disease indicate difficulty for minerals to nucleate and grow on the collagen peptide films formed from the mutant collagen peptides. In contrast, significantly increased mineral size and density are observed for the native-like collagen peptide film [102]. Similarly, dynamic force microscopy was used to observe the demineralized intact collagen fibrils on normal and severely fluorosed dentin surfaces. The data indicate a loose arrangement of fibrils for fluorosed dentin, rather than closely packed fibrils observed in normal dentin, which may affect the ultrastructure of mineral crystallites and lead to the formation of dental caries [103]. Microscopic investigation using AFM provided information with respect to the dentin and dental enamel morphology upon *in vitro* demineralization and remineralization in

the presence of a casein phosphopeptide-amorphous calcium phosphate (CPP-ACP) paste, indicating effectiveness of the CPP-ACP paste in preventing dentin / dental enamel erosion produced by a soft drink [104]. Regeneration of enamel mineralized tissue by an agarose hydrogel biomimetic mineralization model under physiological conditions was visualized by three-dimensional AFM operated in tapping-mode [105].

1.5 Raman spectroscopy and biomineralization

The field of vibrational spectroscopy, which includes infrared (IR) and Raman spectroscopy, has many practical applications in biomedicine as a result of the technological progress achieved over the last few decades [106, 107]. Vibrational spectroscopy is used to study the mineralization process and the interactions between prosthetic inserts and body tissues. Based on the molecular vibrations performed by molecules, it can provide objective information on chemical structure and composition of the samples under investigation, as well as define chemical modifications associated with bone ailments [106, 108].

The characterization of biominerals is essential for a better understanding of abnormal functional changes that may occur in biological mineralized tissues or in synthetic apatitic biomaterials [8]. The Raman spectroscopy technique is widely used in mineral analysis and provided new insights into the mechanisms of mineralization [109]. In addition, Raman spectroscopy proved to be a proficient tool for the characterization of the collagen and mineral phases at a near submicron-length scale [110] and permits one to obtain quantitative information concurrently on the mineral phase and the organic matrix [107].

The intrinsic advantages of both IR and Raman vibrational spectroscopic methods are the simplicity of sample preparation requiring minimal sample processing and

very small amounts of sample (micrograms to nanograms), the speed of measurement with collection times in the range of seconds or minutes, and the non-destructive characterization of a sample's biochemistry allowing in the same time the investigation of functional groups, bonding types and molecular conformations [13, 106]. While both IR and Raman spectroscopies are sensitive to alterations in mineral substituents or protein secondary structure, Raman spectroscopy provides an enhanced spatial resolution vis à vis the IR [107] and does not have strong interferences from water [111].

The major Raman band assignments for bone tissue and synthetic hydroxyapatites and other calcium phosphate phases are presented in detail in Chapter 2. However, of particular interest in the interpretation of Raman spectra for bone and collagen-based mineralized biomaterials are the phosphate ν_1 band at approximately 960 cm^{-1} and the bands attributed to collagen: amide III at $\sim 1250\text{ cm}^{-1}$, CH_2 wag at $\sim 1450\text{ cm}^{-1}$, and amide I at $\sim 1665\text{ cm}^{-1}$ [111].

Raman spectroscopy has been used to investigate the composition of human cortical bone tissue [13], the mineral and collagen organization in bone as well as variations in mineral structure and collagen content due to ageing and various bone diseases [107, 112]. In addition to the IR and Raman spectroscopy study of high purity calcium hydroxyapatite exposed to high external pressures [113], the increased development of Raman spectroscopy permitted researchers to investigate the response of the individual collagen fibrils and mineral crystallites in bovine cortical bone when subjected to induced mechanical load, in either plastic or elastic deformation regimes, based on altered bone spectra that indicated spectral shifts as a result from chemical damage [111].

Raman spectroscopy is capable of distinguishing between various calcium phosphate phases, which helps in the understanding and elucidation of the mechanism involved in the mineralization of hard collagen tissues, such as bone and dentin, and

in the identification of the mineral phases which may act as intermediates in the formation of hydroxyapatite. For instance, this technique has been used to show the presence of transient calcium phosphate phases, like octacalcium phosphate (OCP), in living mouse calvarial tissue, which has been known to be thermodynamically unstable with respect to hydroxyapatite [114]. A comparative study of hydroxyapatite and polycrystalline β -tricalcium phosphate, a closely related calcium phosphate compound, indicated that Raman spectroscopy was able to differentiate between these two calcium phosphates when precipitated on the surface of bioceramic materials based on the vibrational modes of the hydroxyl group in hydroxyapatite and the phosphate group internal modes associated with different crystalline structure [115].

All these attributes confirm Raman spectroscopy as a valuable tool in the scientific community for the analysis of mineralized tissues and chemical composition of crystalline materials.

1.6 NMR and polysaccharides

Nuclear magnetic resonance (NMR) spectroscopy methods, such as solution NMR, are recognized as valuable analytical tools in the chemical structural analysis of polysaccharides [116]. The resolution achieved in solution NMR can provide detailed structural information on composition, distribution of individual polysaccharides and is used effectively in the food industry to identify the type and the proportions of different sugar residues [117, 118].

NMR spectroscopy is capable of showing the presence of glycosidic linkages and allows one to distinguish between anomeric configurations, thus being suitable for the determination of the chemical structure of polysaccharides [119]. NMR has been previously used for the structure elucidation of new uronic acids [120] and was also

employed in establishing the structure of more complex systems containing repeating oligosaccharide units [121] and for the characterization and structure determination of polyglucuronic acids [122].

1.7 Summary

In Chapter 2, I examine the effect of calcium and phosphate ions' concentration on the collagen mineralization *in vitro*. The collagen fibrillogenesis for this experiment was conducted by two different approaches: surface-induced fibril growth and alignment [123] and the cold-start method [124, 125]. Surface-supported growth makes for clearer imaging conditions, allowing for *in situ* imaging by AFM of the collagen mineralization.

It is believed that carboxylate groups can act as a nucleation site for mineral growth by binding calcium ion. Glycosaminoglycans present in the extracellular matrix may interact with the collagen matrix during the fibrillogenesis, resulting in more carboxylate groups, originating from the uronic acids in glycosaminoglycans, to be available for calcium binding. This phenomenon impacts the mineralization process by increasing the number of crystal nucleation sites. To gain insight into the early stages of the collagen mineralization in the presence of uronic acids originating from glycosaminoglycans present in the extracellular matrix, in Chapter 3, I use AFM and Raman spectroscopy to study the structural modifications that selected uronic acids can bring to the collagen matrix and their effect on the alignment of collagen fibrils on mica. The uronic acids selected for this study were glucuronic acid, since it is contained in the structure of the majority of glycosaminoglycans (e.g. hyaluronic acid), and, for comparison, galacturonic acid, which is an epimer of glucuronic acid at the C4 atom.

The AFM images of collagen fibrils formed in the presence of glucuronic and galacturonic acids revealed disruptions in the usual, parallel alignment of collagen fibrils on mica surface, bringing up the necessity to understand the behaviour of uronic acids in solution. Therefore, in Chapter 4, I observe by AFM the glucuronic acid aggregation under various pH conditions ranging from acidic (pH 2) to basic pH (pH 13). In acidic pH the glucuronic acid monomeric units polymerized leading to the synthesis of α -polyglucuronic acid, its structure being elucidated by NMR spectroscopy.

Bibliography

- [1] S. Weiner and P. M. Dove. An overview of biomineralization processes and the problem of the vital effect. *Reviews in Mineralogy and Geochemistry*, 54(1):1–29, 2003.
- [2] A. L. Boskey. Biomineralization: an overview. *Connective Tissue Research*, 44(1):5–9, 2003.
- [3] F. Z. Cui, Y. Wang, Q. Cai, and W. Zhang. Conformation change of collagen during the initial stage of biomineralization of calcium phosphate. *Journal of Materials Chemistry*, 18(32):3835–3840, 2008.
- [4] S. V. Dorozhkin. Calcium orthophosphates: occurrence, properties, biomineralization, pathological calcification and biomimetic applications. *Biomatter*, 1(2):121–164, 2011.
- [5] S. Weiner. Biomineralization: a structural perspective. *Journal of Structural Biology*, 163(3):229–234, 2008.

- [6] A. George and A. Veis. Phosphorylated proteins and control over apatite nucleation, crystal growth, and inhibition. *Chemical Reviews*, 108(11):4670–4693, 2008.
- [7] Q. Liu, S. Huang, J. P. Matinlinna, Z. Chen, and H. Pan. Insight into biological apatite: physiochemical properties and preparation approaches. *BioMed Research International*, 929748:1–13, 2013.
- [8] G. Penel, C. Delfosse, M. Descamps, and G. Leroy. Composition of bone and apatitic biomaterials as revealed by intravital Raman microspectroscopy. *Bone*, 36(5):893–901, 2005.
- [9] P. Fratzl, H. S. Gupta, E. Paschalis, and P. Roschger. Structure and mechanical quality of the collagen–mineral nano-composite in bone. *Journal of Materials Chemistry*, 14(14):2115–2123, 2004.
- [10] L. C. Palmer, C. J. Newcomb, S. R. Kaltz, E. D. Spoerke, and S. I. Stupp. Biomimetic systems for hydroxyapatite mineralization inspired by bone and enamel. *Chemical Reviews*, 108(11):4754–4783, 2008.
- [11] S. Habelitz, M. Balooch, S. J. Marshall, G. Balooch, and G. W. Marshall. In situ atomic force microscopy of partially demineralized human dentin collagen fibrils. *Journal of Structural Biology*, 138(3):227–236, 2002.
- [12] S. Weiner and H. D. Wagner. The material bone: structure-mechanical function relations. *Annual Review of Materials Science*, 28(1):271–298, 1998.
- [13] R. Smith and I. Rehman. Fourier transform Raman spectroscopic studies of human bone. *Journal of Materials Science: Materials in Medicine*, 5(9-10):775–778, 1994.

- [14] H. Fernandes, L. Moroni, C. van Blitterswijk, and J. de Boer. Extracellular matrix and tissue engineering applications. *Journal of Materials Chemistry*, 19(31):5474–5484, 2009.
- [15] J. K. Kular, S. Basu, and R. I. Sharma. The extracellular matrix: structure, composition, age-related differences, tools for analysis and applications for tissue engineering. *Journal of Tissue Engineering*, 5:1–17, 2014.
- [16] B. Alberts, A. Johnson, J. Lewis, M. Raff, K. Roberts, P. Walter, et al. The extracellular matrix of animals. In *Molecular Biology of the Cell*. Garland Science, New York, 2002.
- [17] S. F. Badylak. The extracellular matrix as a scaffold for tissue reconstruction. *Seminars in Cell & Developmental Biology*, 13(5):377–383, 2002.
- [18] R. O. Hynes. The extracellular matrix: not just pretty fibrils. *Science*, 326(5957):1216–1219, 2009.
- [19] L. G. Griffith and G. Naughton. Tissue engineering—current challenges and expanding opportunities. *Science*, 295(5557):1009–1014, 2002.
- [20] B. P. Chan and K. W. Leong. Scaffolding in tissue engineering: general approaches and tissue-specific considerations. *European Spine Journal*, 17(4):467–479, 2008.
- [21] S. F. Badylak. The extracellular matrix as a biologic scaffold material. *Biomaterials*, 28(25):3587–3593, 2007.
- [22] D. W. Hutmacher. Scaffolds in tissue engineering bone and cartilage. *Biomaterials*, 21(24):2529–2543, 2000.

- [23] L. E. Freed, G. Vunjak-Novakovic, R. J. Biron, D. B. Eagles, D. C. Lesnoy, S. K. Barlow, and R. Langer. Biodegradable polymer scaffolds for tissue engineering. *Nature Biotechnology*, 12(7):689–693, 1994.
- [24] D. L. Christiansen, E. K. Huang, and F. H. Silver. Assembly of type I collagen: fusion of fibril subunits and the influence of fibril diameter on mechanical properties. *Matrix Biology*, 19(5):409–420, 2000.
- [25] Y. Wang, T. Azaïs, M. Robin, A. Vallée, C. Catania, P. Legriel, G. Pehau-Arnaudet, F. Babonneau, M.-M. Giraud-Guille, and N. Nassif. The predominant role of collagen in the nucleation, growth, structure and orientation of bone apatite. *Nature Materials*, 11(8):724–733, 2012.
- [26] W. Friess. Collagen–biomaterial for drug delivery. *European Journal of Pharmaceutics and Biopharmaceutics*, 45(2):113–136, 1998.
- [27] K. J. L. Burg, S. Porter, and J. F. Kellam. Biomaterial developments for bone tissue engineering. *Biomaterials*, 21(23):2347–2359, 2000.
- [28] D. J. S. Hulmes. Collagen diversity, synthesis and assembly. In P. Fratzl, editor, *Collagen: Structure and Mechanics*, pages 15–47. Springer, New York, USA, 2008.
- [29] K. Kadler, D. Holmes, J. Trotter, and J. Chapman. Collagen fibril formation. *Biochemical Journal*, 316:1–11, 1996.
- [30] D. E. Birk and P. Bruckner. Collagen suprastructures. *Topics in Current Chemistry*, 247:185–205, 2005.
- [31] J. D. Prockop. Collagens: molecular biology, diseases, and potentials for therapy. *Annual Review of Biochemistry*, 64(1):403–434, 1995.

- [32] S. Strasser, A. Zink, M. Janko, W. M. Heckl, and S. Thalhammer. Structural investigations on native collagen type I fibrils using AFM. *Biochemical and Biophysical Research Communications*, 354(1):27–32, 2007.
- [33] G. N. Ramachandran and G. Kartha. Structure of collagen. *Nature*, 174(4423):269–270, 1954.
- [34] J. A. Petruska and A. J. Hodge. A subunit model for the tropocollagen macromolecule. *Proceedings of the National Academy of Sciences of the United States of America*, 51(5):871, 1964.
- [35] J. Gosline, M. Lillie, E. Carrington, P. Guerette, C. Ortlepp, and K. Savage. Elastic proteins: biological roles and mechanical properties. *Philosophical Transactions of the Royal Society B: Biological Sciences*, 357(1418):121–132, 2002.
- [36] T. Gutsmann, G. E. Fantner, J. H. Kindt, M. Venturoni, S. Danielsen, and P. K. Hansma. Force spectroscopy of collagen fibers to investigate their mechanical properties and structural organization. *Biophysical Journal*, 86(5):3186–3193, 2004.
- [37] F. H. Silver, J. W. Freeman, and G. P. Seehra. Collagen self-assembly and the development of tendon mechanical properties. *Journal of Biomechanics*, 36(10):1529–1553, 2003.
- [38] M. Gale, M. S. Pollanen, P. Markiewicz, and M. C. Goh. Sequential assembly of collagen revealed by atomic force microscopy. *Biophysical Journal*, 68(5):2124–2128, 1995.
- [39] J. E. Scott. Supramolecular organization of extracellular matrix glycosaminoglycans, in vitro and in the tissues. *The FASEB Journal*, 6(9):2639–2645, 1992.

- [40] J. E. Scott. Physiological function and chemical composition of pericellular proteoglycan (an evolutionary view). *Philosophical Transactions of the Royal Society of London B: Biological Sciences*, 271(912):235–242, 1975.
- [41] J. E. Scott. Structure and function in extracellular matrices depend on interactions between anionic glycosaminoglycans. *Pathologie Biologie*, 49(4):284–289, 2001.
- [42] M. Raspanti, M. Viola, A. Forlino, R. Tenni, C. Gruppi, and M. E. Tira. Glycosaminoglycans show a specific periodic interaction with type I collagen fibrils. *Journal of Structural Biology*, 164(1):134–139, 2008.
- [43] M. E. Maitland and A. L. Arsenault. A correlation between the distribution of biological apatite and amino acid sequence of type I collagen. *Calcified Tissue International*, 48(5):341–352, 1991.
- [44] A. L. Boskey. Noncollagenous matrix proteins and their role in mineralization. *Bone and Mineral*, 6(2):111–123, 1989.
- [45] H. P. Wiesmann, U. Meyer, U. Plate, and H. J. Höhling. Aspects of collagen mineralization in hard tissue formation. *International Review of Cytology*, 242:121–156, 2004.
- [46] W. J. Landis and F. H. Silver. Mineral deposition in the extracellular matrices of vertebrate tissues: identification of possible apatite nucleation sites on type I collagen. *Cells, Tissues, Organs*, 189(1-4):20–24, 2008.
- [47] F. Nudelman, K. Pieterse, A. George, P. H. H. Bomans, H. Friedrich, L. J. Brylka, P. A. J. Hilbers, G. de With, and N. A. J. M. Sommerdijk. The role of collagen in bone apatite formation in the presence of hydroxyapatite nucleation inhibitors. *Nature Materials*, 9(12):1004–1009, 2010.

- [48] S. Weiner and W. Traub. Organization of hydroxyapatite crystals within collagen fibrils. *FEBS Letters*, 206(2):262–266, 1986.
- [49] W. J. Landis, K. J. Hodgens, M. J. Song, J. Arena, S. Kiyonaga, M. Marko, C. Owen, and B. F. McEwen. Mineralization of collagen may occur on fibril surfaces: evidence from conventional and high-voltage electron microscopy and three-dimensional imaging. *Journal of Structural Biology*, 117(1):24–35, 1996.
- [50] W. Landis, M. Song, A. Leith, L. McEwen, and B. McEwen. Mineral and organic matrix interaction in normally calcifying tendon visualized in three dimensions by high-voltage electron microscopic tomography and graphic image reconstruction. *Journal of Structural Biology*, 110(1):39–54, 1993.
- [51] M. J. Olszta, X. Cheng, S. S. Jee, R. Kumar, Y.-Y. Kim, M. J. Kaufman, E. P. Douglas, and L. B. Gower. Bone structure and formation: a new perspective. *Materials Science and Engineering: R: Reports*, 58(3):77–116, 2007.
- [52] G. Binnig, C. F. Quate, and C. Gerber. Atomic force microscope. *Physical Review Letters*, 56(9):930–933, 1986.
- [53] B. Drake, C. B. Prater, A. Weisenhorn, S. A. C. Gould, T. R. Albrecht, C. F. Quate, D. Cannell, H. G. Hansma, and P. K. Hansma. Imaging crystals, polymers, and processes in water with the atomic force microscope. *Science*, 243(4898):1586–1589, 1989.
- [54] C. A. J. Putman, K. O. Van der Werf, B. G. De Groot, N. F. Van Hulst, and J. Greve. Tapping mode atomic force microscopy in liquid. *Applied Physics Letters*, 64(18):2454–2456, 1994.

- [55] M. F. Paige, J. K. Rainey, and M. C. Goh. Fibrous long spacing collagen ultrastructure elucidated by atomic force microscopy. *Biophysical Journal*, 74(6):3211–3216, 1998.
- [56] M. F. Paige, J. K. Rainey, and M. C. Goh. A study of fibrous long spacing collagen ultrastructure and assembly by atomic force microscopy. *Micron*, 32(3):341–353, 2001.
- [57] H. G. Hansma, K. J. Kim, D. E. Laney, R. A. Garcia, M. Argaman, M. J. Allen, and S. M. Parsons. Properties of biomolecules measured from atomic force microscope images: a review. *Journal of Structural Biology*, 119(2):99–108, 1997.
- [58] L. Ng, A. J. Grodzinsky, P. Patwari, J. Sandy, A. Plaas, and C. Ortiz. Individual cartilage aggrecan macromolecules and their constituent glycosaminoglycans visualized via atomic force microscopy. *Journal of Structural Biology*, 143(3):242–257, 2003.
- [59] T. E. Fisher, A. F. Oberhauser, M. Carrion-Vazquez, P. E. Marszalek, and J. M. Fernandez. The study of protein mechanics with the atomic force microscope. *Trends in Biochemical Sciences*, 24(10):379–384, 1999.
- [60] D. R. Baselt, J.-P. Revel, and J. D. Baldeschwieler. Subfibrillar structure of type I collagen observed by atomic force microscopy. *Biophysical Journal*, 65(6):2644–2655, 1993.
- [61] I. Revenko, F. Sommer, D. T. Minh, R. Garrone, and J.-M. Franc. Atomic force microscopy study of the collagen fibre structure. *Biology of the Cell*, 80(1):67–69, 1994.

- [62] R. Tejero, S. Bierbaum, T. Douglas, A. Reinstorf, H. Worch, and D. Scharnweber. Glucuronic acid and phosphoserine act as mineralization mediators of collagen I based biomimetic substrates. *Journal of Materials Science: Materials in Medicine*, 21(2):407–418, 2010.
- [63] A. C. Lin and M. C. Goh. Investigating the ultrastructure of fibrous long spacing collagen by parallel atomic force and transmission electron microscopy. *Proteins: Structure, Function, and Bioinformatics*, 49(3):378–384, 2002.
- [64] L. Bozec and M. Odlyha. Thermal denaturation studies of collagen by microthermal analysis and atomic force microscopy. *Biophysical Journal*, 101(1):228–236, 2011.
- [65] C. Bustamante, C. Rivetti, and D. J. Keller. Scanning force microscopy under aqueous solutions. *Current Opinion in Structural Biology*, 7(5):709–716, 1997.
- [66] A. Engel, C.-A. Schoenenberger, and D. J. Müller. High resolution imaging of native biological sample surfaces using scanning probe microscopy. *Current Opinion in Structural Biology*, 7(2):279–284, 1997.
- [67] D. J. Müller, F. A. Schabert, G. Büldt, and A. Engel. Imaging purple membranes in aqueous solutions at sub-nanometer resolution by atomic force microscopy. *Biophysical Journal*, 68(5):1681–1686, 1995.
- [68] C. Bustamante and D. Keller. Scanning force microscopy in biology. *Physics Today*, 48(12):32–38, 2008.
- [69] K. Rippe, N. Mücke, and J. Langowski. Superhelix dimensions of a 1868 base pair plasmid determined by scanning force microscopy in air and in aqueous solution. *Nucleic Acids Research*, 25(9):1736–1744, 1997.

- [70] J. H. Hoh and P. K. Hansma. Atomic force microscopy for high-resolution imaging in cell biology. *Trends in Cell Biology*, 2(7):208–213, 1992.
- [71] S. Karrasch, R. Hegerl, J. H. Hoh, W. Baumeister, and A. Engel. Atomic force microscopy produces faithful high-resolution images of protein surfaces in an aqueous environment. *Proceedings of the National Academy of Sciences*, 91(3):836–838, 1994.
- [72] S. Manne, H. J. Butt, S. A. C. Gould, and P. K. Hansma. Imaging metal atoms in air and water using the atomic force microscope. *Applied Physics Letters*, 56(18):1758–1759, 1990.
- [73] S. Karrasch, M. Dolder, F. Schabert, J. Ramsden, and A. Engel. Covalent binding of biological samples to solid supports for scanning probe microscopy in buffer solution. *Biophysical Journal*, 65(6):2437–2446, 1993.
- [74] C. A. Siedlecki and R. E. Marchant. Atomic force microscopy for characterization of the biomaterial interface. *Biomaterials*, 19(4):441–454, 1998.
- [75] J. B. Thompson, G. T. Palocz, J. H. Kindt, M. Michenfelder, B. L. Smith, G. Stucky, D. E. Morse, and P. K. Hansma. Direct observation of the transition from calcite to aragonite growth as induced by abalone shell proteins. *Biophysical Journal*, 79(6):3307–3312, 2000.
- [76] C. Sikes, A. Wheeler, A. Wierzbicki, R. Dillaman, and L. De Luca. Oyster shell protein and atomic force microscopy of oyster shell folia. *The Biological Bulletin*, 194(3):304–316, 1998.
- [77] C. Sikes, A. Wheeler, A. Wierzbicki, A. Mount, and R. Dillaman. Nucleation and growth of calcite on native versus pyrolyzed oyster shell folia. *The Biological Bulletin*, 198(1):50–66, 2000.

- [78] A. Wierzbicki, C. Sikes, J. Madura, and B. Drake. Atomic force microscopy and molecular modeling of protein and peptide binding to calcite. *Calcified Tissue International*, 54(2):133–141, 1994.
- [79] K. Subburaman, N. Pernodet, S. Y. Kwak, E. DiMasi, S. Ge, V. Zaitsev, X. Ba, N. L. Yang, and M. Rafailovich. Templated biomineralization on self-assembled protein fibers. *Proceedings of the National Academy of Sciences*, 103(40):14672–14677, 2006.
- [80] K. Henriksen, J. R. Young, P. R. Bown, and S. L. S. Stipp. Coccolith biomineralisation studied with atomic force microscopy. *Palaeontology*, 47(3):725–743, 2004.
- [81] M. Hildebrand, M. J. Doktycz, and D. P. Allison. Application of AFM in understanding biomineral formation in diatoms. *Pflügers Archiv-European Journal of Physiology*, 456(1):127–137, 2008.
- [82] J. L. Hutter and J. Bechhoefer. Calibration of atomic-force microscope tips. *Review of Scientific Instruments*, 64(7):1868–1873, 1993.
- [83] A. L. Arsenault. A comparative electron microscopic study of apatite crystals in collagen fibrils of rat bone, dentin and calcified turkey leg tendons. *Bone and Mineral*, 6(2):165–177, 1989.
- [84] A. Bigi, M. Gandolfi, N. Roveri, and G. Valdre. In vitro calcified tendon collagen: an atomic force and scanning electron microscopy investigation. *Biomaterials*, 18(9):657–665, 1997.
- [85] S. Lees, K. Prostak, V. Ingle, and K. Kjoller. The loci of mineral in turkey leg tendon as seen by atomic force microscope and electron microscopy. *Calcified Tissue International*, 55(3):180–189, 1994.

- [86] L. Siperko and W. Landis. Aspects of mineral structure in normally calcifying avian tendon. *Journal of Structural Biology*, 135(3):313–320, 2001.
- [87] D. Erts, L. Gathercole, and E. Atkins. Scanning probe microscopy of intrafibrillar crystallites in calcified collagen. *Journal of Materials Science: Materials in Medicine*, 5(4):200–206, 1994.
- [88] G. W. Marshall, I. C. Wu-Magidi, L. G. Watanabe, N. Inai, M. Balooch, J. H. Kinney, and S. J. Marshall. Effect of citric acid concentration on dentin demineralization, dehydration, and rehydration: atomic force microscopy study. *Polymer Reviews*, 42(4):500–507, 1998.
- [89] H.-P. Wiesmann, L. Chi, U. Stratmann, U. Plate, H. Fuchs, U. Joos, and H. J. Höhling. Sutural mineralization of rat calvaria characterized by atomic-force microscopy and transmission electron microscopy. *Cell and Tissue Research*, 294(1):93–97, 1998.
- [90] J. Ge, F.-Z. Cui, X. Wang, and Y. Wang. New evidence of surface mineralization of collagen fibrils in wild type zebrafish skeleton by AFM and TEM. *Materials Science and Engineering: C*, 27(1):46–50, 2007.
- [91] T. Hassenkam, G. E. Fantner, J. A. Cutroni, J. C. Weaver, D. E. Morse, and P. K. Hansma. High-resolution AFM imaging of intact and fractured trabecular bone. *Bone*, 35(1):4–10, 2004.
- [92] T. Hassenkam, H. L. Jørgensen, M. B. Pedersen, A. H. Kourakis, L. Simonsen, and J. B. Lauritzen. Atomic force microscopy on human trabecular bone from an old woman with osteoporotic fractures. *Micron*, 36(7):681–687, 2005.
- [93] G. E. Fantner, O. Rabinovych, G. Schitter, P. Thurner, J. H. Kindt, M. M. Finch, J. C. Weaver, L. S. Golde, D. E. Morse, E. A. Lipman, et al. Hierarchi-

- cal interconnections in the nano-composite material bone: fibrillar cross-links resist fracture on several length scales. *Composites Science and Technology*, 66(9):1205–1211, 2006.
- [94] L. Bozec, J. de Groot, M. Odlyha, B. Nicholls, and M. A. Horton. Mineralised tissues as nanomaterials: analysis by atomic force microscopy. In *IEEE Proceedings-Nanobiotechnology*, volume 152, pages 183–186. IET, 2005.
- [95] W. Tong, M. J. Glimcher, J. L. Katz, L. Kuhn, and S. J. Eppell. Size and shape of mineralites in young bovine bone measured by atomic force microscopy. *Calcified Tissue International*, 72(5):592–598, 2003.
- [96] S. J. Eppell, W. Tong, J. L. Katz, L. Kuhn, and M. J. Glimcher. Shape and size of isolated bone mineralites measured using atomic force microscopy. *Journal of Orthopaedic Research*, 19(6):1027–1034, 2001.
- [97] H. Chen, C. Robinson, R. Shore, S. Brookes, J. Zhang, D. Smith, B. Clarkson, and J. Kirkham. Nanoscale analysis of bone mineral crystals. *Technical Proceedings of the 2006 NSTI Nanotechnology Conference and Trade Show*, 2:95–98, 2006.
- [98] L. M. Siperko and W. J. Landis. Atomic scale imaging of hydroxyapatite and brushite in air by force microscopy. *Applied Physics Letters*, 61(21):2610–2612, 1992.
- [99] K. Onuma, A. Ito, T. Tateishi, and T. Kameyama. Growth kinetics of hydroxyapatite crystal revealed by atomic force microscopy. *Journal of Crystal Growth*, 154(1):118–125, 1995.

- [100] K. Onuma, A. Ito, T. Tateishi, and T. Kameyama. Surface observations of synthetic hydroxyapatite single crystal by atomic force microscopy. *Journal of Crystal Growth*, 148(1):201–206, 1995.
- [101] K. Flade, C. Lau, M. Mertig, and W. Pompe. Osteocalcin-controlled dissolution-precipitation of calcium phosphate under biomimetic conditions. *Chemistry of Materials*, 13(10):3596–3602, 2001.
- [102] P. Xu, J. Huang, P. Cebe, and D. L. Kaplan. Osteogenesis imperfecta collagen-like peptides: self-assembly and mineralization on surfaces. *Biomacromolecules*, 9(6):1551–1557, 2008.
- [103] K. Waidyasekera, T. Nikaido, D. Weerasinghe, A. Watanabe, S. Ichinose, F. Tay, and J. Tagami. Why does fluorosed dentine show a higher susceptibility for caries: an ultra-morphological explanation. *Journal of Medical and Dental Sciences*, 57(1):17–23, 2010.
- [104] C. Poggio, M. Lombardini, P. Vigorelli, and M. Ceci. Analysis of dentin/enamel remineralization by a CPP-ACP paste: AFM and SEM study. *Scanning*, 35(6):366–374, 2013.
- [105] Y. Cao, M. L. Mei, Q.-L. Li, E. C. M. Lo, and C. H. Chu. Agarose hydrogel biomimetic mineralization model for the regeneration of enamel prislime tissue. *ACS Applied Materials & Interfaces*, 6(1):410–420, 2013.
- [106] D. Naumann. Vibrational spectroscopy in microbiology and medical diagnostics. In P. Lasch and J. Kneipp, editors, *Biomedical vibrational spectroscopy*, pages 1–8. John Wiley & Sons, Inc., Hoboken, NJ, USA, 2008.

- [107] M. D. Morris and W. F. Finney. Recent developments in Raman and infrared spectroscopy and imaging of bone tissue. *Spectroscopy: An International Journal*, 18(2):155–159, 2004.
- [108] A. Carden and M. D. Morris. Application of vibrational spectroscopy to the study of mineralized tissues (review). *Journal of Biomedical Optics*, 5(3):259–268, 2000.
- [109] A. L. Boskey. Mineral analysis provides insights into the mechanism of biomineralization. *Calcified Tissue International*, 72(5):533–536, 2003.
- [110] J. S. Nyman, A. J. Makowski, C. A. Patil, T. P. Masui, E. C. O’Quinn, X. Bi, S. A. Guelcher, D. P. Nicollela, and A. Mahadevan-Jansen. Measuring differences in compositional properties of bone tissue by confocal Raman spectroscopy. *Calcified Tissue International*, 89(2):111–122, 2011.
- [111] A. Carden, R. M. Rajachar, M. D. Morris, and D. H. Kohn. Ultrastructural changes accompanying the mechanical deformation of bone tissue: a Raman imaging study. *Calcified Tissue International*, 72(2):166–175, 2003.
- [112] J. A. Timlin, A. Carden, M. D. Morris, R. M. Rajachar, and D. H. Kohn. Raman spectroscopic imaging markers for fatigue-related microdamage in bovine bone. *Analytical Chemistry*, 72(10):2229–2236, 2000.
- [113] J. Xu, D. F. R. Gilson, I. S. Butler, and I. Stangel. Effect of high external pressures on the vibrational spectra of biomedical materials: calcium hydroxyapatite and calcium fluoroapatite. *Journal of Biomedical Materials Research*, 30(2):239–244, 1996.
- [114] N. J. Crane, V. Popescu, M. D. Morris, P. Steenhuis, and M. A. Ignelzi. Raman spectroscopic evidence for octacalcium phosphate and other transient mineral

- species deposited during intramembranous mineralization. *Bone*, 39(3):434–442, 2006.
- [115] R. Cusco, F. Guitian, S. De Aza, and L. Artus. Differentiation between hydroxyapatite and β -tricalcium phosphate by means of μ -Raman spectroscopy. *Journal of the European Ceramic Society*, 18(9):1301–1305, 1998.
- [116] W. A. Bubb. NMR spectroscopy in the study of carbohydrates: characterizing the structural complexity. *Concepts in Magnetic Resonance Part A*, 19(1):1–19, 2003.
- [117] H. N. Cheng and T. G. Neiss. Solution NMR spectroscopy of food polysaccharides. *Polymer Reviews*, 52(2):81–114, 2012.
- [118] C. A. Bush, M. Martin-Pastor, and A. Imbery. Structure and conformation of complex carbohydrates of glycoproteins, glycolipids, and bacterial polysaccharides. *Annual Review of Biophysics and Biomolecular Structure*, 28(1):269–293, 1999.
- [119] L. Yang and L.-M. Zhang. Chemical structural and chain conformational characterization of some bioactive polysaccharides isolated from natural sources. *Carbohydrate Polymers*, 76(3):349–361, 2009.
- [120] M. Ito, Y. Matsumuro, S. Yamada, T. Kitamura, S. Itonori, and M. Sugita. Isolation and characterization of a novel uronic acid-containing acidic glycosphingolipid from the ascidian *halocynthia roretzi*. *Journal of Lipid Research*, 48(1):96–103, 2007.
- [121] E. Katzenellenbogen, N. A. Kocharova, A. S. Shashkov, S. Górska-Frączek, M. Bogulska, A. Gamian, and Y. A. Knirel. Structure of the O-polysaccharide

- of *Edwardsiella tarda* PCM 1150 containing an amide of d-glucuronic acid with l-alanine. *Carbohydrate Research*, 368:84–88, 2013.
- [122] C. Delattre, G. Pierre, C. Gardarin, M. Traikia, R. Elboutachfaiti, A. Isogai, and P. Michaud. Antioxidant activities of a polyglucuronic acid sodium salt obtained from TEMPO-mediated oxidation of xanthan. *Carbohydrate Polymers*, 116:34–41, 2015.
- [123] M. Sun, A. Stetco, and E. F. Merschrod S. Surface-templated formation of protein microfibril arrays. *Langmuir*, 24(10):5418–5421, 2008.
- [124] D. F. Holmes, M. J. Capaldi, and J. A. Chapman. Reconstitution of collagen fibrils in vitro; the assembly process depends on the initiating procedure. *International Journal of Biological Macromolecules*, 8(3):161–166, 1986.
- [125] A. George and A. Veis. FTIRS in water demonstrates that collagen monomers undergo a conformational transition prior to thermal self-assembly in vitro. *Biochemistry*, 30(9):2372–2377, 1991.

Co-authorship Statement

This dissertation is prepared in manuscript format and presents the research as a collection of published papers or papers prepared for publication, written by the candidate under the supervision of Prof. Erika F. Merschrod S. Ionela Alina Stetco wrote the first draft and revisions of each chapter, including the published paper presented in Chapter 4, with feedback from Prof. Erika F. Merschrod S. and from journal reviewers. As the principal author of all the manuscripts in her thesis, Ionela Alina Stetco made a major intellectual and practical contribution to all work that is reported herein, including design of the research proposal, practical aspects of the research, data analysis, and manuscript preparation.

For the work presented in Chapter 2, entitled “Incipient stages of collagen mineralization monitored by atomic force microscopy”, and Chapter 3, entitled “Structural effects of uronic acids on collagen-based mineralization matrices”, which are papers prepared for publication, Ionela Alina Stetco conducted, under the guidance of Prof. Erika F. Merschrod S., all the experiments described, including material preparation and testing, operation of atomic force microscope and Raman spectrometer, data collection and analysis.

Chapter 4, entitled “Supramolecular structure and anomer-selective formation of polyglucuronic acid”, published in *Polymer Int* peer-reviewed journal, describes the synthesis of α polyglucuronic acid and the confirmation of its structure. Ionela Alina

Stetco carried out, under the guidance of Prof. Erika F. Merschrod S., the preparation of the solutions and their analysis using the atomic force microscope operated in air and in fluid, as well as the NMR spectrometer for the acquisition of ^{13}C NMR spectra in solution. Dr. Céline Schneider (Department of Chemistry and CREAT, Memorial University) acquired the solid-state NMR spectrum of glucuronic acid and assisted with the NMR experiments and analysis.

Chapter 2

Incipient stages of collagen mineralization monitored by atomic force microscopy

2.1 Introduction

Biom mineralization is defined as the process that leads to the formation of mineral-rich tissues in living organisms and relies on the capability of proteins to initiate and control crystal growth [1, 2]. A fundamental aspect of biom mineralization is that no spontaneous precipitation is observed for the free ions which are precursors of a particular inorganic phase and which are present in the tissue-specific extracellular matrix, but rather the mineralization process occurs through a mechanism which controls the amount of inorganic solid formed, the size, and the orientation of the crystals [1].

Bone is a mineralized tissue comprising mainly type I collagen and a calcium phosphate mineral, hydroxyapatite [3], which is the most stable form of calcium phosphate

under physiological conditions, being the least soluble of all calcium phosphates [4]. Previous studies suggest that hydroxyapatite-collagen composites might be suitable as bone substitutes [5]. Hence, the mechanism by which the collagen mineralization occurs was extensively studied in order to gain insight on how collagens induce mineralization and template the crystal growth [6–12].

The atomic force microscope (AFM) has proven to be a suitable tool for the analysis of fibrillar collagen structures in calcified tissue [13–17] and has provided the three-dimensional visual evidence of the size and shape of native protein-free mineralites isolated from mature bovine bone [18]. AFM was employed for *in situ* investigation at the atomic scale of hydroxyapatite crystal growth under physiological conditions [19] and to observe the early stages of biomineralization *in vitro* [2].

The mixing of phosphate and calcium ions' sources at physiological pH leads to the formation of various calcium phosphate phases, with the exception of hydroxyapatite, which is formed exclusively in the presence of collagen. Additionally, electron microscopy and FTIR studies indicate that the rate of hydroxyapatite formation at 38 °C via an acid-base reaction between calcium phosphate precursors in the presence of collagen matrix increases with an increase in the proportion of collagen present. This suggests a collagen capability to provide nucleation sites for hydroxyapatite crystallization [5] by binding calcium ions to the carboxylate groups of collagen [20–23]. Thus, it is believed that it is collagen that stimulates the formation of hydroxyapatite and justifies the need for controlled mineralization *in vitro*.

Since it is known that collagen monomers, in the form of tropocollagen protofibrils, are not capable of inducing crystal nucleation [1], we conducted our collagen mineralization study on collagen fibrils assembled by one of two distinct experimental approaches: mica-induced fibril growth and alignment, and “cold start” incubation.

The aim of this chapter consists of monitoring of the incipient stages of collagen/-

calcium phosphate composite formation *in situ*, as well as the influence of the calcium and phosphate ion concentration upon mineralization and calcium phosphate phase formation. An AFM was used to visualise the nucleation sites of calcium phosphate crystals during collagen mineralization *in vitro* that were achieved through controlled deposition of the mineral phases.

2.2 Materials and methods

Two methods were employed for growing collagen fibrils for mineralization: mica-induced fibril growth and alignment, and the cold start method. The first one involves bringing the pH of the collagen to 7.5 with phosphate buffer, while for the second one the pH is raised to a value of 7.5 with a basic NaOH solution.

2.2.1 Materials

Acidified type I bovine dermal collagen (3.0 mg/mL in 0.012 M HCl, pH \sim 2.0, Inamed Biomaterials) was used as received. ACS-grade salts (Sigma) were used for the NaOH solution, 0.01 M CaCl₂ solution, and sodium and potassium phosphate buffers (0.05 M PO₄³⁻, 0.2 M Na⁺/K⁺ and 0.1 M Cl⁻, pH 7.45). Solutions were prepared with ultrapure water (Barnstead, 18.2 M Ω ·cm).

Sodium phosphate buffer solution pH = 7.45, [Na⁺] = 200 mM, [P] = 50 mM was prepared from NaH₂PO₄ · 2H₂O, Na₂HPO₄, and NaCl. Potassium phosphate buffer solution pH = 7.43, [K⁺] = 200 mM, [P] = 50 mM was prepared from KH₂PO₄, K₂HPO₄ · 3H₂O, KCl.

2.2.2 Methods for growing collagen fibrils

Cold start method for growing collagen fibrils enriched with calcium

Collagen solution in NaOH and CaCl₂ (230 $\mu\text{g}/\text{mL}$, pH 7–8, 0.07 M Ca²⁺, 0.2 M OH⁻) were placed in a water bath at 34–37°C [24, 25] for 24 hours.

Sample preparation on mica. 100 μL of the resultant suspension was placed on freshly cleaved mica and allowed to adsorb for 15 minutes, after which the excess was removed and the sample was rinsed twice, before drying, with 50 μL ultrapure water to remove excess ions and to avoid salt deposition during drying. Immediately the sample was imaged in ultrapure water for control, (Figure 2.1 (A)), after which 50 μL potassium phosphate buffer solution were added to the imaging spot (Figure 2.1 (B–D)), without removing the existing imaging water and without raising the AFM head.

Growing collagen fibrils by incubation on mica

Collagen solutions in sodium phosphate buffer (5 $\mu\text{g}/\text{mL}$ collagen for *in situ* mineralization, Figure 2.2, and 10 $\mu\text{g}/\text{mL}$ collagen for crystal growth by exposure to calcium ions, Figure 2.3) were deposited on a freshly cleaved muscovite mica substrate ($\sim 1 \text{ cm}^2$). After 20 minutes, the substrate was exposed to potassium phosphate buffer and incubated, also under potassium phosphate buffer, for 16 hours [26, 27], at room temperature, followed by the removal of the buffer solution. The sample prepared for *in situ* mineralization (collagen fibrils 5 $\mu\text{g}/\text{mL}$), Figure 2.2, was immediately transferred to the AFM and imaged in the presence of potassium phosphate buffer solution, after which 20 μL 0.01M CaCl₂ solution were added every 60 minutes to the imaging spot, immersed in potassium phosphate buffer solution, without raising the AFM head, for a duration of eight hours. In the case of crystal growth by exposure

to calcium ions (Figure 2.3) after the removal of the potassium phosphate buffer solution, the collagen fibrils grown on mica (10 $\mu\text{g}/\text{mL}$) were immediately exposed once (Figure 2.3 (A)) to 100 μL 0.01M CaCl_2 , or twice (Figure 2.3 (B)), to 100 μL 0.01M CaCl_2 each time, by pouring the solution over the sample, held in a vertical position. Samples were left to dry in air before imaging.

2.2.3 AFM

AFM imaging (AC mode) at room temperature was carried out on an Asylum Research MFP-3D system using silicon cantilevers with aluminum-coated backsides (Mikromasch, 150–300 kHz resonant frequencies). Images were acquired in dry and fluid environment and are shown with no post-processing beyond a zero order flattening for Figures 2.1 and 2.3, and first order flattening for Figure 2.2, using Asylum Research procedures within IGOR 6.1.

2.2.4 Raman spectroscopy

Raman scattering spectra were obtained using a confocal configuration with 532 nm excitation (LabRAM, Jobin Yvon Horiba). All samples were dried in air at room temperature, in a fume hood, for at least 24 hours. Referring to Figure 2.4, the sample for spectrum (A) was a freshly cleaved mica crystal. For (B), collagen monomers on mica, 100 μL collagen at pH 2 were left to dry on mica by exposure to air at room temperature. Spectrum (C), collagen fibrils on mica, was from a sample as prepared for AFM. (D), calcium phosphate phases on mica, were prepared from 100 μL 0.01 M CaCl_2 mixed with 100 μL potassium phosphate buffer (KPB) at pH 7.43. Spectrum (E) was for a sample of collagen fibrils on mica exposed once to 100 μL 0.01M CaCl_2 solution, while spectrum (F) was from collagen fibrils on mica saturated with 100 μL 0.01M CaCl_2 and 100 μL KPB and dried at room temperature.

2.3 Results and discussion

2.3.1 Collagen mineralization revealed by AFM

It is generally believed that the mineral nucleation occurs in the “hole zones” of the collagen fibrils [28] and that the collagen is responsible for the formation of hydroxyapatite *in vitro* [29]. Our experiments represent an attempt in understanding the early stages of mineral formation, therefore we applied *in situ* procedures. For this purpose, we showed that AFM scanning in AC mode offered a good visualization of the collagen fibrils and the appearance of calcium phosphate phases crystals as they formed *in situ*.

Our first approach consisted in growing collagen fibrils enriched with calcium by employing the cold start method, when the pH is adjusted with NaOH. The fibrils grown were immobilized on mica and imaged in fluid in the same location (Figure 2.1). The first AFM image acquired, Figure 2.1 (A), represents the sample imaged in ultrapure water and was used as a control image. Subsequently, an aliquot (50 μL) of potassium phosphate buffer solution ([P] 50 mM) was added at the scanning location and the changes of the same surface over time, as they happened, were examined by AFM and are presented in Figure 2.1 (B–D). In time, we observed the disappearance of the least mature collagen fibrils, which might have detached from the surface during scanning.

Although biomacromolecules that are weakly adsorbed to a solid support can easily be displaced during scanning [30], these fibrils may also have been either “dissolved” in the presence of both phosphate buffer and calcium ion solutions or they were almost completely covered by minerals, due to uncontrolled precipitation. The last hypothesis is sustained by a drop observed in the height of the collagen fibrils over time.

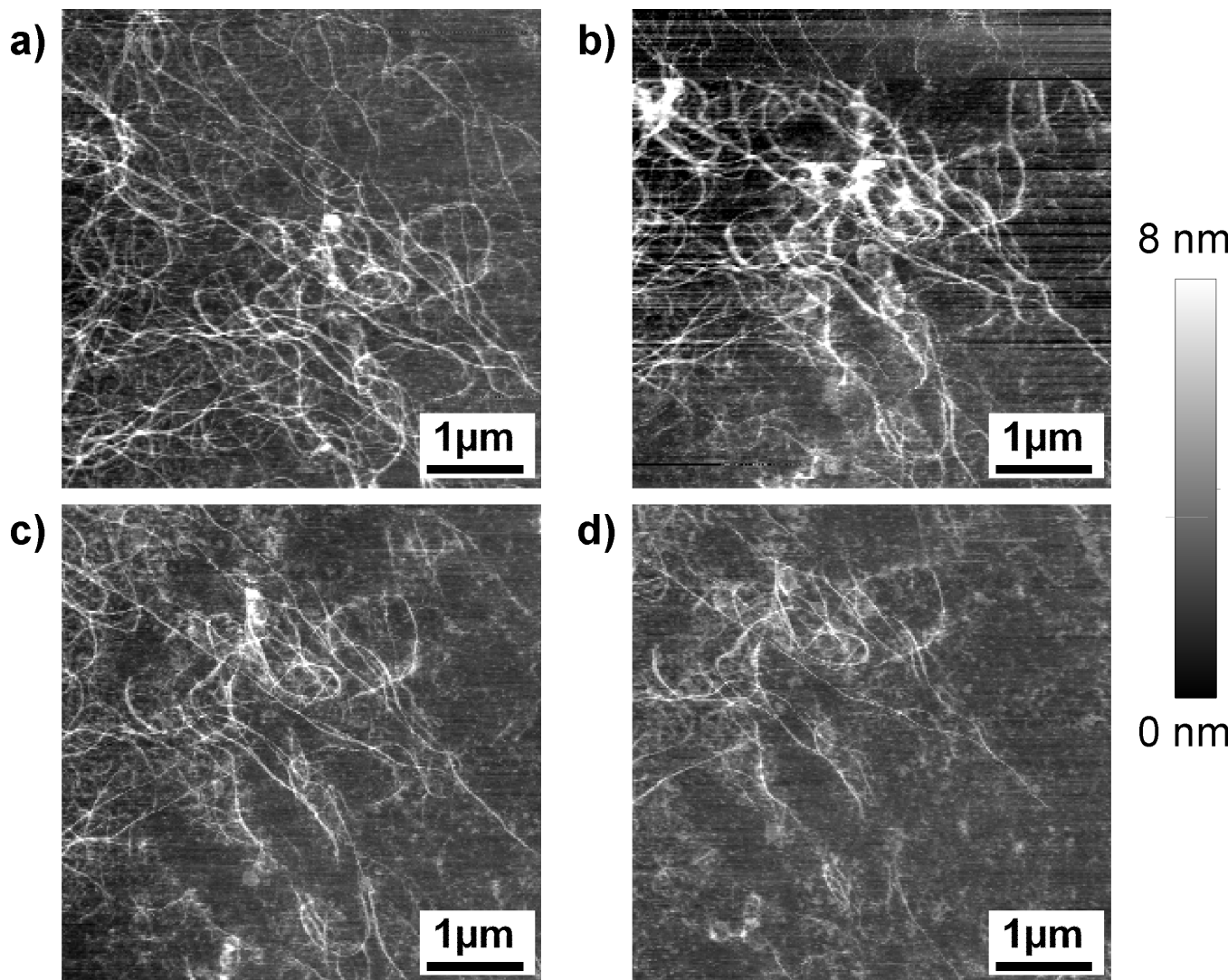


Figure 2.1: Phosphate ion addition to cold start collagen protofibrils enriched with calcium leads to partial disappearance of collagen fibrils. A) Collagen protofibrils enriched with calcium, imaged in water (control image) B) 20 minutes after the addition of 50 μL KPb - dramatic change in fibrils thickness is observed due to mineral precipitation on top of the fibrils C) after 40 minutes since the addition of KPb (the next scan) - deposition of calcium phosphate occurs more even on the imaged surface, not only on collagen fibrils where the calcium concentration was the highest, leading to thinner fibrils D) after 80 minutes since the addition of KPb - the fibrils are becoming less prominent and fewer in number Note: the duration of an AFM image is approximately 20 minutes; all images $5 \mu\text{m} \times 5 \mu\text{m}$.

***In situ* mineralization of fibrils grown on a mica substrate**

An eight-hour experiment was designed for collagen fibrils grown and aligned on mica and imaged in potassium phosphate buffer solution. Every hour, 20 μL of 1 mM CaCl_2 were added. The area was inspected by AFM imaging throughout the length of the experiment (Figure 2.2). At the end of the experiment the collagen fibrils were covered by minerals (Figure 2.2 (D)). It is observable that the height of the collagen fibrils after calcium solution is added is decreasing, thus indicating that the minerals formed are deposited in a small part on the fibrils, but mostly in between the fibrils.

While this experiment aims to control the mineralization concentration of the calcium ion in a more strict way than the mineralization experiment with cold start collagen fibrils enriched with calcium, in which the concentration of calcium in suspension is about seventy times higher, it is still possible to observe that some fibrils are disappearing over time largely due to mineral coverage, but at the same time some depositions are growing in size throughout the duration of the experiment. This indicates that the concentration of the calcium and phosphate ions in the mineralization process *in vitro* has to be controlled even more rigorously.

Since the concentration of calcium ion affects the amount of precipitate formed, incipient stages of calcium phosphate phase formation were obtained just by scarce exposure of the samples containing collagen fibrils incubated on mica to a solution of 10 mM CaCl_2 . When using this slight exposure approach to control the amount of minerals formed (Figure 2.3), the resulting calcium phosphate crystals are mostly in association with the surface of collagen fibrils, presumably within collagen hole and overlap zones. After the mineralization has been initiated by exposure to the calcium solution once (Figure 2.3 (A)), by applying a second exposure (Figure 2.3 (B)) the mineralization continued. The AFM images revealed that, as mineralization advanced, the size of the crystallites increased (Figure 2.3 (B)). Despite the intensification in

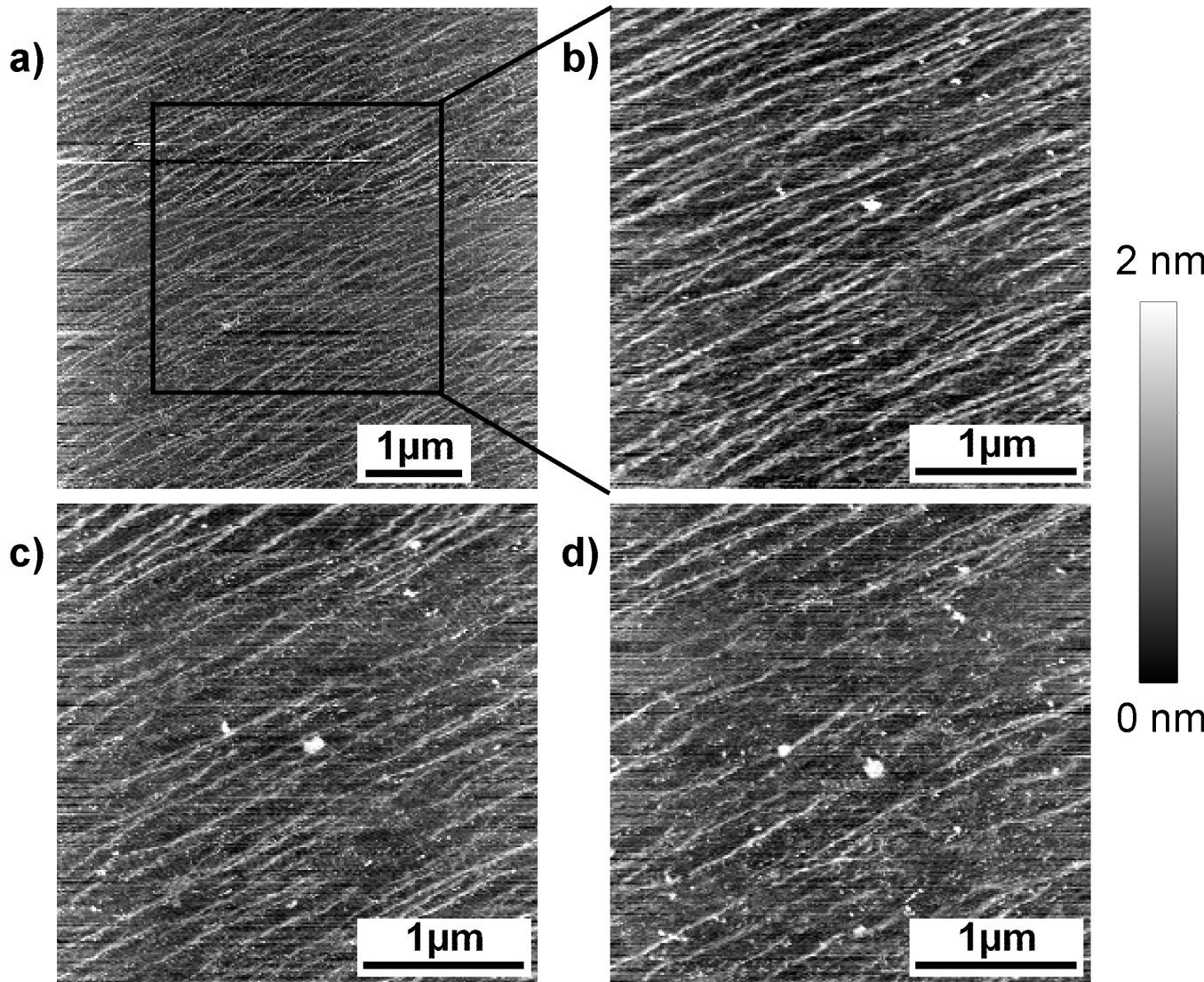


Figure 2.2: The effect of calcium ion concentration upon the *in situ* mineralization process with imaging in phosphate buffer pH 7.5. 20 μL 1 mM CaCl₂ solution are added every 60 minutes at the imaging spot. A) No calcium is added. B) After 5 hours the amount of added CaCl₂ is 100 μL; image shows the mineralized fibrils. C) The next scanned image after addition of CaCl₂ shows the growth in size of the crystallite objects at the expense of decrease in height of the collagen fibrils. D) After 6 hours there is more mineral coverage. Image sizes are (A) 5 μm × 5 μm and (B)-(D) 3 μm × 3 μm.

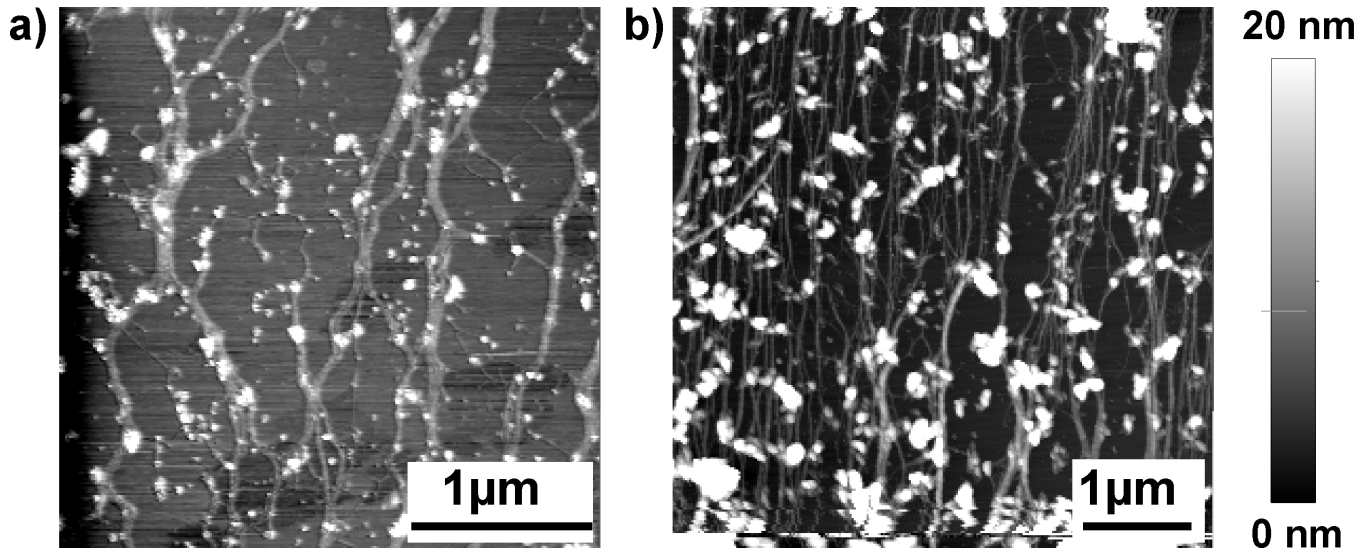


Figure 2.3: Mineralization of the collagen scaffold created by incubation on mica by slight exposure to calcium ion solution. AC mode capture of the incipient stages of mineralization stimulated by collagen fibrils (on top of fibrils) exposed A) once ($3 \mu\text{m} \times 3 \mu\text{m}$) or B) twice ($5 \mu\text{m} \times 5 \mu\text{m}$) to CaCl_2 .

mineralization, the crystallites seem to be nucleated on the fibril surface, and once nucleated, they grow outwards or may serve as nuclei for the formation of new crystals, without affecting the parallel alignment of the collagen fibrils. These observations confirm that, at the concentrations of calcium and phosphate ions used, collagen stimulates and provides the site of mineral nucleation.

2.3.2 Calcium phosphate mineral phases characterized by Raman spectroscopy

The calcium phosphate mineral phases obtained as a result of mineralization can be identified by Raman spectroscopy. The distinction between various calcium phosphate mineral phases is done mainly by analyzing the peaks for the ν_1 symmetric stretch of the phosphate group, which has the highest intensity [31], and the ν_3 asymmetric stretch of the phosphate. The Raman bands corresponding to ν_2 and ν_4 are weaker

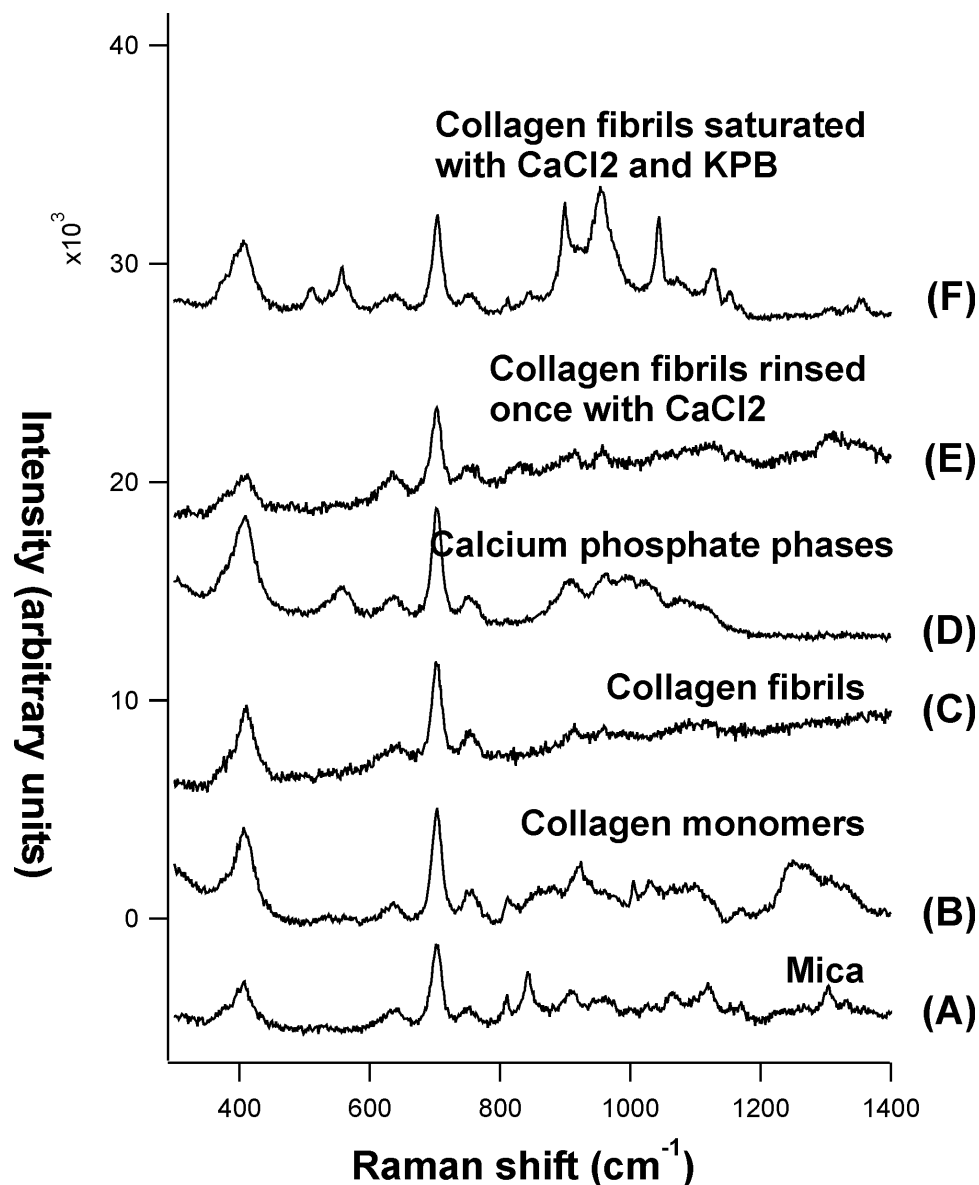


Figure 2.4: Raman spectra: A) mica (intensity multiplied by 2) B) collagen monomers on mica (original intensity; x axis offset of 12.5 cm^{-1}) C) collagen fibrils on mica (intensity multiplied by 2) D) mica and calcium phosphate phases (mixed KPB and CaCl_2) (original intensity; x axis offset of 12.5 cm^{-1}) E) collagen fibrils incubated on mica in KPB exposed once to CaCl_2 (intensity multiplied by 2); F) collagen fibrils incubated on mica in KPB saturated with CaCl_2 and KPB (intensity multiplied by 2). Note: The offset along the x axis was adjusted for some spectra so that the major mica Raman band at 701 cm^{-1} is aligned in all spectra in this plot. The intensity of selected spectra in this plot was doubled with the purpose of enhancing the visualisation of the spectral features of interest and to facilitate their interpretation.

in intensity, making their identification more challenging. Due to the fact that the amount of precipitate in our samples is reduced in quantity, the interpretation of the Raman spectra is substantially based on the Raman shift for the Raman high intensity symmetric stretching phosphate mode ν_1 . The Raman band assignments characteristic to calcium phosphate phases observed in our spectra are listed in Table 2.1.

Table 2.1: Raman band assignment of calcium phosphate phases

Raman Shift (cm^{-1})	Assignment of vibrational mode	Calcium phosphate phase	Reference
413	$\text{HPO}_4^{2-}; \nu_2 (\text{PO}_4^{3-})$	Octacalcium phosphate	[32, 33]
556	$\nu_4 (\text{HPO}_4^{2-})$	Octacalcium phosphate	[32, 34]
875–878	$\nu_1 (\text{HPO}_4^{2-})$	Brushite	[32, 35, 36]
900	$\nu_1 (\text{H}_2\text{PO}_4^-)$	Monetite	[35]
955–957	$\nu_1 (\text{PO}_4^{3-})$	Octacalcium phosphate	[32, 34]
957–960	$\nu_1 (\text{PO}_4^{3-})$	Hydroxyapatite	[32, 34, 36]
980–988	P–O stretch, HPO_4^{2-}	Brushite	[32, 34–36]
988	H_2PO_4^-	Monetite	[35]
1010–1013	HPO_4^{2-}	Octacalcium phosphate	[32, 34]
1044	$\nu_3 (\text{PO}_4^{3-})$	Phosphate	[31]
1071	$\nu_1 (\text{CO}_3^{2-})$	Carbonate	[31]

The substrate used for our samples is muscovite mica, therefore, its spectrum was recorded for reference and is presented in Figure 2.4(A). The characteristic peaks of mica in the range $300\text{--}1200 \text{ cm}^{-1}$, which are of interest for our samples given that this is the range where the phosphate modes occur, are the following: 408 cm^{-1} , 640 cm^{-1} , 701 cm^{-1} , and 752 cm^{-1} and they are all within $\pm 2 \text{ cm}^{-1}$ agreement with the

values reported in literature for muscovite mica [37, 38]. All the presented spectra in Figure 2.4 are aligned to the mica major Raman band at 701 cm^{-1} , corresponding to the symmetric stretching of the bridging oxygen, Si–O–Si [39], the other peaks representing weak bands.

Spectra presented in Figure 2.4(B) and (C) represent the collagen in monomeric and fibrillar form, respectively. The collagen monomer spectrum features the most important mica Raman bands and one single distinctive wide band between $1236\text{--}1274\text{ cm}^{-1}$, corresponding to the collagen matrix, the amide III band [31, 32]. However, the Raman bands at 560 cm^{-1} (amide III band) and 1095 cm^{-1} (C–N stretch) associated with fibrillar collagen [40] are not visible in the collagen fibrils spectrum, Figure 2.4(C). This may be attributable to the fact that the collagen fibrils analyzed are in a very thin (order of nanometers) film, thus the peaks corresponding to the collagen matrix are very weak and are not distinctive in Figure 2.4(C).

The spectrum in Figure 2.4(D) shows a mixture of phases that are formed upon mixing of phosphate buffer with calcium ion solution on mica, in the absence of collagen. The spectrum features peaks that are small in intensity at 555 cm^{-1} and 877 cm^{-1} , and broad peaks in the regions $899\text{--}917\text{ cm}^{-1}$, $956\text{--}964\text{ cm}^{-1}$, 986 cm^{-1} , $992\text{--}1014\text{ cm}^{-1}$, $1015\text{--}1025\text{ cm}^{-1}$, and 1110 cm^{-1} . The peaks at 877 cm^{-1} and 986 cm^{-1} are assigned to brushite and are within $\pm 2\text{ cm}^{-1}$ agreement with the values published in literature [35, 36]. The Raman shifts at 900 cm^{-1} and 988 cm^{-1} , according to what has been reported in literature [35], correspond to monetite. However, since monetite is not likely to form in our system, we probably obtained here a mixture of brushite and octacalcium phosphate (OCP), and some precipitated salt peak (broad peak 900 cm^{-1}) from the buffer, which counts for the H_2PO_4^- ion peak, present also in monetite, and potentially other uncontrolled precipitation products. The presence of the phosphate stretch ν_1 between $950\text{--}963\text{ cm}^{-1}$ confirms the presence of the phosphate

groups [36].

In the presence of collagen, by slightly exposing the collagen fibrils incubated in phosphate buffer to CaCl_2 solution (spectrum E), no significant fingerprints as proof for mineralization were found in the Raman spectrum as compared to spectrum C of collagen fibrils only, without minerals. While this type of sample, collagen fibrils slightly exposed to calcium ions, is suitable for AFM imaging and characterization of the crystals formed on the surface, it proved not to have the amount of crystals needed to give the Raman markers for the identification of the calcium phosphate mineral phases. Therefore, for obtaining a suitable Raman response, we chose to create a sample by saturating the collagen fibrils immobilized on mica with calcium chloride and phosphate buffer solutions. The sample was dried in air prior to being analyzed, spectrum Figure 2.4 (F).

It is observable that the peaks are narrower in spectrum 2.4(F) than in spectrum 2.4(D), suggesting increased crystallinity of the phases formed in the presence of collagen as opposed to when it is absent. The vibrational Raman bands seen are the following: 512 cm^{-1} weak, 540 cm^{-1} weak, 558 cm^{-1} stronger, 900 cm^{-1} strong, 955 cm^{-1} strong, $1010\text{--}1013\text{ cm}^{-1}$ very weak, 1044 cm^{-1} strong, 1066 cm^{-1} weak. Based on the Raman fingerprints corresponding to the phosphate group, spectrum 2.4(F) indicates that octacalcium phosphate formed in our system, its characteristic bands being at 558 cm^{-1} and, the symmetric stretching mode of phosphate group, at 955 cm^{-1} , within $\pm 2\text{ cm}^{-1}$ agreement with literature reported values for OCP [32,34].

The peak corresponding to ν_2 , which should appear at 413 cm^{-1} for OCP [32,33], is not visible in our sample due to overlapping with the broad mica peak at 408 cm^{-1} . However, the most characteristic band for OCP, according to [32,34], is the very small band at $1010\text{--}1013\text{ cm}^{-1}$, which was identified in our spectrum.

The excess phosphate buffer solution added for the purpose of mineralization also

led to simple precipitation of the salts, unregulated by collagen. The P–OH stretch that we see at 900 cm^{-1} could be due to the presence of the HPO_4^{-2} ion, which is the principal component of our phosphate buffer solution as a potassium salt. The peak at 1044 cm^{-1} corresponds to the ν_3 phosphate modes [31], and the weak band at 1066 cm^{-1} is a sign that carbonate may be present [31] in a small extent in the crystalline phases, originating from atmospheric CO_2 .

Despite the observed salt precipitation of the excess ions present in solution, our study indicates that, in the presence of collagen, the mineralization occurred with the formation of a preferred calcium phosphate phase, i.e. octacalcium phosphate, which is a precursor of synthetic hydroxyapatite [36, 41] and of biological hydroxyapatite *in vitro* [32]. In the absence of collagen, the simple mixing of the same solutions employed to study the collagen mineralization led to a mixture of phases that are difficult to assign.

2.4 Conclusions

We performed *in situ* AFM studies on reconstituted collagen fibrils to visualize the incipient stages of collagen/calcium phosphate composite formation and to study the calcium and phosphate ions' concentrations as factors involved in the initiation and progression of mineralization. Two different methodologies were applied for collagen fibrillogenesis: mica-induced fibril growth and alignment, and “cold start” incubation in the presence of calcium ions. The growth of calcium phosphate minerals in the collagen matrix, as it happened, was achieved by imaging the collagen fibrils in phosphate buffer, and, in the case of mica-induced fibrils, local addition of a calcium ion solution. Moreover, the effect of the calcium ion concentration on mineral deposition was examined by the exposure of the collagen sample to the calcium ion solution once

or twice, in order to restrict the contact between the mica-aligned collagen fibrils, the reminiscent phosphate buffer in the collagen matrix, and the calcium ion. The AFM images show that different calcium ion concentrations led to distinct degrees of mineralization, and that, increased calcium and phosphate ion levels in the mineralization system led to accelerated mineralization, as well as a greater extent of mineralization. Our experimental approaches have enabled the visualisation of mineral depositions on top of the fibrils, suggesting that the collagen matrix is responsible for inducing crystal nucleation. Raman spectroscopy allowed the identification of the various calcium phosphate phases formed and showed that, in the presence of collagen, octacalcium phosphate was present.

Bibliography

- [1] M. J. Glimcher, A. J. Hodge, and F. O. Schmitt. Macromolecular aggregation states in relation to mineralization: the collagen-hydroxyapatite system as studied in vitro. *Proceedings of the National Academy of Sciences of the United States of America*, 43(10):860–867, 1957.
- [2] K. Subburaman, N. Pernodet, S. Y. Kwak, E. DiMasi, S. Ge, V. Zaitsev, X. Ba, N. L. Yang, and M. Rafailovich. Templated biomineralization on self-assembled protein fibers. *Proceedings of the National Academy of Sciences*, 103(40):14672–14677, 2006.
- [3] L. Bozec, J. de Groot, M. Odlyha, B. Nicholls, and M. A. Horton. Mineralised tissues as nanomaterials: analysis by atomic force microscopy. In *IEEE Proceedings-Nanobiotechnology*, volume 152, pages 183–186. IET, 2005.

- [4] A. George and A. Veis. Phosphorylated proteins and control over apatite nucleation, crystal growth, and inhibition. *Chemical Reviews*, 108(11):4670–4693, 2008.
- [5] K. S. Tenhuisen, R. I. Martin, M. Klimkiewicz, and P. W. Brown. Formation and properties of a synthetic bone composite: hydroxyapatite–collagen. *Journal of Biomedical Materials Research*, 29(7):803–810, 1995.
- [6] M. J. Glimcher. Mechanism of calcification: role of collagen fibrils and collagen-phosphoprotein complexes in vitro and in vivo. *The Anatomical Record*, 224(2):139–153, 1989.
- [7] W. J. Landis, K. J. Hodgens, M. J. Song, J. Arena, S. Kiyonaga, M. Marko, C. Owen, and B. F. McEwen. Mineralization of collagen may occur on fibril surfaces: evidence from conventional and high-voltage electron microscopy and three-dimensional imaging. *Journal of Structural Biology*, 117(1):24–35, 1996.
- [8] H. Cölfen. Biomineralization: a crystal-clear view. *Nature Materials*, 9(12):960–961, 2010.
- [9] H. P. Wiesmann, U. Meyer, U. Plate, and H. J. Höhling. Aspects of collagen mineralization in hard tissue formation. *International Review of Cytology*, 242:121–156, 2004.
- [10] H. C. Anderson. Mechanism of mineral formation in bone. *Laboratory Investigation; a Journal of Technical Methods and Pathology*, 60(3):320–330, 1989.
- [11] F.-Z. Cui, Y. Li, and J. Ge. Self-assembly of mineralized collagen composites. *Materials Science and Engineering: R: Reports*, 57(1):1–27, 2007.

- [12] C. Du, F. Z. Cui, W. Zhang, Q. L. Feng, X. D. Zhu, and K. De Groot. Formation of calcium phosphate/collagen composites through mineralization of collagen matrix. *Journal of Biomedical Materials Research*, 50(4):518–527, 2000.
- [13] S. Habelitz, M. Balooch, S. J. Marshall, G. Balooch, and G. W. Marshall. In situ atomic force microscopy of partially demineralized human dentin collagen fibrils. *Journal of Structural Biology*, 138(3):227–236, 2002.
- [14] T. Hassenkam, G. E. Fantner, J. A. Cutroni, J. C. Weaver, D. E. Morse, and P. K. Hansma. High-resolution AFM imaging of intact and fractured trabecular bone. *Bone*, 35(1):4–10, 2004.
- [15] S. Lees, K. S. Probst, V. K. Ingle, and K. Kjoller. The loci of mineral in turkey leg tendon as seen by atomic force microscope and electron microscopy. *Calcified Tissue International*, 55(3):180–189, 1994.
- [16] J. Ge, F.-Z. Cui, X. Wang, and Y. Wang. New evidence of surface mineralization of collagen fibrils in wild type zebrafish skeleton by AFM and TEM. *Materials Science and Engineering: C*, 27(1):46–50, 2007.
- [17] A. Bigi, M. Gandolfi, N. Roveri, and G. Valdre. In vitro calcified tendon collagen: an atomic force and scanning electron microscopy investigation. *Biomaterials*, 18(9):657–665, 1997.
- [18] W. Tong, M. J. Glimcher, J. L. Katz, L. Kuhn, and S. J. Eppell. Size and shape of mineralites in young bovine bone measured by atomic force microscopy. *Calcified Tissue International*, 72(5):592–598, 2003.
- [19] K. Onuma, A. Ito, T. Tateishi, and T. Kameyama. Growth kinetics of hydroxypapatite crystal revealed by atomic force microscopy. *Journal of Crystal Growth*, 154(1):118–125, 1995.

- [20] S.-H. Rhee, J. D. Lee, and J. Tanaka. Nucleation of hydroxyapatite crystal through chemical interaction with collagen. *Journal of the American Ceramic Society*, 83(11):2890–2892, 2000.
- [21] S.-H. Rhee and J. Tanaka. Effect of citric acid on the nucleation of hydroxyapatite in a simulated body fluid. *Biomaterials*, 20(22):2155–2160, 1999.
- [22] S. Mann, B. R. Heywood, S. Rajam, and J. D. Birchall. Controlled crystallization of CaCO_3 under stearic acid monolayers. *Nature*, 334(6184):692–695, 1988.
- [23] S. Weiner, W. Traub, and S. B. Parker. Macromolecules in mollusc shells and their functions in biomineralization [and Discussion]. *Philosophical Transactions of the Royal Society B: Biological Sciences*, 304(1121):425–434, 1984.
- [24] D. F. Holmes, M. J. Capaldi, and J. A. Chapman. Reconstitution of collagen fibrils in vitro; the assembly process depends on the initiating procedure. *International Journal of Biological Macromolecules*, 8(3):161–166, 1986.
- [25] A. George and A. Veis. FTIRS in water demonstrates that collagen monomers undergo a conformational transition prior to thermal self-assembly in vitro. *Biochemistry*, 30(9):2372–2377, 1991.
- [26] M. Sun, A. Stetco, and E. F. Merschrod S. Surface-templated formation of protein microfibril arrays. *Langmuir*, 24(10):5418–5421, 2008.
- [27] F. Jiang, H. Hörber, J. Howard, and D. J. Müller. Assembly of collagen into microribbons: effects of pH and electrolytes. *Journal of Structural Biology*, 148(3):268–278, 2004.
- [28] W. Zhang, S. S. Liao, and F. Z. Cui. Hierarchical self-assembly of nano-fibrils in mineralized collagen. *Chemistry of Materials*, 15(16):3221–3226, 2003.

- [29] W. J. Landis and F. H. Silver. Mineral deposition in the extracellular matrices of vertebrate tissues: identification of possible apatite nucleation sites on type I collagen. *Cells Tissues Organs*, 189(1-4):20–24, 2009.
- [30] S. Karrasch, M. Dolder, F. Schabert, J. Ramsden, and A. Engel. Covalent binding of biological samples to solid supports for scanning probe microscopy in buffer solution. *Biophysical Journal*, 65(6):2437–2446, 1993.
- [31] R. A. de Souza, D. P. Jerônimo, H. A. Gouvêa, M. Xavier, M. T. de Souza, H. Miranda, M. G. Tosato, A. A. Martin, and W. Ribeiro. Fourier-transform Raman spectroscopy study of the ovariectomized rat model of osteoporosis. *The Open Bone Journal*, 2(1):24–31, 2010.
- [32] G. R. Sauer, W. B. Zunic, J. R. Durig, and R. E. Wuthier. Fourier transform Raman Spectroscopy of synthetic and biological calcium phosphates. *Calcified Tissue International*, 54(5):414–420, 1994.
- [33] B. O. Fowler, M. Markovic, and W. E. Brown. Octacalcium phosphate. 3. Infrared and Raman vibrational spectra. *Chemistry of Materials*, 5(10):1417–1423, 1993.
- [34] N. J. Crane, V. Popescu, M. D. Morris, P. Steenhuis, and M. A. Ignelzi Jr. Raman spectroscopic evidence for octacalcium phosphate and other transient mineral species deposited during intramembranous mineralization. *Bone*, 39(3):434–442, 2006.
- [35] G. Penel, N. Leroy, P. V. Landuyt, B. Flautre, P. Hardouin, J. Lemaitre, and G. Leroy. Raman microspectrometry studies of brushite cement: in vivo evolution in a sheep model. *Bone*, 25(2):81S–84S, 1999.
- [36] S. Stewart, D. A. Shea, C. P. Tarnowski, M. D. Morris, D. Wang, R. Franceschi, D.-L. Lin, and E. Keller. Trends in early mineralization of murine calvarial os-

- teoblastic cultures: a Raman microscopic study. *Journal of Raman Spectroscopy*, 33(7):536–543, 2002.
- [37] A. Tlili, D. C. Smith, J.-M. Beny, and H. Boyer. A Raman microprobe study of natural micas. *Mineralogical Magazine*, 53(2):165–179, 1989.
- [38] D. A. McKeown, M. I. Bell, and E. S. Etz. Vibrational analysis of the dioctahedral mica: $2M_1$ muscovite. *American Mineralogist*, 84(7-8):1041–1048, 1999.
- [39] A. K. Misra, S. K. Sharma, C. H. Chio, P. G. Lucey, and B. Lienert. Pulsed remote Raman system for daytime measurements of mineral spectra. *Spectrochimica Acta Part A: Molecular and Biomolecular Spectroscopy*, 61(10):2281–2287, 2005.
- [40] M. R. Kumar, E. F. Merschrod S., and K. M. Poduska. Correlating mechanical properties with aggregation processes in electrochemically fabricated collagen membranes. *Biomacromolecules*, 10(7):1970–1975, 2009.
- [41] S. V. Dorozhkin and M. Epple. Biological and medical significance of calcium phosphates. *Angewandte Chemie International Edition in English*, 41(17):3130–3146, 2002.

Chapter 3

Structural effects of sugar acids on collagen-based mineralization matrices

3.1 Introduction

The process of collagen mineralization represents a current challenge in tissue engineering and is extensively studied, since collagen and calcium phosphate are the main constituents of natural human bone. *In vitro* biomineralization of collagen can lead to biomaterials appropriate for use as bone substitutes and implants in medical fields [1,2].

The extracellular matrix is involved in formation of connective tissue such as bone. Bone formation is based on collagen mineralization, which occurs through the deposition of calcium phosphate crystals in the extracellular matrix. Glycosaminoglycans (GAGs) are carbohydrate polymers found in the extracellular matrix, which also contains collagen fibrils and a small amount of non-collagenous proteins. Negatively

charged carboxylate groups are suggested to have an ability to bind calcium ions and induce the nucleation of biominerals [3–6]. Previous studies of collagen mineralization mention the use of GAGs in the biomineralization process, mainly hyaluronic acid, which is composed from a repeated disaccharide unit of glucuronic acid and N-acetylglucosamine [7]. The improvement in the mineralization efficiency brought by the presence of hyaluronic acid or other GAGs is due to the extra free carboxylate group, not involved in the peptidic bond, which can bind calcium. It is believed that the binding of the calcium ion is the first step in the mechanism of collagen mineralization, and that it is mediated by the free carboxyl group from glutamate and aspartate amino acids [3, 8, 9]. A previous study on rat tail tendon mentions the existence of interactions *in vivo* between the GAGs contained in the proteoglycan decorin, namely chondroitin sulphate or dermatan sulphate, and the surface of collagen fibrils [10].

As a way to increase the efficiency of mineralization *in vitro* at physiological pH (7.4), some studies report the use of polyaspartate [11], or sugar acids like glucuronic acid [12] or hyaluronic acid [7], containing free carboxylate groups.

The aim of this study is to present the different structural changes in the collagen matrix due to the presence of two sugar acids, glucuronic acid (GlcA) and galacturonic acid (GalA), as monitored by atomic force microscopy (AFM). GlcA is the monomer component of various proteoglycans, and GalA is an epimer of glucuronic acid at the C4 atom, but which is not found in GAGs. Raman spectroscopy shows the presence of the sugar acids in the collagen matrix, and in spectra not shown here we also confirm the ability of these composite matrices to induce mineralization.

3.2 Experimental

3.2.1 Reagents and apparatus

Solutions of D-glucuronic acid (sodium salt, Sigma) and D-galacturonic acid (sodium salt, Fluka) were prepared with ultrapure water (Barnstead, 18.2 M Ω ·cm) to 1 mg/mL. Acidified type I bovine dermal collagen (3.0 mg/mL in 0.012 M HCl, Inamed Biomaterials) was used as received. ACS-grade salts (Sigma) were used for NaOH solution and sodium and potassium phosphate buffers (0.05 M PO₄³⁻, 0.2 M Na⁺/K⁺ and 0.1 M Cl⁻, pH 7.45).

Raman scattering spectra were obtained using a confocal configuration with 532 nm excitation (LabRAM, Jobin Yvon Horiba). AFM imaging (AC mode) was carried out on an Asylum Research MFP-3D system using silicon cantilevers with aluminum-coated backsides (Mikromasch, 150–300 kHz resonant frequencies). Images are shown with no post-processing beyond a simple planefit.

3.2.2 Methods for growing collagen fibrils

Growing collagen fibrils by incubation on mica

Collagen solutions in sodium phosphate buffer (5 μ g/mL collagen) were deposited on a freshly cleaved muscovite mica substrate. After 20 minutes, the substrate was rinsed with potassium phosphate buffer and incubated, also under potassium phosphate buffer, for 16 hours [13]. The buffer solution was then removed and the sample was left to dry in air before imaging. In the case of the samples that contained GlcA and GalA, the acids were included in the sodium phosphate buffer (pH 7.43) used initially with the collagen monomers. The mass ratio collagen:GlcA and collagen:GalA was 1:6.6. This higher ratio was chosen, given that the disruption of collagen fibrillogenesis

is dependent on the concentration of glucuronic acid used and no disruption was observed by AFM at a collagen:GlcA 1:0.5 mass ratio.

Cold start method for growing collagen fibrils

Collagen solutions in NaOH (650–750 $\mu\text{g}/\text{mL}$, pH 7–8), with or without GlcA/GalA, were placed in a water bath at 34–37°C [14] for at least 3 days. The GlcA/Gal was added to the collagen solution, in a mass ratio pure collagen:pure GlcA = 4.5:1, such that the GlcA was present in both suggested phases of nucleation and growth of collagen fibrils [15].

Sample preparation on mica. 150 μL of the resultant suspension was placed on freshly cleaved mica and allowed to adsorb for 30 minutes, after which the excess was removed and the sample was left to dry in air before imaging.

3.3 Results and discussion

3.3.1 Collagen on mica

Type I collagen is a protein found in many structures in mammals, having the property to self-assemble *in vivo* into fibrils of a few millimetres long [16]. In the process of growing collagen fibrils *in vitro*, one can obtain parallel fibrils if the process is induced on mica [13, 17], while the presence of sugar acids seems to disrupt the fibrillogenesis and to induce the formation of circular holes. *In vivo*, the process of collagen mineralization is believed to be stimulated by mature collagen fibrils [18]. In the absence of sugar acids, the collagen fibrils grown in our lab by alignment on mica reach a length of more than 90 μm (the maximum limit for x and y dimensions of our instrument) and with a height from 6 up to 22 nm (Figure 3.1a).

3.3.2 Collagen with sugar acids on mica

In the presence of the studied sugar acids the collagen fibrils still form and they preserve their general trend for parallel alignment, but striking pores appear in the resultant film. These structures are suggestive of film drying or dewetting effects, and control experiments in high or low humidity showed consistent pore formation, with variations in pore size and number.

There are examples in the literature of dewetting of thin films of collagen monomers on highly oriented pyrolytic graphite and mica [19–21], with a hexagonal network as a final pattern. This dewetting phenomenon is believed to depend on the rate of solvent evaporation and the thickness of the film. Studies of thin films of collagen on polystyrene showed that the rupture of the film takes place only when the film is adsorbed on the surface for a short time and then is exposed to slow drying, while a longer incubation leads to stronger collagen-collagen interactions and no discontinuity in the pattern formed [22]. Similarly, a thin film of collagen in phosphate buffered saline deposited on poly(methyl methacrylate) will form a net-like pattern due to slow drying and a continuous film for fast drying [23]. In the case of dewetting studied on surfaces of hydroxyapatite crystals and controlled humidity of 95%, films of collagen monomers having low or high collagen concentration in phosphate buffered saline showed pores which differed in shape and diameter for slow drying, but without any particular pattern besides the thin monomers for fast drying [24].

The above-mentioned studies strengthen the idea that the patterns formed during dewetting depend on the drying rate or solvent evaporation rate, humidity, and concentration of the solution used or thickness of the film. However, our pore structure appears to be specific to collagen-sugar acid film.

In our experiments collagen was mixed with GlcA and exposed to slow drying in air, without controlling humidity. The resultant pores have a diameter up to 10

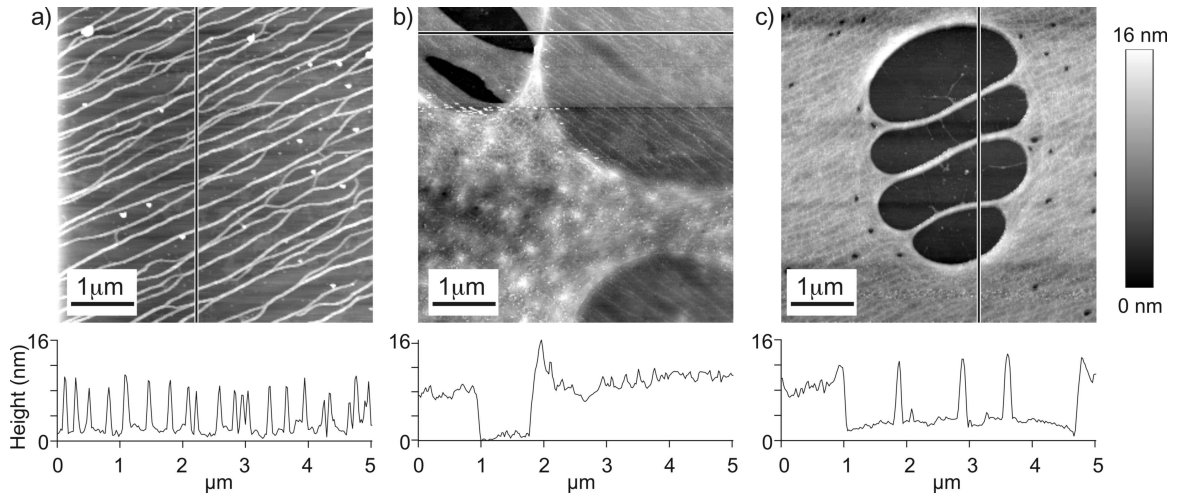


Figure 3.1: AFM images of glucuronic acid’s effects on a collagen matrix. a) Collagen fibrils grown by incubation on mica. b) Collagen fibrils grown with the sugar acid (early stages of hole formation). c) Mature collagen/sugar film showing the “laddered stockings” motif.

μm (Figure 3.1b and c). The pores are round in shape and eventually can form a pattern as shown in Figure 3.1c, reminiscent of a run or ladder in nylon stockings. The pores are externally defined by a rim with a pronounced height ($\sim 8\text{--}13\text{ nm}$), with the surface immediately surrounding the rim $\sim 2.5\text{ nm}$ lower than the rim height. The remainder of the surface shows fluctuations in height in the range $7\text{--}10\text{ nm}$ due to the presence of the collagen fibrils.

Comparing panels b and c in Figure 3.1, it appears that the pores initiate with an early stage when the collagen fibrils are pushed aside due to dewetting, leaving behind a circular shape with high rims, creating the pore. The topographic images suggest that inside the pores is a flat surface, which could be bare mica or the surface could be covered with a very thin layer of the evaporating solvent [25]. The phase images (not shown), a measure of surface friction, present very distinctively the patterns formed on the surface, sustaining the idea that inside and outside the pores there could be two different materials: inside – the substrate, outside – the collagen matrix with sugar acids.

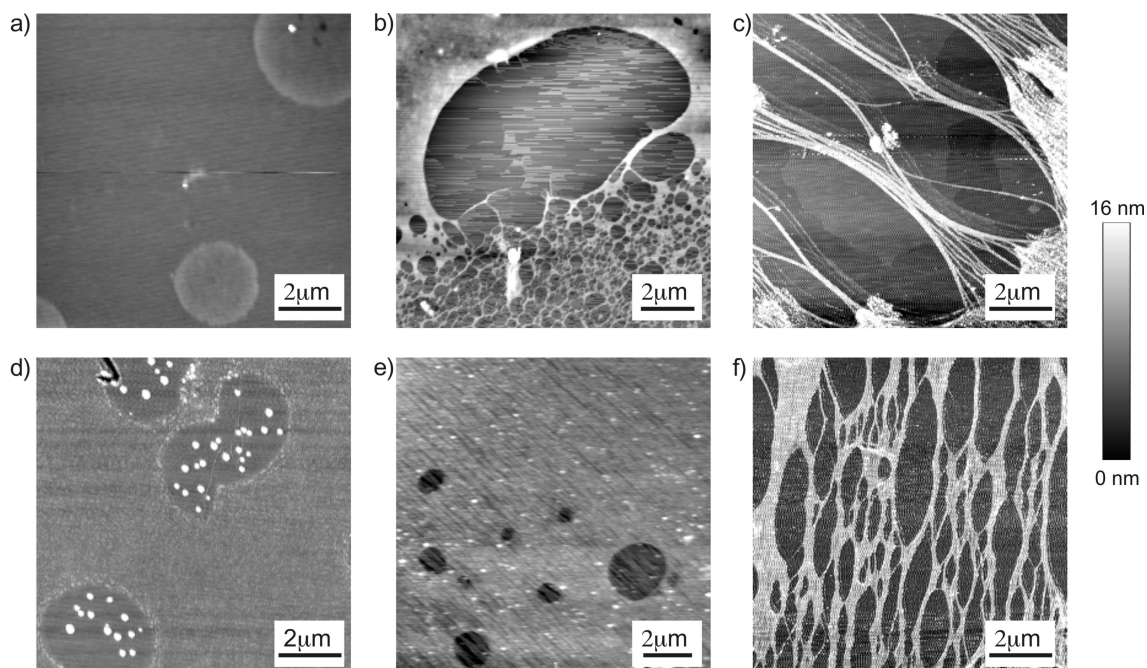


Figure 3.2: AFM images showing how sugar interactions with mica initiate the pore formation. GlcA on mica looks like a), while collagen films grown on a pre-treated surface of mica saturated with GlcA look like b), which is similar to the films from pre-mixed GlcA/collagen c). Similar images for GalA are shown in d)–f), with the GalA film on mica in d), the collagen film grown on a GalA-treated mica surface in e), and a film of pre-mixed coll/GalA in f).

Similar experiments with GalA produced fewer disruptions of the collagen matrix, leaving openings in the film whose widths were smaller ($3 \mu\text{m}$ at most) than the diameter of pores observed with GlcA (see Figure 3.2f).

3.3.3 Collagen on mica pre-treated with sugar acids

The sugar acids present during matrix formation change the collagen-mica interaction: the driving force for hole formation in the matrix appears to arise from the dewetting of the sugar acid layer. Separate experiments with pure acid films also shows dewetting, with pores of similar size. It is important to note that these pores are on a different length scale than the features observed for water alone on mica (images not shown).

For pure films of either GlcA or GalA on mica, after drying it was possible to

observe with the AFM the formation of round holes with diameters in the range of 2–3.5 μm (Figure 3.2 a,d). Their height varied from 2 to 5 nm.

For mica pretreated with GlcA, the images show the formation of pores in the subsequently applied collagen films, with a width up to 10 μm and a height of the rim and of the bridge inside the pore of ~ 12 nm (Figure 3.2b). In contrast with these large pores, when the mica surface was pretreated with a 1 mg/mL solution of GalA (Figure 3.2e), the AFM images showed less disruption of the overlaid collagen film, with hole diameters varying between 0.5 μm to 3 μm . The depth of the pores varies between 4–6.5 nm, and preserve the alignment of the collagen fibrils, with a height of ~ 1.5 nm.

The final hole formation with GalA, whether through pretreatment of the surface or by inclusion during fibril formation, is comparable to the early stages in pore evolution with GlcA, as seen in the similarities between Figure 3.2e,f and Figure 3.1b. This suggests that the GalA is less active in disrupting the collagen-mica interactions and inducing dewetting.

The driving force for pore formation is presumably not due to solvent evaporation from aqueous solution, since pores are not observable in the collagen matrix without sugar acids and occur on different length scales than the dewetting of water alone. Therefore, the dewetting induced by the sugar acids, whether alone or in the collagen matrix, must be the impetus for the pore formation. The mixed films (*e.g.* Figure 3.1b) show features with similar height increments as the samples described here with collagen growth on mica pre-treated with sugar acids. This suggests a similar model of a dewetting sugar layer below a collagen fibril layer for both systems, implying some segregation of the sugars within the mixed films analogous to the imposed layering with the pretreated surfaces.

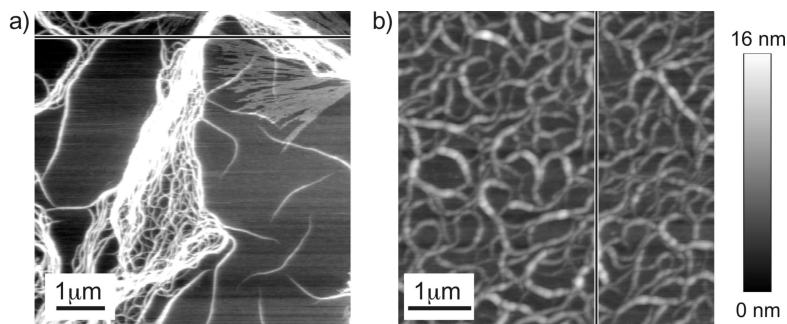


Figure 3.3: AFM images of a) collagen and b) collagen and glucuronic acid, after cold-start treatment.

3.3.4 Collagen fibrils with sugar acids by the cold start method

The sugar acids also affect collagen-collagen interactions, as seen in experiments on collagen fibrillogenesis without mica incubation. Images of collagen fibrils from the cold start method without sugar acids feature clumps of long protofibrils (Figure 3.3 a), while the fibrils grown with GlcA (1:4.5) are thicker and curled (Figure 3.3 b). No fibrils were observed for the sample with GalA (1:4.5), despite a long incubation time, after which the solution remained clear.

While the sample of collagen with GlcA shows the fibrils having a height of $\sim 9\text{--}10$ nm, the collagen blank sample shows fibrils mostly ~ 3 nm in height, although some larger fibrils also appear. As well, the fibril widths are more than doubled in the sample with GlcA. Even accounting for the contribution from the tip shape, this still indicates a much larger fibril with GlcA. These results suggest that GlcA stimulates collagen-collagen aggregation, leading to the thicker fibrils seen after pore formation in the films.

This is consistent with literature findings. The process of collagen self-assembly in the presence of polysaccharides such as alginate, hyaluronic acid, chitosan, chondroitin sulphate, and heparin, investigated as a function of their concentration, showed an increase in the collagen fibrils' diameter for a small concentration of the polysaccha-

rides [15, 26].

3.3.5 Raman spectroscopy

Our sugar-collagen matrices, although structurally modified, do promote phase-selective mineralization. Preliminary experiments on mica-supported films show Raman peaks characteristic of calcium phosphate phases.

Given the evidence for crosslinking of collagen by sugar acids from the enhanced fibril formation observed by AFM, we may also expect to see some signals in Raman spectra indicating collagen-sugar acid binding. There are two groups on the sugar acids which could bind amines on the side chains of lysine in collagen: a carboxylate, and a carbonyl present in the open chain form.

Our recorded Raman spectra on the GlcA solution, made from a sodium salt, should show two peaks for the ionized carboxylate group [27, 28]: one for symmetric stretching of COO^- at 1410 cm^{-1} or between $1360\text{--}1400\text{ cm}^{-1}$, and one for antisymmetric stretching of COO^- at 1606 cm^{-1} or between $1580\text{--}1590\text{ cm}^{-1}$ (Figure 3.4a).

For a suspension containing collagen and GlcA (1:67 by mass), the persistence of the Raman peaks at $\sim 1410\text{ cm}^{-1}$ and in the range of $1580\text{--}1590\text{ cm}^{-1}$ (Figure 3.4b) suggest that indeed there has been no binding with the collagen through the carboxylate group on the sugar acid. (The peaks in the $1580\text{--}1590\text{ cm}^{-1}$ region are nearly obscured by the broad water bending mode [29] at 1640 cm^{-1} .) The spectrum remained unchanged even with samples aged for up to seven days at room temperature.

These continuing free carboxylate signatures could simply be a result of the high proportion of GlcA in the mixture, with excess unbound GlcA dominating the spectrum. At the other extreme, the Raman spectra for the cold start samples with GlcA (Figure 3.4c) do not show the bands specific for the carboxylate group due to the fact

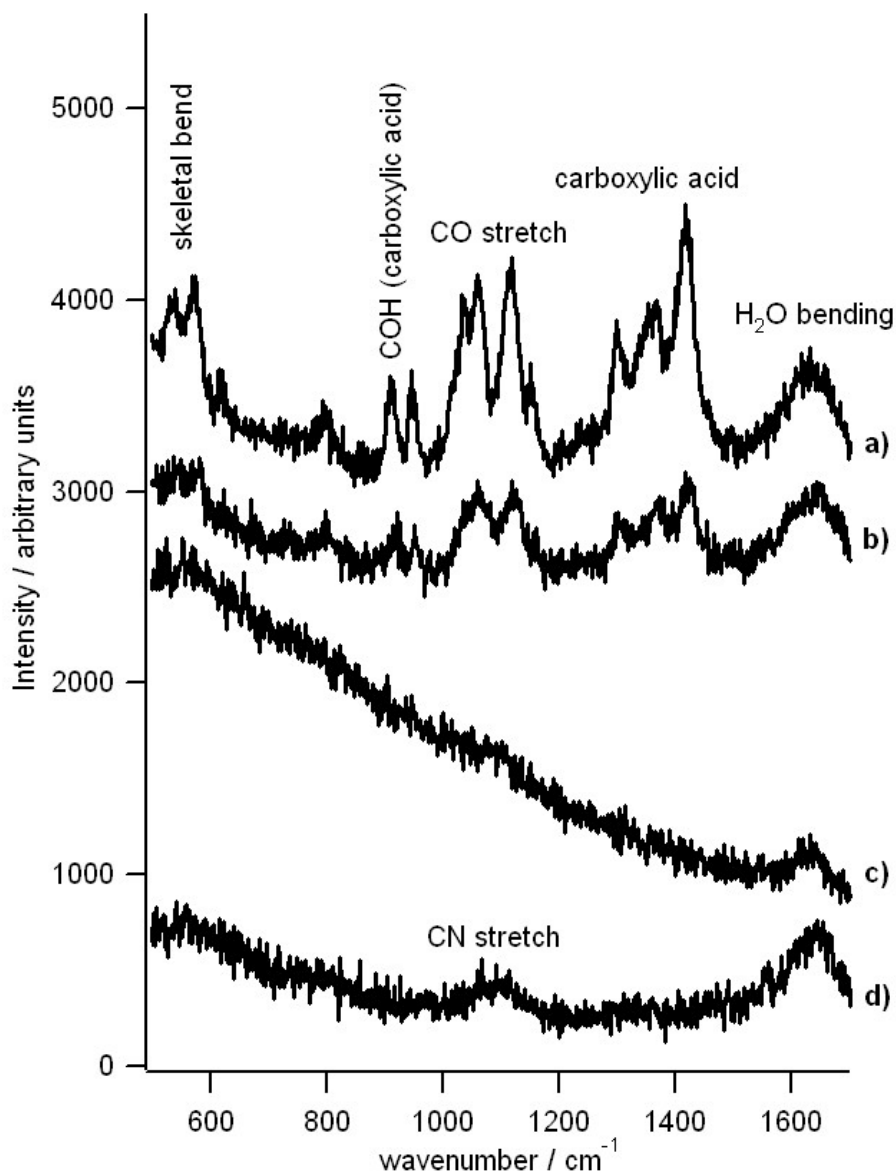


Figure 3.4: Raman spectra of: a) glucuronic acid, b) a sample of collagen monomers with glucuronic acid, c) collagen with GlcA after cold start, d) collagen after cold start.

that the collagen:GlcA ratio is 4.5:1 by mass, a concentration of 0.14 mg GlcA/mL aliquot which was to detect any signal. The spectra from cold-start samples (Figure 3.4c,d) is characterized by a low intensity collagen signal which is otherwise eclipsed in the presence of higher concentrations of GlcA. The broad peak at $\sim 1093\text{--}1100\text{ cm}^{-1}$ arises from C-N stretches in the protein backbone [30], and the wide peak at 1640 cm^{-1} is attributed to the bending mode of water, as mentioned above.

We also looked to the carbonyl moiety as a more likely candidate for evidence of collagen binding. If GlcA were to interact with collagen through the carbonyl group present in the open chain, as in a Maillard reaction [12, 31], this would leave the carboxylate group of the GlcA free and available for binding calcium in the incipient stages of mineralization. The skeletal modes of the monosaccharides and their corresponding sugar acids [32] are in the region $300\text{--}575\text{ cm}^{-1}$. A shift or a change in these peaks, especially the one at 573 cm^{-1} , may suggest a crosslink between GlcA and collagen, involving an amino group of collagen and the aldehyde group of GlcA. Our spectra show a lower intensity for the 573 cm^{-1} peak in the mixture of collagen and GlcA (Figure 3.4c *vs.* Figure 3.4b), but although it supports the crosslinking inferred from AFM imaging, this finding alone is not conclusive since the intensity of several peaks for the mixture is lower than those for the GlcA alone.

3.4 Conclusions

The mixture of sugar acids and collagen represents a feasible scaffold for the process of artificial collagen mineralization, the resulting material being used for hard tissue repair and implants.

In this study we presented the influence of sugar acids on the structure of the collagen matrix. AFM imaging leads to the conclusion that the sugar acids disrupt

the collagen-collagen and collagen-mica interactions of mica supported collagen fibril arrays, leading to the formation of pores and the thickening of the collagen fibrils. Stimulated dewetting by the sugar acids, possibly as a segregated underlayer, initiates the process, with collagen crosslinking by the sugar acids joining the fibrils into larger, pore displaced, rims. It seems that GlcA is more chemically active than GalA, since the features observed with GlcA form quicker and at a larger scale than with GalA.

The role that these sugars play in binding this protein and in the rate of stimulation for the mineralization process is still not completely elucidated, but an overall conclusion is that sugar acids alone, without collagen, do not stimulate mineralization, but that composite films do so, as seen by calcium phosphate signatures from Raman spectra in preliminary experiments, presented in Appendix A. This enhanced collagen mineralization in the presence of sugar acids may arise not only from initiation through binding of calcium cations by the acids, but also from sugar acid-enhanced collagen aggregation.

Bibliography

- [1] U. Meyer and H. P. Wiesmann. *Bone and cartilage engineering*. New York : Springer, Berlin, 2006.
- [2] D. Wahl and J. Czernuszka. Collagen-hydroxyapatite composites for hard tissue repair. *European Cells and Materials*, 11:43–56, 2006.
- [3] S.-H. Rhee and J. Do Lee. Nucleation of hydroxyapatite crystal through chemical interaction with collagen. *Journal of the American Ceramic Society*, 83(11):2890–2892, 2000.

- [4] S.-H. Rhee and J. Tanaka. Effect of citric acid on the nucleation of hydroxyapatite in a simulated body fluid. *Biomaterials*, 20(22):2155–2160, 1999.
- [5] S. Mann, B. R. Heywood, S. Rajam, and J. D. Birchall. Controlled crystallization of CaCO_3 under stearic acid monolayers. *Nature*, 334(6184):692–695, 1988.
- [6] S. Weiner, W. Traub, and S. B. Parker. Macromolecules in mollusc shells and their functions in biomineralization [and Discussion]. *Philosophical Transactions of the Royal Society B: Biological Sciences*, 304(1121):425–434, 1984.
- [7] Y. Wang, C. Yang, X. Chen, and N. Zhao. Development and characterization of novel biomimetic composite scaffolds based on bioglass-collagen-hyaluronic acid-phosphatidylserine for tissue engineering applications. *Macromolecular Materials and Engineering*, 291(3):254–262, 2006.
- [8] T. Schepersa, J. Brickmann, O. Hochrein, and D. Zahn. Atomistic simulation study of calcium, phosphate and fluoride ion association to the teleopeptide-tails of collagen – initial steps to biomineral formation. *Zeitschrift für Anorganische und Allgemeine Chemie*, 633(3):411–414, 2007.
- [9] W. Zhang, Z.-L. Huang, S.-S. Liao, and F.-Z. Cui. Nucleation sites of calcium phosphate crystals during collagen mineralization. *Journal of the American Ceramic Society*, 86(6):1052–1054, 2003.
- [10] M. Raspanti, A. Alessandrini, V. Ottani, and A. Ruggeri. Direct visualization of collagen-bound proteoglycans by tapping-mode atomic force microscopy. *Journal of Structural Biology*, 119(2):118–122, 1997.
- [11] J.-H. Bradt, M. Mertig, A. Teresiak, and W. Pompe. Biomimetic mineralization of collagen by combined fibril assembly and calcium phosphate formation. *Chemistry of Materials*, 11(10):2694–2701, 1999.

- [12] H. Ehrlich, T. Douglas, D. Scharnweber, T. Hanke, R. Born, S. Bierbaum, and H. Worch. Hydroxyapatite crystal growth on modified collagen I-templates in a model dual membrane diffusion system. *Zeitschrift für Anorganische Chemie*, 631(10):1825–1830, 2005.
- [13] F. Jiang, H. Horber, J. Howard, and D. J. Muller. Assembly of collagen into microribbons: effects of pH and electrolytes. *Journal of Structural Biology*, 148(3):268–278, 2004.
- [14] A. George and A. Veis. FTIRS in water demonstrates that collagen monomers undergo a conformational transition prior to thermal self-assembly in vitro. *Biochemistry*, 30(9):2372–2377, 1991.
- [15] G. C. Wood. The formation of fibrils from collagen solutions 3. Effect of chondroitin sulphate and some other naturally occurring polyanions on the rate of formation. *Biochemical Journal*, 75(3):605–612, 1960.
- [16] K. E. Kadler, D. F. Holmes, J. A. Trotter, and J. A. Chapman. Collagen fibril formation. *Biochemical Journal*, 316(Pt1):1–11, 1996.
- [17] M. Sun, A. Stetco, and E. F. Merschrod S. Surface-templated formation of protein microfibril arrays. *Langmuir*, 24(10):5418–5421, 2008.
- [18] A. Veis. *Biom mineralization*, volume 54 of *Reviews in Mineralogy and Geochemistry*, chapter Mineralization in organic matrix frameworks, pages 249–289. Mineralogical Society of America, Series editor J. J. Rosso, 2003.
- [19] M. Mertig, U. Thiele, J. Bradt, D. Klemm, and W. Pompe. Dewetting of thin collagenous precursor films. *Applied Physics A*, 66(7):S565–S568, 1998.

- [20] M. Mertig, U. Thiele, J. Bradt, G. Leibiger, W. Pompe, and H. Wendrock. Scanning force microscopy and geometric analysis of two-dimensional collagen network formation. *Surface and Interface Analysis*, 25(7-8):514–521, 1997.
- [21] U. Thiele, M. Mertig, and W. Pompe. Dewetting of an evaporating thin liquid film: heterogeneous nucleation and surface instability. *Physical Review Letters*, 80(13):2869–2872, 1997.
- [22] I. Jacquemart, E. Pamuła, V. D. Cupere, P. Rouxhet, and C. Dupont-Gillain. Nanostructured collagen layers obtained by adsorption and drying. *Journal of Colloid and Interface Science*, 278(1):63–70, 2004.
- [23] C. C. Dupont-Gillain, B. Nysten, and P. G. Rouxhet. Collagen adsorption on poly(methyl methacrylate): net-like structure formation upon drying. *Polymer International*, 48(4):271–276, 1999.
- [24] A. Monkawa, T. Ikoma, S. Yunoki, K. Ohta, and J. Tanaka. A dewetting process to nano-pattern collagen on hydroxyapatite. *Materials Letters*, 60(29):3647–3650, 2006.
- [25] D. Gan, S. Lu, and Z. Wang. Dewetting of a fluorinated polymer on mica. *Journal of Macromolecular Science, Part B: Physics*, B40(2):199–206, 2001.
- [26] S.-W. Tsai, R.-L. Liu, F.-Y. Hsu, and C.-C. Chen. A Study of the influence of polysaccharides on collagen self-assembly: nanostructure and kinetics. *Biopolymers*, 83(4):381–388, 2006.
- [27] A. Synytsya, M. Urbanová, V. Setnička, M. Tkadlecová, J. Havlíček, I. Raich, P. Matějka, A. Synytsya, J. Čopíková, and K. Volka. The complexation of metal cations by D-galacturonic acid: a spectroscopic study. *Carbohydrate Research*, 339(14):2391–2405, 2004.

- [28] M. Meziane-Tani, P. Lagant, A. Semmoud, and G. Vergoten. The SPASIBA force field for chondroitin sulfate: vibrational analysis of D-glucuronic and N-acetyl-D-galactosamine 4-sulfate sodium salts. *The Journal of Physical Chemistry A*, 110(39):11359–11370, 2006.
- [29] G. E. Walrafen and L. A. Blatz. Weak Raman bands from water. *The Journal Chemical Physics*, 59(5):2646–2650, 1973.
- [30] T. Ikoma, H. Kobayashi, J. Tanaka, D. Walsh, and S. Mann. Physical properties of type I collagen extracted from fish scales of *Pagrus major* and *Oreochromis niloticus*. *International Journal of Biological Macromolecules*, 32(3):199–204, 2003.
- [31] Š. Horvat and A. Jakas. Peptide and amino acid glycation: new insights into the Maillard reaction. *Journal of Peptide Science*, 10(3):119–137, 2004.
- [32] C. Y. She, N. D. Dinh, and A. T. Tu. Laser raman scattering of glucosamine N-acetylglucosamine, and glucuronic acid. *Biochimica et Biophysica Acta (BBA)-General Subjects*, 372(2):345–357, 1974.

Chapter 4

Supramolecular structure and anomer-selective formation of polyglucuronic acid*

Polyglucuronic acids provide a biocompatible matrix for industries ranging from pharmaceuticals to agriculture. Here we provide a method for selectively producing α -polyglucuronic acid, a simple alternative to the oxidation of cellulose or amylose with 2,2,6,6-tetramethylpiperidine-1-oxyl radical (TEMPO) or isolation from bacterial cultures. Atomic force micrographs show the pH-dependent formation and persistence of polyglucuronic acid fibrils, while NMR studies demonstrate the selectivity of the glycosidic linkage. By controlling pH, oligoglucuronate chains are created, with both NMR and AFM data showing the preservation of this linkage in basic medium after formation under acid. Clear evidence for the formation of the C–O–C glycosidic bond comes from peaks in the ^{13}C NMR spectra, revealing a linkage through the anomeric

*This chapter is a modified version of “Supramolecular structure and anomer-selective formation of polyglucuronic acid”, Stetco, I.A. and Merschrod S., E.F., *Polymer International* **62**, 804–810 (2013).

carbon atom and also a linkage with a ring carbon atom.

4.1 Introduction

Polyglucuronic acids represent a subject with increased popularity in recent years due to their pharmaceutical applications as gelling and thickening agents [1,2], their biological and antiflocculation properties [3], their usage as biofertilizers and pesticides [4] and their possible use for biodegradable packaging and coating materials [5]. Additional uses are collected in a review [6].

Amylose, cellulose, and curdlan are natural polymers and represent precursors for polyglucuronic acid. The most used method for the preparation of polyglucuronic acids is through the 2,2,6,6-tetramethylpiperidine-1-oxyl radical (TEMPO) mediated regioselective oxidation of the primary hydroxy groups in polymer precursors like cellulose to form cellouronic acid featuring a β -(1,4) linkage [3,7–10], the oxidation of starch to form α -(1,4)-polyglucuronic acid (amylouronate) [11,12] or recently through the oxidation of curdlan [13,14] to give β -(1,3)-polyglucuronic acid, all obtained polyglucuronic acids being water soluble products.

The polyglucuronic acids can also be isolated from bacterial cultures, the literature reporting β -(1,4)-glucuronan as an excretion product of bacteria from the *Rhizobiaceae* family [1], while another study discovered the *Gluconacetobacter hansenii* bacterial strain that produced α -(1,4)-oligoglucuronic acid [15] rather than β . The β -(1,4)-polyglucuronic acid was identified to be part of the mycelial wall of the fungal strain *Mucor rouxii* [16] and another paper [17] reports a polyglucuronic acid with alternating α -(1,4) and β -(1,4) linkages in the cell wall of alkalophilic *Bacillus* strain C-125.

Since glucuronic acid is used in biomaterials and food products, it is important and

interesting to understand its physical properties under a range of aqueous conditions and at different pH. An AFM study of the morphology of starch and amylose films is reported in the literature [18], and there is one example of AFM imaging of the products of oxidation of cellulose which may include polyglucuronic acids [19]. NMR is increasingly employed for the structural investigations of carbohydrates including complex oligosaccharides [20–22].

We present here the results of AFM and NMR experiments, techniques which when combined provide a powerful means of characterizing the pH-dependent morphology and chemical structure of uronic acid polymers and films. In the process of better understanding the structure and chemical interactions of these important systems, we have also developed an easy method to synthesize α -polyglucuronic acid. In the presence of HCl monosaccharides can form a glycosidic bond [23], which in our method leads to polymerization and fibre formation. To our knowledge this direct method was not used before to form polyglucuronic acid starting from monomers.

4.2 Materials and methods

4.2.1 Materials

Solutions of D-glucuronic acid monomers (sodium salt monohydrate, Sigma, Oakville, Canada) were prepared with ultrapure water (Barnstead, Thermo Scientific, Asheville, USA, 18.2 M Ω cm) to 1 mg mL⁻¹ for AFM and 5 mg mL⁻¹ for NMR experiments. All experiments were carried out at room temperature. Afterward the pH was adjusted to acidic with concentrated HCl (Sigma) or 3 mol L⁻¹ HCl (diluted with ultrapure water) and to basic with NaOH (Sigma) in 6 mol L⁻¹ or 4% solutions.

4.2.2 Methods for growing polyglucuronic fibrils on mica for AFM

Muscovite mica squares (*ca* 1 cm²) were used as substrates to image the polyglucuronic fibrils. First, 50 μL of a 1 mg mL⁻¹ solution of glucuronic acid in ultrapure water, with unadjusted pH or pH adjusted to acidic or basic depending on the case, was added to freshly cleaved mica and allowed to adsorb for 20 min. Then the solution was wicked away with Kimwipes and the sample was dried in air before imaging. Some samples were rehydrated with solutions of the same or different pH to monitor the robustness of the fibrils; some samples were not allowed to dry before imaging under fluid.

4.2.3 AFM

AFM imaging (AC mode) at room temperature was carried out on an Asylum Research (Santa Barbara, USA) MFP3D system. Dry samples were imaged using silicon cantilevers with aluminum-coated backsides (Mikromasch, San Jose, USA 150–300 kHz resonant frequencies). Fluid imaging employed gold-coated silicon nitride cantilevers (Mikromasch, 0.05–0.3 N m⁻¹ spring constant). Images are shown with no post-processing beyond a zero order flattening using Asylum Research procedures within IGOR 6.1 (Wavemetrics, Inc, Portland, USA).

4.2.4 Solid-state NMR

The spectra were obtained at 298 K using a Bruker (Milton, Canada) Avance II 600 spectrometer equipped with a SB Bruker 3.2 mm MAS triple-tuned probe operating at 600.33 MHz for ¹H and 150.97 MHz for ¹³C. Chemical shifts are referenced to tetramethylsilane using adamantane as an external standard for ¹³C. The samples

were spun at 20 kHz. The cross-polarization spectrum was collected using 1024 scans, with a Hartmann-Hahn match at 62.5 kHz and 100 kHz ^1H decoupling. The recycle delay was 2 s. The contact time was 2000 ms for ^{13}C NMR.

4.2.5 ^{13}C - solution NMR

NMR ^{13}C spectra were recorded on a Bruker Avance III 300 spectrometer operating at a frequency of 75.487 MHz using a 30° pulse with proton decoupling. Samples were studied at room temperature in solvent containing $\text{H}_2\text{O}:\text{D}_2\text{O} = 90:10$ (v/v), in tubes with 5 mm outer diameter. The spectra are referenced to the ^{13}C shift of the methyl in acetone, used as an internal standard, with $\delta = 31.5$ ppm relative to Me_4Si . The number of scans for all presented spectra is 4096.

4.3 Results and discussion

4.3.1 Polyglucuronic acid fibres on mica revealed by AFM

In our experiments, glucuronic acid presents various forms of aggregation at different pH. Our AFM and NMR data show the ability of glucuronic acid to aggregate at acidic pH to form oligoglucuronates. Based on information provided by NMR experiments we propose that a glycosidic linkage, rather than hydrogen bonding, leads to the formation of polyglucuronate, although hydrogen bonding may exist between the oligomeric chains.

For AFM, an imaging concentration of 1 mg mL^{-1} was preferred to the 5 mg mL^{-1} used for NMR, keeping in mind that lower concentration allows a better visualization of separate fibres. A similar situation has been observed for a sulfated polysaccharide that contains glucuronic acid units [24]. A concentration of 5 mg mL^{-1} , which is suitable for obtaining a high enough ^{13}C NMR signal, may produce a thermoreversible

gel [1], making the AFM imaging difficult. However, $^1\text{H-NMR}$ spectra confirm that a concentration of 1 mg mL^{-1} versus a concentration of 5 mg mL^{-1} does not affect the chemical structure; thus the ^{13}C shifts should be the same. Therefore the 1 mg mL^{-1} AFM images should relate to the 5 mg mL^{-1} ^{13}C NMR data.

AFM images of an untreated solution of glucuronic acid sodium salt (pH 6) dried on mica illustrate that the fibres are not present in solution prior to acid or base addition. The image of glucuronic acid monomers on mica (Figure 4.1(a)) shows circular deposits (discs) of glucuronic acid *ca* 2.5 nm high upon drying and no evidence of fibrils. When the pH of a sodium glucuronate solution is modified from 6 to 2 by adding HCl, the AFM images of the dry sample on mica indicate the formation of an abundance of fibres (Figure 4.1(b)), with their height between 0.6 and 1.5 nm, their length reaching $10\ \mu\text{m}$ and their width between *ca* 70 and 100 nm. In contrast, the AFM images of glucuronic acid dried from a pH 13 solution onto mica (Figure 4.2(b)) show discs as with the untreated monomer solution seen in Figure 4.1(a). The pH of the solution was modified with 6 mol L^{-1} NaOH.

In order to understand the formation of these fibres, the reversibility of that formation and the stability of the fibres, we also switched the pH from acidic to basic and from basic to acidic. The stability of the fibres once dried on mica was monitored by imaging them subsequently in ultrapure water.

It is known that monosaccharides are able to form glycosidic bonds in the presence of HCl, and that this is a reversible process in acidic environment but that these created bonds can be preserved in neutral or basic solutions. The sample which had its pH first modified by adding HCl was imaged dry in air and showed fibres, indicating that the bonds are preserved by removal of the acidic solution (Figure 4.2(a)). After imaging, 4% NaOH was added to that same sample.

After 30 min the excess solution was removed and the sample was dried in air.

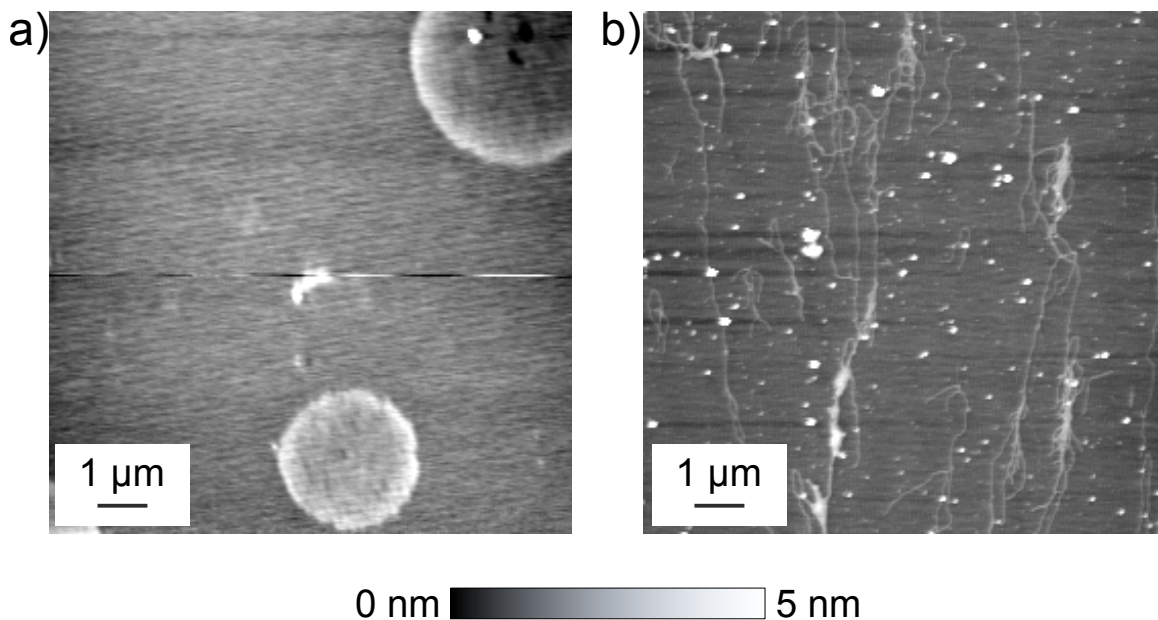


Figure 4.1: Atomic force micrograph of (a) glucuronic acid monomers, unadjusted pH, and (b) polyglucuronate fibrils prepared in an acidified solution and dried on a mica substrate.

The images for the acidic-to-basic sample show that the fibres formed in acidic pH are preserved in basic pH (Figure 4.2(c)), where they appear to be sitting on top of discs characteristic for basic pH. The height of the discs in these samples is *ca* 1.9–2 nm and the height of the fibres is 2–3 nm.

Another sample was prepared in basic solution (pH 13 from added NaOH) and deposited on mica (Figure 4.2(b)). After the excess solution was removed, 3 mol L⁻¹ HCl was added to the mica-supported sample for 10 min. Excess solution was removed and the sample was dried before imaging. The sample shows the presence of both the discs characteristic for basic pH and the early beginnings of fibres (Figure 4.2(d)).

The real-time formation of fibres is not observed if the imaging is done using the pH 2 sodium glucuronate solution as the imaging fluid (images not shown here), possibly due to the linkage reversibility in the presence of acid, forming monomers.

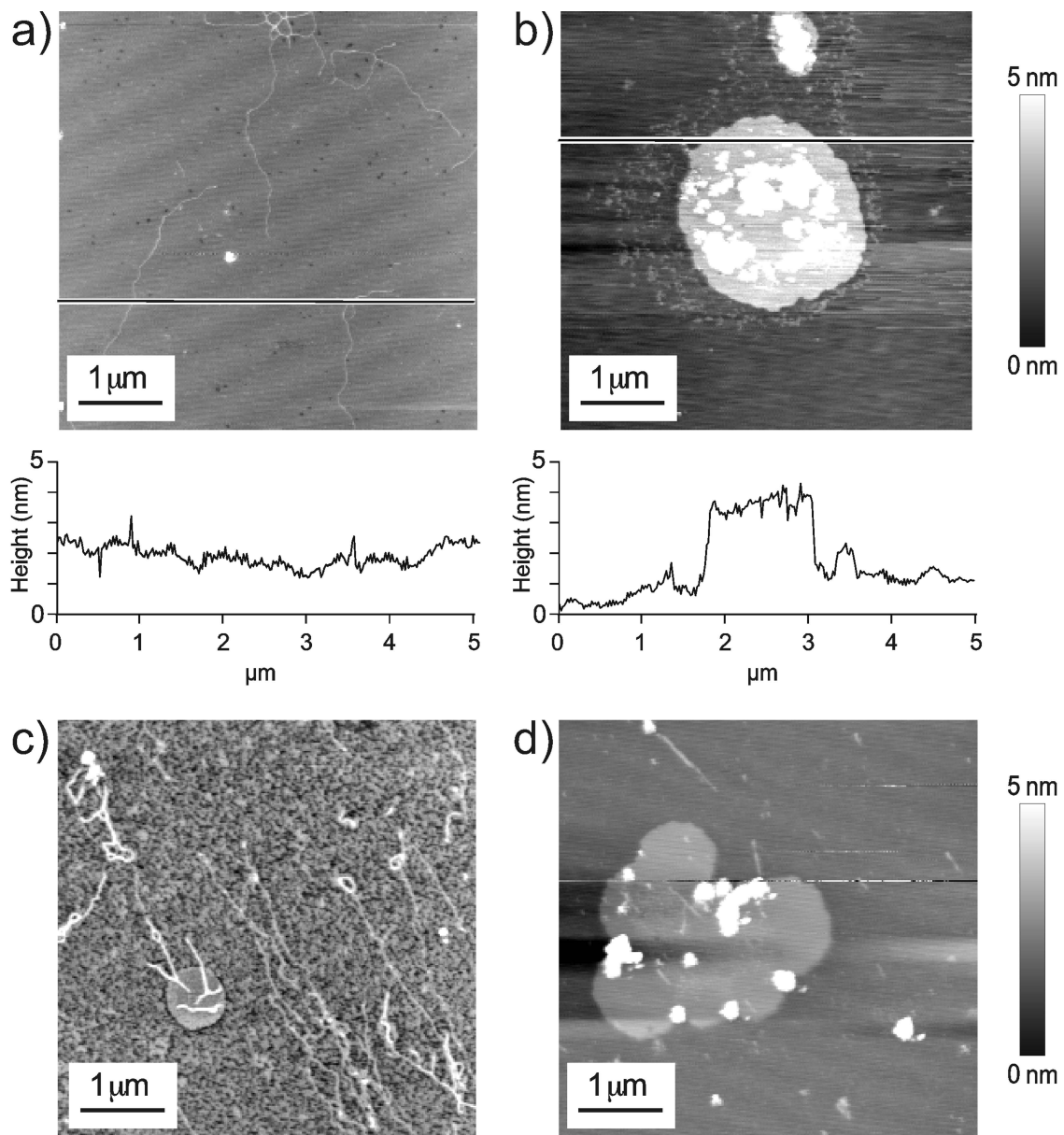


Figure 4.2: AFM images of a sample dried from a glucuronic acid solution (a) at pH 2, (b) at pH 13, (c) at pH 2 switched to basic pH and (d) at pH 13 switched to acidic pH.

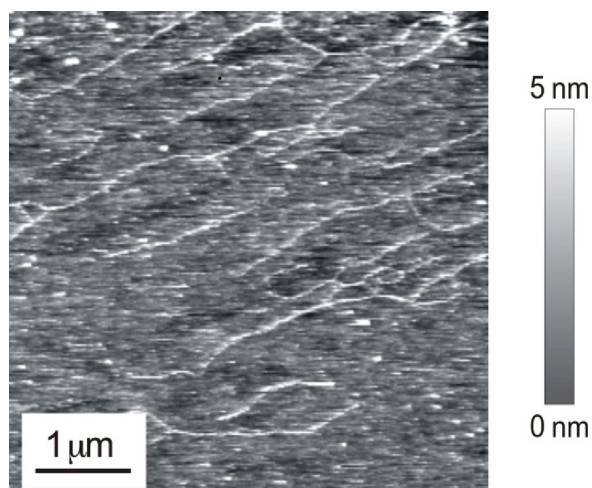


Figure 4.3: Atomic force micrograph of polyglucuronate fibrils prepared in an acidified solution, dried on a mica substrate, and imaged in ultrapure water to check stability.

Once adsorbed on mica and dried, however, the chains exhibit good stability and a strong adsorption when AFM imaged in ultrapure water. Even after 30 min under ultrapure water they are not dissolved, as seen in Figure 4.1.

Given that the polymer formation is fully reversible in acidic solution, the absence of the fibrils in the real-time experiments confirm that mica, used as a support for AFM monitoring, does not induce polymerization. The neutrality of the mica substrate with respect to the behaviour of glucuronic acid at different pH conditions is supported by the NMR spectra presented later, revealing that the formation of polyglucuronic acid by a glycosidation reaction can occur in the absence of mica. By removing the water from the sample (through wiping and also drying of the mica surface), which is the reaction byproduct and also the solvent, the equilibrium of the glycosidation reaction is shifted towards polymer formation, with AFM exposing the fibres formed under acidic conditions.

These experiments suggest that the low pH of the solution is the driving force for the formation of fibres, and not the substrate. However, we did need to rule out the possibility of substrate-induced fibre formation [25] given the apparent alignment

of fibres in Figure 4.3. (This type of alignment was observed with AFM for homogalacturonan in pectin [26].) Images for similar solutions on highly oriented pyrolytic graphite, a quite different substrate, also showed fibrils for low pH, further supporting our conclusion that the fibril formation is not mica-induced.

Based on the height (up to 1.5 nm) and the width (70–100 nm) of the fibres, the obtained fibres represent a lateral association of at least 45 to 65 polymeric individual chains and a stacking of at least four to five single chains. (There is inherent overestimation in width measurements by AFM since the width also includes a contribution from the imaging tip.) The dried fibres on mica that we obtained are similar in height to the “single” molecules or small aggregates of pectin, which is mainly galacturonan. For orange pectin the observed height was 0.43 nm [27] and for tomato pectin 0.5–0.7 nm [28].

The apparent height of the fibrils is bigger in water, up to 4 nm. In aqueous solution, hydrogen bonding can occur between the polymer chains and also between the OH of the polymers and the solvent (water). When the measurements are taken under water, due to polymer swelling and hydration, the diameter and height of the fibres are larger than the actual values or when the measurements are made for the dried, unswelled polymer.

The size of the fibres observed in our experiments indicates that there is massive lateral aggregation present between polymer chains. Since no clear evidence for crosslinking was observed in the NMR data, we attribute the increased association between single chains to the tendency of the glucuronic acid polymers to associate through interchain hydrogen bonding.

To our knowledge this is the first time that glucuronic acid was imaged over a range of pH, showing the formation of oligomers starting from monomers. While galacturonan has been investigated by AFM, being the main component of pectin,

glucuronan and polyglucuronic acid have not. The fibre length we observe is greater than the one observed with the AFM for homogalacturonan from sugar beet pectin on mica, which is much less than 1 micron [26]. The fibres seen are not branched most of the time, which indicates a preference for one type of glycosidic linkage to form long chains. This proposition is confirmed with NMR experiments, as described in the next section.

4.3.2 Polyglucuronic acid fibres characterized by NMR

Solid state and solution state NMR spectra of glucuronic acid in acidic and basic environments

At acidic pH, in the presence of HCl, glucuronic acid monomers link to form oligomers. The linkage occurs between the anomeric carbon (carbon 1 in Figures 4.4(a) and 4.4(b)) and one other carbon atom from the ring, presumably carbon 4. Based on comparison of the NMR spectra obtained with those reported in the literature [11,29], and α -(1,4) linkage was assigned to the obtained structure (Figure 4.4(c)). This process is reversible at acidic pH, but the linkage formed is stable in base [23]. ^{13}C NMR spectra recorded for solutions of commercial glucuronic acid sodium salt, with pH modified to 2 with HCl and subsequently modified to basic (pH 13) with NaOH, prove the formation of a glycosidic linkage between the glucuronic acid monomers.

The $^{13}\text{C}\{^1\text{H}\}$ cross polarization magic angle spinning (CPMAS) NMR spectrum of the glucuronic acid sodium salt (Figure 4.5(a)) shows six peaks indicating the presence of one anomer only, in monomeric form, in concordance with data published for α -D-galacturonic acid [30]. (The solid state spectrum has the intensity lowered to be comparable in intensity to the other presented spectra in Figure 4.5).

The aqueous solution prepared from the solid glucuronic acid sodium salt had an

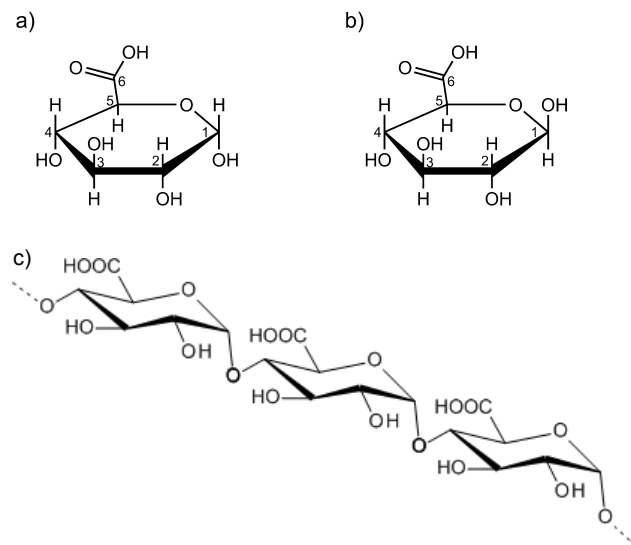


Figure 4.4: Structure of glucuronic acid monomer and polymer: (a) α anomer and (b) β anomer. The carbon atoms are numbered, as referred to in the text. (c) Possible structure of synthesized polyglucuronic acid featuring the α -(1,4) linkage.

unadjusted pH of 6, and the ^{13}C NMR spectrum in solution (Figure 4.5(b)) is similar to the spectrum reported in literature for glucuronic acid sodium salt in D_2O [31]. The spectrum contains 12 peaks, six for each of the α and β anomers of the glucuronic acid monomer, which form by the mutarotation process that takes place in aqueous solution. The peak intensities are similar for both anomers. The assignment of the peaks is done based on literature reported values; thus the peaks at 178.1 ppm and 177.1 ppm represent the carboxylate group at the C6 atom [22], and the peaks at 97.2 ppm and 93.4 ppm are assigned to the C1 carbon atoms for the β anomer and for the α anomer, respectively [22,31,32] (see Figures 4.4(a) and 4.4(b) for carbon numbers). The other grouped peaks in the region 70–80 ppm correspond to the resonances of the ring carbon atoms C2–C5 [22].

In basic solution (pH 13), the same 12 peaks for both α and β anomers are observed (Figure 4.5(c)), and it is worth noting that the spectrum changes are insignificant compared to the unadjusted pH 6, all the peaks having similar intensities and

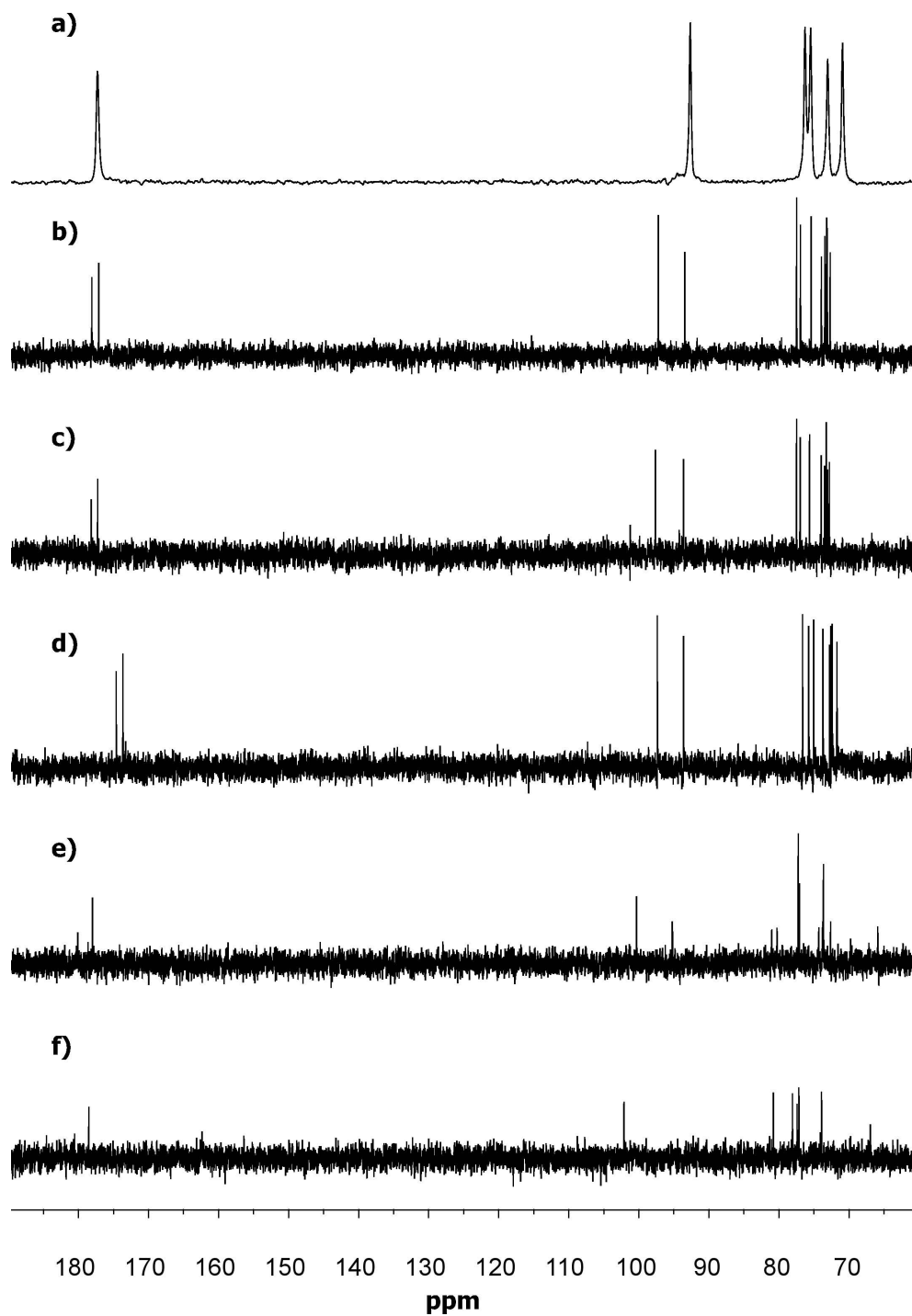


Figure 4.5: ^{13}C NMR spectra of glucuronic acid in monomeric and polymeric forms: (a) solid state CPMAS; (b) unadjusted pH 6, monomer; (c) basic pH 13, monomer; (d) acidic pH 2, monomer; (e) acidic to basic after 10 min, mixture monomer-polymer; (f) acidic to basic after 30 min, polymer. The intensity in the solid state spectrum (a) is scaled to match those of the solution spectra (b)–(f).

distribution and staying within the 0.1–0.3 ppm shift range.

When the pH is modified with HCl to a value of ≤ 2 (Figure 4.5(d)), very slight shifts are observed from the unadjusted pH spectrum (Figure 4.5(b)) for the anomeric and the ring carbon atoms, while the peaks assigned to the carboxylate groups are shifted from 178.1 ppm and 177.1 ppm to 174.6 ppm and 173.9 ppm, respectively. The chemical shift values are similar to the ones reported in literature: for pH 7.8 the carboxylate signal would be at 176.9 ppm for α anomer and 177.6 for β anomer, which changes once the pH is modified to 1.8, with the C6 peak of the α anomer being at 172.9 ppm and for β at 173.8 ppm [22, 33]. The reason for this 3.5 ppm shift for the C6 from the carboxylate groups may be the protonation of glucuronate, which is now not present as a sodium salt but as glucuronic acid.

Solution NMR spectra following pH changes

The spectra for the acidic turned to basic samples were recorded at two different reaction times, in order to see if product formation was complete. One reaction was quenched after 10 min of glucuronic acid in HCl pH 2 (Figure 4.5(e)) and the other after 30 min in HCl ((Figure 4.5(f)) by changing the pH to basic (pH 13) with NaOH. Although others have reported degradation of polyuronic acid through a β -elimination mechanism when allowed to remain in base at room temperature [10], this is actually degradation of precursor polymer in the specific conditions of the TEMPO-based process [34], which does not apply in our method.

During the linkage process in acidic turned to basic samples, the spectral interpretation leads to the idea that the product of a 10 min reaction time represents an intermediate in obtaining the product of a 30 min reaction time, the first spectrum showing more resonances than the latter one and therefore containing more species. A difference in linkage is that the peak at 100.3 ppm for 10 min reaction time shifts

to 102.1 ppm for 30 min reaction time, but in both cases, due to the presence of only one anomeric resonance, it is established that it is the same glucuronate unit that is repeated [35].

When the linking reaction that would occur at acidic pH is quenched after 10 min by adding base ($6 \text{ mol L}^{-1} \text{ NaOH}$) and pH is changed to *ca* 13 from *ca* 2, the NMR spectrum of the solution shows an intense peak at 100.3 ppm corresponding to the C–O–C glycosidic linkage in which the anomeric carbon is involved (Figure 4.5(e)). The other evidence for this type of linkage is the presence of the peaks at *ca* 80 ppm. For this solution two peaks are present at 81.0 ppm and 80.3 ppm, of similar intensities, which may mean that the glycosidic bond formed could be between the anomeric carbon and two distinct carbon atoms in the ring, having different positions.

The presence of the peak at 95.2 ppm suggests that the monomeric β anomer is present in solution or that the polyglucuronic acid formed may have β reducing ends. This is supported also by the presence of the two peaks in the spectral region where the carboxylic carbon atoms resonate, one corresponding to the glucuronic acid monomer with β anomeric configuration and the other to the α -polyglucuronic acid formed. The other chemical shifts present are for carbon atoms from the ring, either for the β -anomeric monomer or for the polyglucuronate, and are not assigned individually. There may be other linkages present in quantities too small to provide a detectable signal.

When the linking reaction is quenched with base after 30 min in HCl (compared with 10 min in the sample above), the peak at 95.2 ppm corresponding to the β anomer of the monomer disappears, suggesting that in solution the polyglucuronate is more abundant than the monomers (Figure 4.5(f)). Furthermore, by allowing more time in the presence of HCl, a preferential position may be achieved for the glycosidic bond based on fewer peaks observed. There may still be some other species present

as well, either monomers or different linkages that can lead to minor branching, but in low concentration.

Although under acidic conditions various types of linkages can form, e.g. glycosidic bonds, esterification between the carboxylic functional unit of one glucuronic acid moiety and a hydroxyl group from another moiety, as well the formation of glucuronolactone type structures, all these linkages are at equilibrium in acid catalysis and fully reversible, as indicated by the spectrum presented in Figure 4.5(d) acquired at acidic pH, in which only the free anomers are present. Under basic conditions, the ester type bonds including the intra-ester linkage of glucurono-lactone is readily hydrolysed to the free glucuronic acid [36], suggesting that the glycosidic bonding should be predominant at basic pH and that the glucurono-lactone type structure is not expected to be present in our spectrum for polymerization, Figure 4.5(f). However, D-glucurono-6,3-lactone can yield an NMR spectrum which partially resembles the one for polyglucuronic acids. Knowing that the β form of D-glucurono-6,3-lactone is predominant in aqueous solution, we compared its ^{13}C NMR spectrum [37] with ours. Close likeness was found between our spectrum for the β free anomer of glucuronic acid (Figure 4.5(b)) and theirs, but there are clear differences between our polymer spectrum (Figure 4.5(f)) and their spectrum for the β form of D-glucurono-6,3-lactone. This hypothesis is supported by the absence in our spectrum of the 85.6 ppm peak reported in this reference, which indicates the bond between C6 and C3 atoms. Based on the spectrum in Figure 4.5(e), it may be possible that the lactone is present as a byproduct in small amounts, which hydrolyses to the free acid, subsequently transformed in polyglucuronic acid.

The absence in spectrum Figure 4.5(f) of signals coming from the anomeric carbon atoms (90–97 ppm) and the presence of the peaks at *ca* 100 ppm and *ca* 80 ppm proves that the type of bonding encountered in the product solution is mainly of glycosidic

type, without excluding the possibility that ester type linkages are present but in insignificant quantity. The peak at *ca* 100 ppm represents evidence that the bond is formed between one of the anomeric carbons, while the peak at *ca* 80 ppm proves that the other atom in the bond is a carbon atom from the ring, which shifts from *ca* 70 ppm. Links between an anomeric hydroxyl and carbon can only lead to the formation of oligosaccharides. Thus, the NMR spectra in Figures 4.5(e) and 4.5(f) are proof of the polymerization of glucuronic acid monomers through glycosylation. If a polyester type structure is to be formed between the C6 carboxyl atom and another OH at a particular position, either the *ca* 100 ppm or the *ca* 80 ppm signals would not be observed. The base promoted hydrolysis of carboxylic acid esters confirms that esters are not the synthesized product of our proposed reaction.

For both spectra for the acidic samples turned to basic, the overall intensity of the peaks drops compared with the spectra for acidic or unadjusted pH samples. One reason could be the formation of the polymer which, due to an increase in viscosity, may not give the same signal strength as the monomers.

We also performed an experiment, spectrum not shown here, where an acidic sample was turned to basic and then back to acidic. Instead of seeing a linkage between the monomers, the characteristic peaks for the α and β anomers of glucuronic acid monomers appeared, the spectrum superimposing with the spectrum for the acidic environment, thus explaining why the formation of the polyglucuronate fibres was not observed when AFM imaging was performed in a pH 2 solution of glucuronic acid sodium salt.

NMR evidence for anomeric selectivity

The NMR spectra demonstrate a preference for one stereomer for the glycosidic linkage, either α or β . In order to elucidate if we have α or β linkages we compared the

chemical shifts in our ^{13}C -spectra for the polyglucuronic acid with those obtained for β -(1,4)-polyglucuronic acid found in the literature. Given the different shift values that we observe overall, we conclude that we do not have a β structure. For example, the carboxylate peak in β linked polyglucuronate is at *ca* 175 ppm for sodium salt [1, 3, 7, 10] while in our experiment it appears at 178.5 ppm.

It is interesting to see that the whole spectrum is comparable with that reported in literature for the amygluronate sodium salt [11, 29], with the carboxylate shift being 178.6 ppm and ours being at 178.5 ppm. There is a difference in the resonance value reported for C1, theirs being at 100 ppm, while the one we obtained was 100.3 ppm after 10 min reaction time in HCl, which shifted to 102 ppm after 30 min reaction in HCl. This suggests that the polyglucuronic acid we obtained is more likely to have an α structure.

Proton magnetic resonance is a valuable method to determine the anomeric configuration of oligosaccharides [20]. Our shifts and coupling constants are similar to those reported in literature [15, 17] for the α anomer of the polyglucuronic acid. This clearly indicates that α anomeric carbons are present and may be forming the linkage between the monomeric units.

The proton spectra recorded (shown in Appendix B, Figures B.1 and B.2) for samples with basic pH, unadjusted pH, and acidic to basic pH after 30 min, all have coupling constants $J_{1,2}$ equal to 3.7 Hz, characteristic for a proton in an α -anomer [15, 20], and appearing as a doublet at *ca* 5.1 ppm. Our values are similar to those reported for glucose to be 3.6 Hz, which is what is expected [21]. Resonances from β anomeric protons, if present, would be covered by the water peak that appears at *ca* 4.2–4.6 ppm, where the β anomeric protons are expected to resonate [7, 17]. However, the ^{13}C spectra indicate that only one linkage (α or β) is present; since the α protons are visible it can be inferred that an α linkage is present.

In summary, our NMR data show that we start from a solid glucuronic acid anomer and find both anomers α and β are identified in solution. When the monomers link they do so through an α -linkage, in contrast to what is found more in nature, the β linkage. Not much literature is found about amygluronate compared with cellouronate or the β linked polyglucuronic acid, which makes this synthesis even more interesting considering that β glucuronan seems to be more abundant in nature, being found in bacterial cultures and fungi, whereas the α linked one is found only in one bacterial culture.

4.4 Conclusions

Here I presented an easy method for the formation of glucuronic acid oligomers in the presence of HCl starting from glucuronic acid monomers, through uncontrolled stereo glycosidation of the glucuronic acid monomeric units. The monomers interconnect through glycosidic linkages to form a water-soluble polyglucuronic acid. The oligomers are characterized with AFM and ^{13}C NMR. AFM images of surface topography illustrate the formation of fibres in acidic medium and their preservation at basic pH, while NMR spectroscopy allows us to see the glycosidic linkage formation between the monomeric glucuronate units which was established from the peaks of the anomeric resonances. For the sample when the pH is switched from acidic to basic after 30 min, the peaks at 102.1 ppm and 80.8 ppm show clearly that the covalent C–O–C bond formed is between the anomeric carbon atom and another carbon atom from the ring.

If the reaction is not given enough time to complete, the presence of the β anomer of the glucuronic acid monomer is signaled by the peak at 95.2 ppm, which disappears if more time is allowed for monomers to sit in acidic medium before changing it to

basic.

The anomer-selective glycosidic linkage is formed at acidic pH modified with HCl without any protection of the OH groups, a fact that is supported by the AFM images showing the fibres adsorbed on mica either dried or by imaging in fluid. To our knowledge this method in the presence of HCl was not used before to form polyglucuronic acid starting from monomers.

Previous study of the oxidation of amylose to α -(1,4)-polyglucuronic acid by TEMPO/NaBr/NaClO oxidation at pH 10 led to almost complete conversion of the C6-OH groups to carboxylate groups, but also depolymerization of polysaccharide chains [38]. The NaClO used for oxidation may cause depolymerization by oxidative cleavage of glycoside bonds [39]. Lower pH conditions consisting in amylose oxidation with 4-acetamide-TEMPO/NaClO/NaClO₂ at pH 4.7 resulted in less depolymerization, but with incomplete conversion of C6-OH groups of polysaccharides to carboxylate groups [38]. A positive aspect of our approach is the presence of the carboxylate moiety on glucuronic acid residues since the beginning of the polymerization process, without the need to use a chlorine-containing oxidant and continuous pH adjustment. However, the degree of polymerization is not yet established and further studies would be required to determine the molecular weight and the number of glucuronic acid residues in a polymer chain. While NMR spectroscopy confirms the selectivity of the polymerization reaction with α -(1,4) linkage being dominant, linkages other than α -(1,4) may occur, therefore, the reaction yield with respect to α -(1,4)-polyglucuronic acid should be assessed in future work.

4.5 Acknowledgments

The authors thank Dr. Céline Schneider (Department of Chemistry and CREAT, Memorial University) for assistance with the NMR experiments and analysis. This work was supported by the Natural Sciences and Engineering Research Council of Canada, the Canada Foundation for Innovation, and the Industrial Research and Innovation Fund.

Bibliography

- [1] A. Heyraud, J. Courtois, L. Dantas, P. Colin-Morel, and B. Courtois. Structural characterization and rheological properties of an extracellular glucuronan produced by a *Rhizobium meliloti* M5N1 mutant strain. *Carbohydrate Research*, 240:71–78, 1993.
- [2] M. L. Tavernier, C. Delattre, E. Petit, and P. Michaud. β -(1, 4)-Polyglucuronic acids—an overview. *The Open Biotechnology Journal*, 2:73–86, 2008.
- [3] D. da Silva Perez, S. Montanari, and M. R. Vignon. TEMPO-mediated oxidation of Cellulose III. *Biomacromolecules*, 4(5):1417–1425, 2003.
- [4] Y. Lienart, A. Heyraud, and O. Sevenou. 1,4 beta-D-glucuronane polymers and related polysaccharide and oligosaccharide pesticides and fertilizers. *PCT International Application*, WO 2001000025, 2001.
- [5] Y. Kato, J. Kaminaga, R. Matsuo, and A. Isogai. Oxygen permeability and biodegradability of polyuronic acids prepared from polysaccharides by TEMPO-mediated oxidation. *Journal of Polymers and the Environment*, 13(3):261–266, 2005.

- [6] R. Elboutachfaiti, C. Delattre, E. Petit, and P. Michaud. Polyglucuronic acids: structures, functions and degrading enzymes. *Carbohydrate Polymers*, 84(1):1–13, 2011.
- [7] C. Tahiri and M. R. Vignon. TEMPO-oxidation of cellulose: synthesis and characterisation of polyglucuronans. *Cellulose*, 7(2):177–188, 2000.
- [8] M. Hirota, N. Tamura, T. Saito, and A. Isogai. Oxidation of regenerated cellulose with NaClO_2 catalyzed by TEMPO and NaClO under acid-neutral conditions. *Carbohydrate Polymers*, 78(2):330–335, 2009.
- [9] N. Follain, S. Montanari, I. Jeacomine, S. Gambarelli, and M. R. Vignon. Coupling of amines with polyglucuronic acid: evidence for amide bond formation. *Carbohydrate Polymers*, 74(3):333–343, 2008.
- [10] S. Gomez-Bujedo, E. Fleury, and M. R. Vignon. Preparation of cellouronic acids and partially acetylated cellouronic acids by TEMPO/ NaClO oxidation of water-soluble cellulose acetate. *Biomacromolecules*, 5(2):565–571, 2004.
- [11] Y. Kato, R. Matsuo, and A. Isogai. Oxidation process of water-soluble starch in TEMPO-mediated system. *Carbohydrate Polymers*, 51(1):69–75, 2003.
- [12] R. ter Haar, J. W. Timmermans, T. M. Slaghek, F. E. M. Van Dongen, H. A. Schols, and H. Gruppen. TEMPO oxidation of gelatinized potato starch results in acid resistant blocks of glucuronic acid moieties. *Carbohydrate Polymers*, 81(4):830–838, 2010.
- [13] C. Delattre, L. Rios, C. Laroche, N. H. T. Le, D. Lecerf, L. Picton, J. Y. Berthon, and P. Michaud. Production and characterization of new families of polyglucuronic acids from TEMPO- NaOCl oxidation of curdlan. *International Journal of Biological Macromolecules*, 45(5):458–462, 2009.

- [14] N. Tamura, M. Wada, and A. Isogai. TEMPO-mediated oxidation of (1→3)- β -d-glucans. *Carbohydrate Polymers*, 77(2):300–305, 2009.
- [15] J. K. Park, T. Khan, and J. Y. Jung. Structural studies of the glucuronic acid oligomers produced by *Gluconacetobacter hansenii* strain. *Carbohydrate Polymers*, 63(4):482–486, 2006.
- [16] J. M. Dow, D. W. Darnall, and V. D. Villa. Two distinct classes of polyuronide from the cell walls of a dimorphic fungus, *Mucor rouxii*. *Journal of Bacteriology*, 155(3):1088–1093, 1983.
- [17] R. Aono. The poly- α - and - β -1,4-glucuronic acid moiety of teichuronopeptide from the cell wall of the alkalophilic *Bacillus* strain C-125. *Biochemical Journal*, 270(2):363–367, 1990.
- [18] Å. Rindlav-Westling and P. Gatenholm. Surface composition and morphology of starch, amylose, and amylopectin films. *Biomacromolecules*, 4(1):166–172, 2003.
- [19] S. Iwamoto, W. Kai, T. Isogai, T. Saito, A. Isogai, and T. Iwata. Comparison study of TEMPO-analogous compounds on oxidation efficiency of wood cellulose for preparation of cellulose nanofibrils. *Polymer Degradation and Stability*, 95(8):1394–1398, 2010.
- [20] J. Lehmann. *Carbohydrates: Structure and Biology*. Thieme, Stuttgart·New York, 2nd edition, 1998.
- [21] J. Ø. Duus, C. H. Gotfredsen, and K. Bock. Carbohydrate structural determination by NMR spectroscopy: modern methods and limitations. *Chemical Reviews*, 100(12):4589–4614, 2000.

- [22] K. Bock and C. Pedersen. Carbon-13 NMR spectroscopy of monosaccharides. *Advances in Carbohydrate Chemistry and Biochemistry*, 41:27–66, 1983.
- [23] A. D. Baker and R. Engel. *Organic Chemistry*. West Publishing Company, St. Paul, 1992.
- [24] S. M. Arad, L. Rapoport, A. Moshkovich, D. van Moppes, M. Karpasas, R. Golan, and Y. Golan. Superior Biolubricant from a Species of Red Microalga. *Langmuir*, 22(17):7313–7317, 2006.
- [25] M. Sun, A. Stetco, and E. F. Merschrod S. Surface-templated formation of protein microfibril arrays. *Langmuir*, 24(10):5418–5421, 2008.
- [26] A. Gromer, A. R. Kirby, A. P. Gunning, and V. J. Morris. Interfacial structure of sugar beet pectin studied by atomic force microscopy. *Langmuir*, 25(14):8012–8018, 2009.
- [27] M. L. Fishman, P. H. Cooke, H. K. Chau, D. R. Coffin, and A. T. Hotchkiss, Jr. Global structures of high methoxyl pectin from solution and in gels. *Biomacromolecules*, 8(2):573–578, 2007.
- [28] A. R. Kirby, A. J. MacDougall, and V. J. Morris. Atomic force microscopy of tomato and sugar beet pectin molecules. *Carbohydrate Polymers*, 71(4):640–647, 2008.
- [29] N. Iihashi, J. Nagayama, N. Habu, N. Konno, and A. Isogai. Enzymatic degradation of amylouronate (α -(1 \rightarrow 4)-linked glucuronan) by α -glucuronidase from *Paenibacillus* sp. TH501b. *Carbohydrate Polymers*, 77(1):59–64, 2009.

- [30] H.-R. Tang, P. S. Belton, S. C. Davies, and D. L. Hughes. Solid state NMR and X-ray diffraction studies of α -D-galacturonic acid monohydrate. *Carbohydrate Research*, 330(3):391–399, 2001.
- [31] Y. Kato, N. Habu, J. Yamaguchi, Y. Kobayashi, I. Shibata, A. Isogai, and M. Samejima. Biodegradation of β -1, 4-linked polyglucuronic acid (cellouronic acid). *Cellulose*, 9(1):75–81, 2002.
- [32] M. U. Roslund, P. Tähtinen, M. Niemitz, and R. Sjöholm. Complete assignments of the ^1H and ^{13}C chemical shifts and JH,H coupling constants in NMR spectra of D-glucopyranose and all D-glucopyranosyl-D-glucopyranosides. *Carbohydrate Research*, 343(1):101–112, 2008.
- [33] P. E. Pfeffer, K. M. Valentine, and F. W. Parrish. Deuterium-induced differential isotope shift carbon-13 NMR. 1. Resonance reassignments of mono- and disaccharides. *Journal of the American Chemical Society*, 101(5):1265–1274, 1979.
- [34] A. E. J. de Nooy, A. C. Besemer, H. van Bekkum, J. A. P. P. van Dijk, and J. A. M. Smit. TEMPO-mediated oxidation of pullulan and influence of ionic strength and linear charge density on the dimensions of the obtained polyelectrolyte chains. *Macromolecules*, 29(20):6541–6547, 1996.
- [35] M. L. Sinnott. *Carbohydrate Chemistry and Biochemistry : Structure and Mechanism*. RSC Publishing, Cambridge, 1st edition, 2007.
- [36] S. Suzuki, S. Hayase, M. Nakano, Y. Oda, and K. Kakehi. Analysis of glucuronolactone and glucuronic acid in drug formulations by high-performance liquid chromatography. *Journal of Chromatographic Science*, 36(7):357–360, 1998.
- [37] H.-A. Tajmir-Riahi. Carbohydrate complexes with lead (II) ion. Interaction of Pb (II) with. BETA.-D-glucurono-6, 3-lactone, D-glucono-1, 5-lactone, and their

acid anions and the effects of metal ion binding on the sugar hydrolysis. *Bulletin of the Chemical Society of Japan*, 62(4):1281–1286, 1989.

- [38] N. Tamura, M. Hirota, T. Saito, and A. Isogai. Oxidation of curdlan and other polysaccharides by 4-acetamide-TEMPO/NaClO/NaClO₂ under acid conditions. *Carbohydrate Polymers*, 81(3):592–598, 2010.
- [39] A. Isogai. Pretreatment of cellulose for further processing. In *Handbook of Green Materials: 1 Bionanomaterials: Separation Processes, Characterization and Properties*, pages 35–51. 2014.

Chapter 5

Conclusions and future perspectives

5.1 Conclusions

Collagen and calcium phosphate are the main constituents of natural human bone. Therefore, many efforts have been employed in the synthesis of calcium phosphate/-collagen composites [1, 2], biomaterials which could resemble the bone structure and would be able to substitute for bones [3, 4]. This bio-inspired synthesis relies mainly on the growth of calcium phosphate minerals on a collagen matrix in aqueous medium [5–7].

Due to the fact that *in vitro* mineralization of collagen contributes to the understanding of mechanisms of mineralization *in vivo*, the research presented in Chapter 2 focused on *in situ* monitoring of the incipient stages of collagen/calcium phosphate composite formation with the help of AFM. There was a particular emphasis on the effect of calcium and phosphate ion concentrations upon the mineralization process, followed by the identification of the calcium phosphate phases formed using Raman

spectroscopy. The results from this study indicate that if excess amounts of calcium and phosphate ions are present in the mineralization system the power of collagen control over the preferred formed phase is limited. The mineralization occurred with the formation of octacalcium phosphate, which is a precursor of synthetic hydroxyapatite [8,9] and of biological hydroxyapatite *in vitro* [10]. In this study we demonstrated the stimulation of mineral deposition by protein and confirmed that collagen can distinctively make a difference in the chemical composition of the mineralization products. The research performed and presented herein provides new insights into collagen mineralization and enhances the current understanding of fibril assembly and the concept of *in vitro* collagen mineralization by controlling the concentration of calcium and phosphate ions.

Glucuronic acid has previously been shown to lead to the formation of hydroxyapatite *in vitro* [11]. Therefore, in Chapter 3, a fibrillar model composed of type I collagen and glucuronic acid served as a mineralization scaffold potentially to be used for bone tissue engineering applications. The model is based on the fibrillogenesis of collagen type I in the presence of glucuronic acid, which is the main component of GAGs in the extracellular matrix, and, for comparison, galacturonic acid, a glucuronic acid epimer. The fibrillogenesis was conducted using two different approaches: “cold start” and mica-induced fibril growth. The fibrillogenesis of collagen in such conditions indicated significantly different morphological characteristics than the pure collagen systems. The effect of glucuronic acid on the morphology and structure of the collagen fibrillar assemblies proved to be dependent on the concentration of uronic acid and the fibrillogenesis approach.

In order to gain insight on how glucuronic acid affects the collagen matrix during fibrillogenesis, as observed in Chapter 3, it was essential to investigate the behaviour of the glucuronic acid, based on its electrostatic properties, in alkaline and acidic media.

This research is presented in Chapter 4 [12], where I also present the synthesis of α -polyglucuronic acid starting from glucuronic acid monomers in an acidic solution. The AFM visualisation of the α -polyglucuronic and structure confirmation by NMR was tailored by varying the pH of the glucuronic acid solution between acidic and alkaline pH range. To our knowledge this is the first time that glucuronic acid was observed by AFM under various pH conditions. This study provides a simple and direct synthesis of α -polyglucuronic acid as an alternative to its isolation from bacterial cultures or TEMPO oxidation of amylose.

5.2 Future perspectives:

5.2.1 Understanding the role of acidic groups in collagen mineralization

The mineralization of type I collagen has been studied in a dual membrane diffusion system in the presence of decorin (a proteoglycan) and glucuronic acid monomer. The formation of hydroxyapatite, which is the desired calcium phosphate phase, was observed only in the case of collagen modified with glucuronic acid [11]. An additional study indicates that the glucuronic acid-rich chondroitin 4-sulphate glycosaminoglycan may bind calcium ions, thus playing an important role in the formation of hydroxyapatite during dentinogenesis [13]. Therefore, the influence of uronic acids deserves more attention in future research in order to understand the role of the acidic group that they carry in binding calcium ions and controlling the calcium phosphate phases formation. The proposed collagen-glucuronic / galacturonic acid model presented in Chapter 3 may be used, *in vitro*, to provide insight with regards to the effect of uronic acid concentration on enhancing collagen mineralization and increasing the mechani-

cal properties of the mineralized collagen fibrils. Additionally, other acids outside of the uronic acid family, e.g. gluconic acid (another carboxylic acid derived from glucose, which does not have a carbonyl functional group), which may bind to collagen differently than uronic acids, may be introduced in the study in order to investigate the effect of acidic groups on the extent of the mineralization.

5.2.2 Mechanical properties of *in vitro* mineralized collagen fibrils

The mineralized collagen fibrils, being the building blocks of the bone matrix, contribute to bone stiffness and decrease in fracture strain. Therefore, it is important to understand how their mechanical properties depend on the amount of mineral particles and their arrangement within the fibrils [14]. An increase in stiffness is expected with increase in mineral density [14]. However, a study aimed to determine whether hardness and modulus of dentin, which is also composed of mineralized collagen fibrils, increase linearly with increase in the proportion of the mineral concentration demonstrated that the mechanical properties of dentin do not always correlate with the mineral concentration [15]. It is essential, therefore, in the light of developing new synthetic materials for tissue engineering, to study the mechanical properties of the mineralized collagen fibrils generated with *in vitro* systems for collagen mineralization.

5.2.3 Characterization of α -polyglucuronic acid

An essential parameter in the characterization of a polymer is the determination of its molecular weight, which might affect its physico-chemical properties. Since increase in viscosity could be quantitatively correlated with the molecular weight of a polymer [16], viscosity measurements of the α -polyglucuronic acid solutions could

lead to the determination of its molecular weight [17].

Bibliography

- [1] M. J. Olszta, X. Cheng, S. S. Jee, R. Kumar, Y.-Y. Kim, M. J. Kaufman, E. P. Douglas, and L. B. Gower. Bone structure and formation: a new perspective. *Materials Science and Engineering: R: Reports*, 58(3):77–116, 2007.
- [2] J. D. Hartgerink, E. Beniash, and S. I. Stupp. Self-assembly and mineralization of peptide-amphiphile nanofibers. *Science*, 294(5547):1684–1688, 2001.
- [3] U. Ripamonti and A. H. Reddi. Tissue engineering, morphogenesis, and regeneration of the periodontal tissues by bone morphogenetic proteins. *Critical Reviews in Oral Biology & Medicine*, 8(2):154–163, 1997.
- [4] R. E. Holmes, R. W. Bucholz, and V. Mooney. Porous hydroxyapatite as a bone-graft substitute in metaphyseal defects. A histometric study. *The Journal of Bone & Joint Surgery*, 68(6):904–911, 1986.
- [5] N. J. Mathers and J. T. Czernuszka. Growth of hydroxyapatite on type 1 collagen. *Journal of Materials Science Letters*, 10(17):992–993, 1991.
- [6] K. I. Clarke, S. E. Graves, A. T. C. Wong, J. T. Triffitt, M. J. O. Francis, and J. T. Czernuszka. Investigation into the formation and mechanical properties of a bioactive material based on collagen and calcium phosphate. *Journal of Materials Science: Materials in Medicine*, 4(2):107–110, 1993.
- [7] C. Du, F. Z. Cui, W. Zhang, Q. L. Feng, X. D. Zhu, and K. De Groot. Formation of calcium phosphate/collagen composites through mineralization of collagen matrix. *Journal of Biomedical Materials Research*, 50(4):518–527, 2000.

- [8] S. V. Dorozhkin and M. Epple. Biological and medical significance of calcium phosphates. *Angewandte Chemie International Edition*, 41(17):3130–3146, 2002.
- [9] S. Stewart, D. A. Shea, C. P. Tarnowski, M. D. Morris, D. Wang, R. Franceschi, D.-L. Lin, and E. Keller. Trends in early mineralization of murine calvarial osteoblastic cultures: a Raman microscopic study. *Journal of Raman Spectroscopy*, 33(7):536–543, 2002.
- [10] G. R. Sauer, W. B. Zunic, J. R. Durig, and R. E. Wuthier. Fourier transform Raman spectroscopy of synthetic and biological calcium phosphates. *Calcified Tissue International*, 54(5):414–420, 1994.
- [11] H. Ehrlich, T. Douglas, D. Scharnweber, T. Hanke, R. Born, S. Bierbaum, and H. Worch. Hydroxyapatite crystal growth on modified collagen I-templates in a model dual membrane diffusion system. *Zeitschrift Fur Anorganische Und Allgemeine Chemie*, 631(10):1825–1830, 2005.
- [12] I. A. Stetco and E. F. Merschrod S. Supramolecular structure and anomer-selective formation of polyglucuronic acid. *Polymer International*, 62(5):804–810, 2013.
- [13] G. Embery, S. Rees, R. Hall, K. Rose, R. Waddington, and P. Shellis. Calcium- and hydroxyapatite-binding properties of glucuronic acid-rich and iduronic acid-rich glycosaminoglycans and proteoglycans. *European Journal of Oral Sciences*, 106(S1):267–273, 1998.
- [14] I. Jäger and P. Fratzl. Mineralized collagen fibrils: a mechanical model with a staggered arrangement of mineral particles. *Biophysical Journal*, 79(4):1737–1746, 2000.

- [15] J. H. Kinney, S. Habelitz, S. J. Marshall, and G. W. Marshall. The importance of intrafibrillar mineralization of collagen on the mechanical properties of dentin. *Journal of Dental Research*, 82(12):957–961, 2003.
- [16] S. Wiegand and W. Köhler. Determination of molecular weights and their distributions. *Molecular Characterization and Analysis of Polymers*, 53:205–251, 2008.
- [17] T. Luan, Y. Fang, S. Al-Assaf, G. O. Phillips, and H. Zhang. Compared molecular characterization of hyaluronan using multiple-detection techniques. *Polymer*, 52(24):5648–5658, 2011.

Appendix A

Raman evidence for mineralization*

To the previously prepared samples of collagen by incubation on mica, mixed or not with the glucuronic or galacturonic acids, as described in Chapter 3, 50 μL of potassium phosphate buffer (pH 7.45) and 50 μL of $\text{Ca}(\text{NO}_3)_2$ 0.01M or CaCl_2 0.01M solution were added. The calcium nitrate and calcium chloride solutions were used as a calcium ions source for mineralization. The samples thus saturated with calcium and phosphate ions were left to dry in air before Raman analysis. The corresponding Raman spectra are presented in Figures A.1 and A.2.

Raman scattering spectra were obtained on air-dried samples using a confocal configuration with 532 nm excitation (LabRAM, Jobin Yvon Horiba).

The spectra of calcium phosphate phases obtained from the samples with glucuronic acid, galacturonic acid, and also for collagen alone, Figure A.2, show the peak for the main phosphate band, corresponding to the symmetric stretch ν_1 in the range 957-959 cm^{-1} , which is assigned to the OCP phase, indicating that the mineralization

*This appendix provides supporting information for Chapter 3

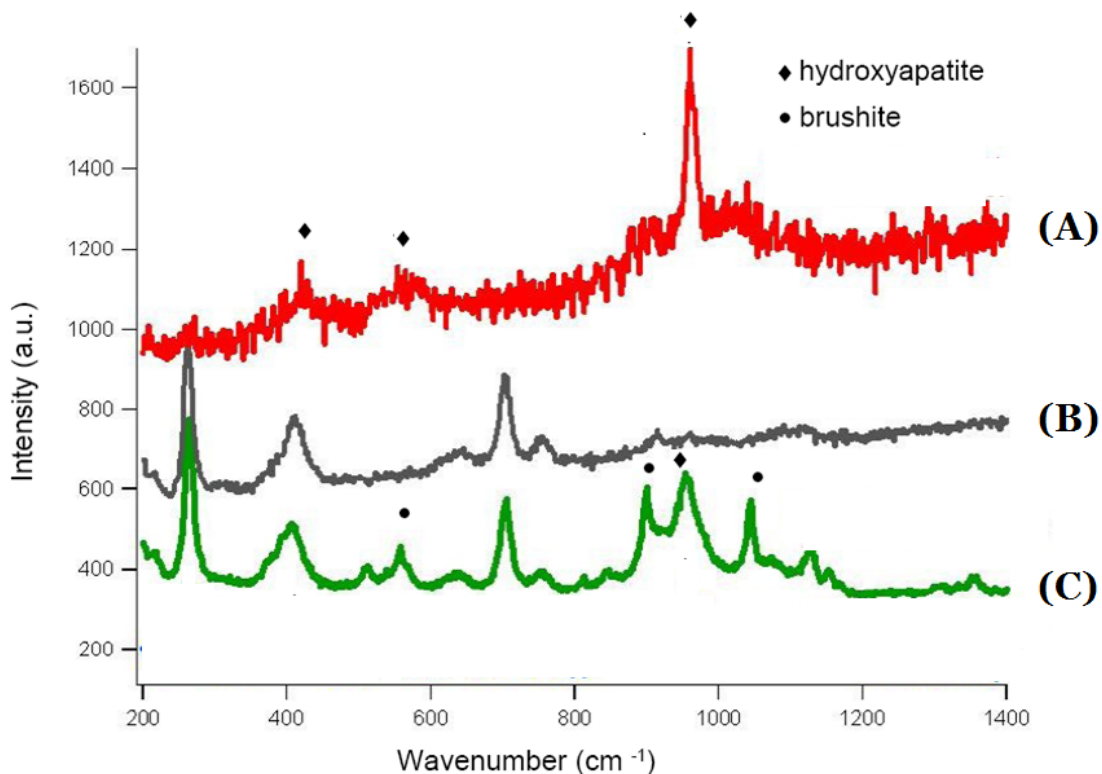


Figure A.1: Raman spectra: A) collagen fibrils incubated on mica in KPB in the presence of glucuronic acid and saturated with CaCl_2 and KPB B) collagen fibrils incubated on mica in KPB C) collagen fibrils incubated on mica in KPB, without addition of glucuronic acid, and saturated with CaCl_2 and KPB.

occurred. Although the collagen alone when it is mineralized shows the presence of this 957 cm^{-1} band, it is interesting to notice that even though the glucuronic and the galacturonic acids change the structure of the fibrillar collagen matrix, these new scaffolds still favorize the presence of the $957\text{-}959\text{ cm}^{-1}$ Raman band. In the case of the collagen sample without being mixed with glucuronic and galacturonic acids, this peak was not as specific, and appeared in a mixture of phases in which the OCP like band was equal or smaller in intensity than the bands for other calcium phosphate phases involved. The peak at 1050 cm^{-1} is assigned to the nitrate ion.

The Raman spectrum of collagen monomers mixed with $50\text{ }\mu\text{L}$ of potassium phosphate buffer (pH 7.45) and $50\text{ }\mu\text{L}$ of $\text{Ca}(\text{NO}_3)_2$ 0.01 M without incubation, Figure

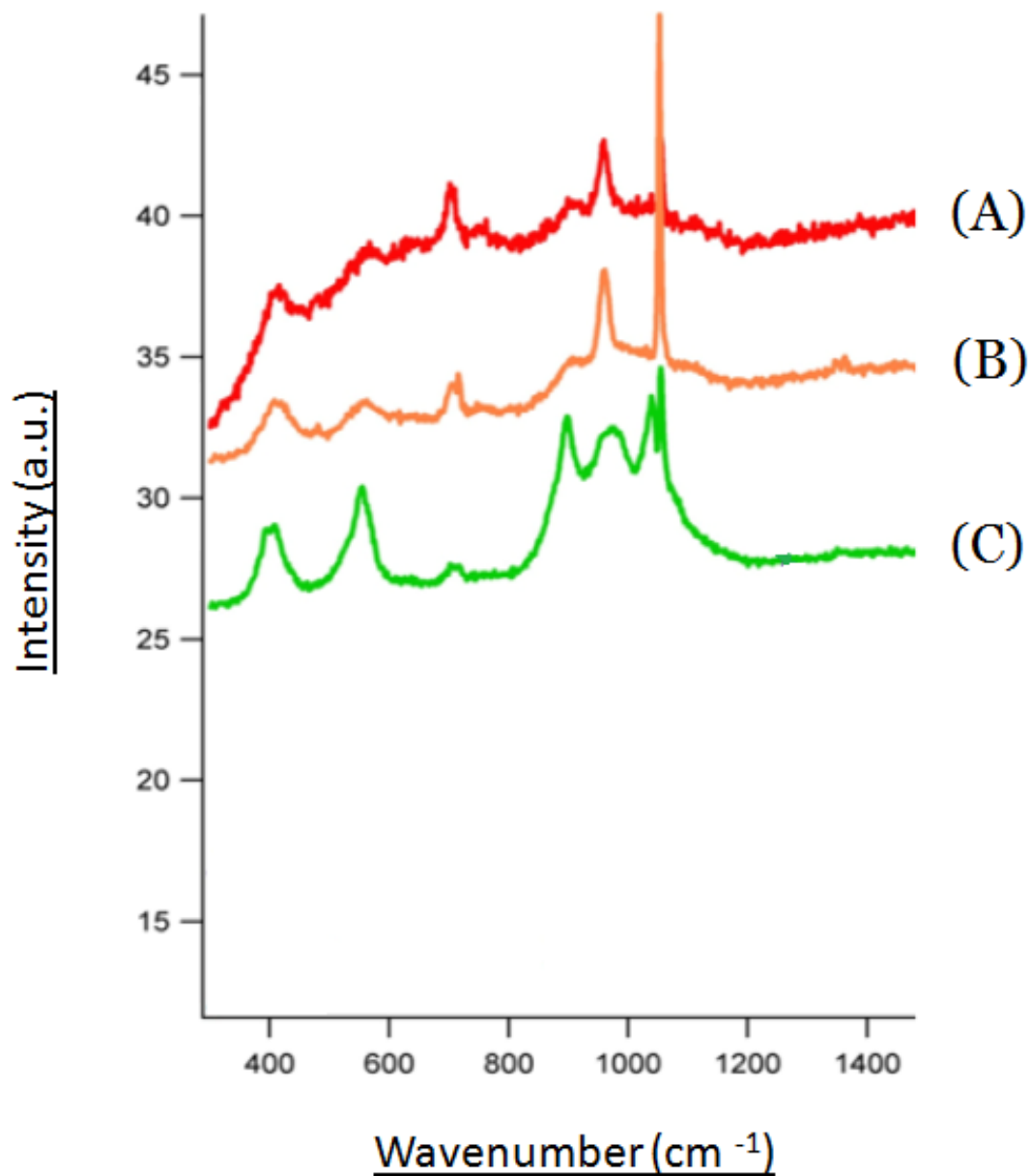


Figure A.2: Raman spectra: A) collagen fibrils incubated on mica in KPB in the presence of glucuronic acid and saturated with $\text{Ca}(\text{NO}_3)_2$ and KPB B) collagen fibrils incubated on mica in KPB in the presence of galacturonic acid and saturated with $\text{Ca}(\text{NO}_3)_2$ and KPB C) collagen fibrils incubated on mica in KPB, without addition of uronic acids, and saturated with $\text{Ca}(\text{NO}_3)_2$ and KPB.

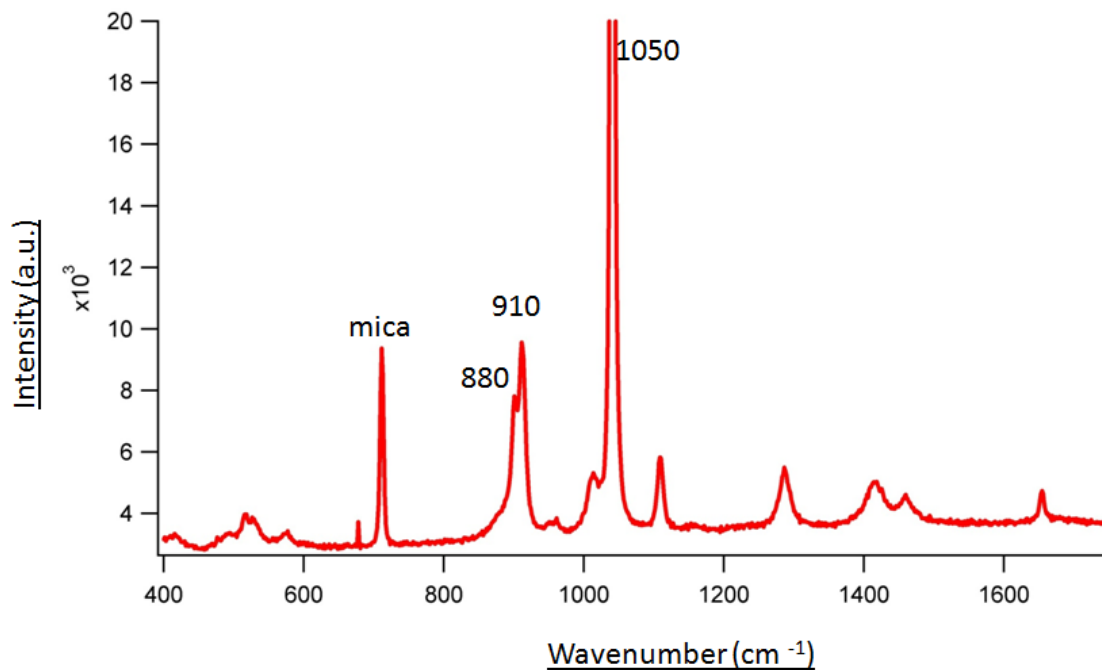


Figure A.3: Raman spectrum of collagen monomers after exposure to calcium and phosphate ions.

A.3, indicates no calcium phosphate signatures of octacalcium phosphate or hydroxyapatite in the range $957\text{-}962\text{ cm}^{-1}$. This fact suggests that collagen fibrils must be present in order to induce their formation.

Appendix B

^1H NMR spectra of glucuronic acid in monomeric and polymeric forms

This appendix provides supporting information for ^1H NMR spectra of glucuronic acid in monomeric and polymeric forms, at different pH, not shown in Chapter 4.

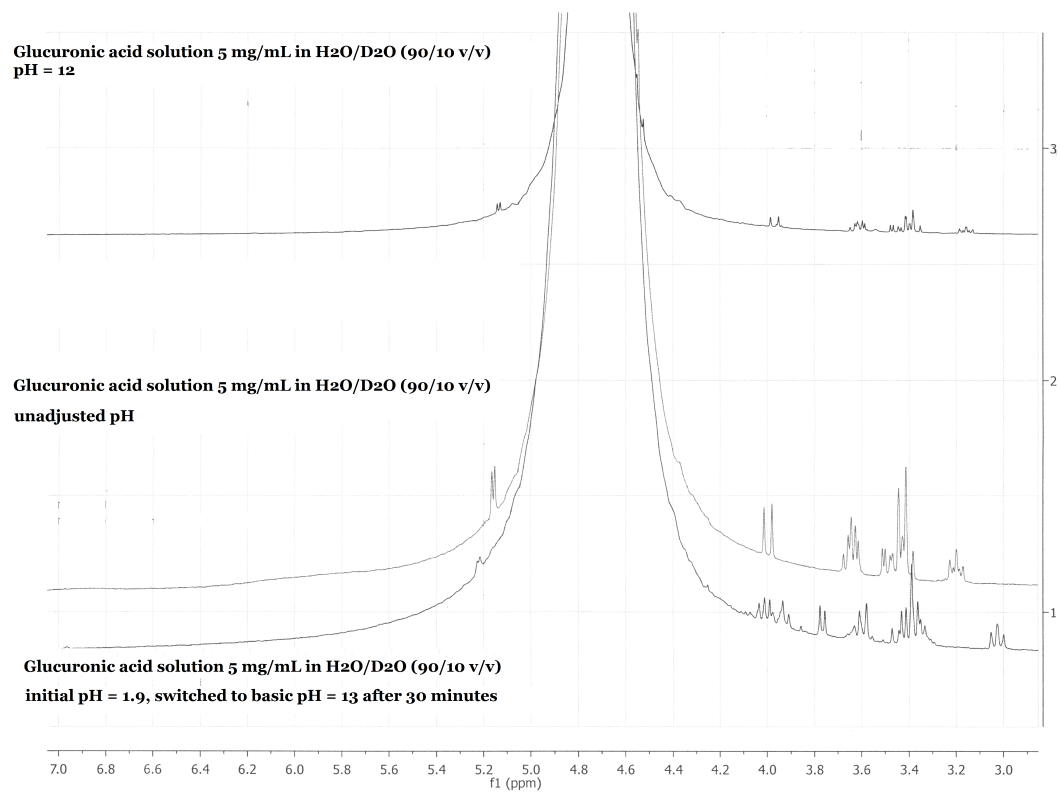


Figure B.1: ^1H NMR spectra of glucuronic acid in monomeric and polymeric forms.

Glucuronic acid solution 5 mg/mL in H₂O/D₂O (90/10 v/v) pH = 12

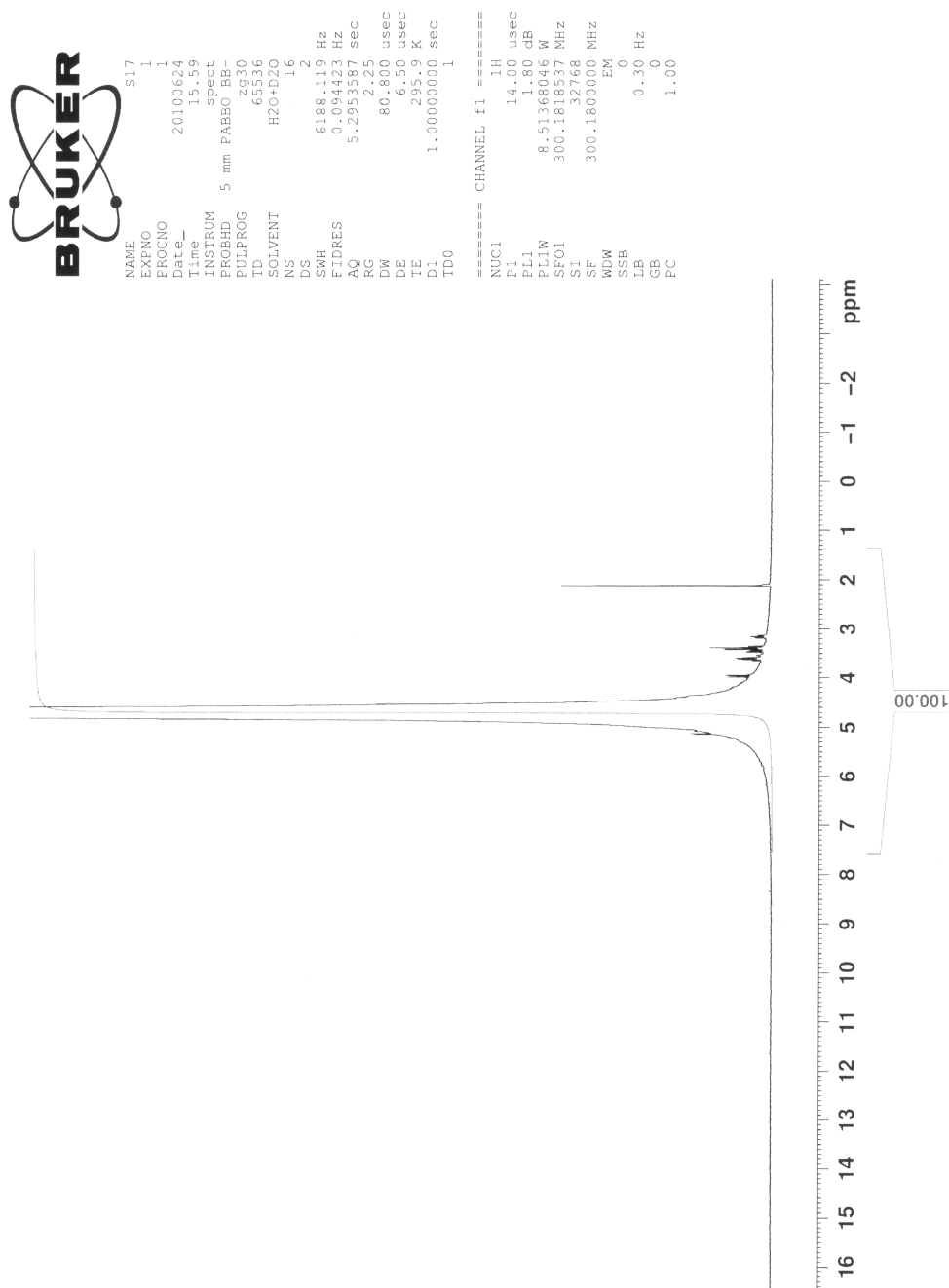


Figure B.2: ¹H NMR spectrum of glucuronic acid in monomeric form at basic pH = 12.